INORGANIC CHEMISTRY

FRONTIERS

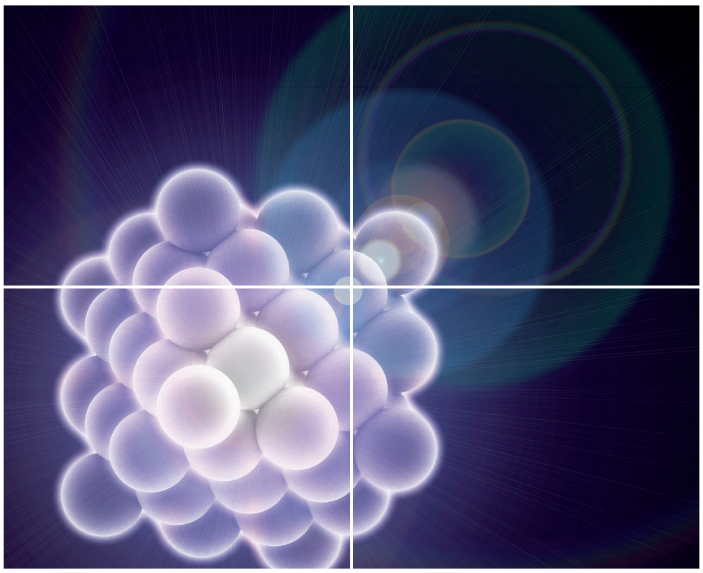

Accepted Manuscript

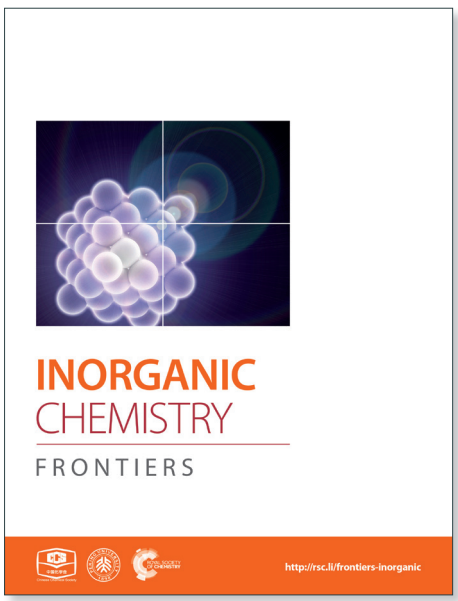

This is an *Accepted Manuscript*, which has been through the Royal Society of Chemistry peer review process and has been accepted for publication.

Accepted Manuscripts are published online shortly after acceptance, before technical editing, formatting and proof reading. Using this free service, authors can make their results available to the community, in citable form, before we publish the edited article. We will replace this *Accepted Manuscript* with the edited and formatted *Advance Article* as soon as it is available.

You can find more information about *Accepted Manuscripts* in the **Information for Authors**.

Please note that technical editing may introduce minor changes to the text and/or graphics, which may alter content. The journal's standard **Terms & Conditions** and the **Ethical guidelines** still apply. In no event shall the Royal Society of Chemistry be held responsible for any errors or omissions in this *Accepted Manuscript* or any consequences arising from the use of any information it contains.

Combining coordination and supramolecular chemistry to explore uranyl assembly in the solid state

Korey P. Carter and Christopher L. Cahill*
Department of Chemistry, The George Washington University, 725 21st Street, NW, Washington, D.C. 20052, United States

Abstract

The syntheses and crystal structures of twelve new compounds containing the UO_2^{2+} cation, a bromo-substituted benzoic acid linker (*m*-bromo-, *p*-bromo, or 3,5-dibromobenzoic acid) and a chelating N-donor (1,10-phenanthroline, 2,2':6',2''-terpyridine, or 4'-chloro-2,2':6',2''-terpyridine) are reported. Single crystal X-ray diffraction analyses of these materials allowed for the exploration of the structural relationship between the benzoic acids and the chelating N-donor, as well as the influence of pH on uranyl speciation. At an unadjusted pH (~3) a mix of uranyl monomers and dimers are observed whereas at higher pH (5-6) uranyl dimers are usually produced with monomers and tetramers also observed. A systematic study of the supramolecular interactions present in these materials was executed by varying the bromine position on the benzoic acid groups along with substituents on the chelating N-donor. Assembly via halogen and hydrogen bonding interactions as well as π-π interactions, including four instances of uranyl oxo-functionalization via halogen bonding, was observed depending on the experimental conditions utilized.

Introduction

Hybrid materials incorporating hexavalent uranium are an area of continued interest due to their penchant for forming structurally diverse coordination polymers and molecular complexes, as well as their relevance to the nuclear fuel cycle.[1-9] Development of crystalline uranyl-organic hybrid materials is generally reliant on largely directional metal-ligand interactions to promote extended structures in 1-, 2- and 3-dimensions.[10] The resulting structural diversity of uranyl hybrid materials provides a platform for understanding the relationship between solution-phase $[UO_2]^{2+}$ speciation and solid-state manifestations thereof, as is relevant for the delineation of structure property relationships such as luminescence or actinide (An) transport in the environment. The unique chemistry of the linear triatomic $[UO_2]^{2+}$ cation, where bonding is generally constrained to the equatorial plane, results in three observed primary building units (square, pentagonal and hexagonal bipyramids) and additional hydrolysis of the U(VI) metal center results in an unpredictable range of secondary building units (dimers, trimers, tetramers, hexamers, sheets, chains, etc.).[11, 12]

Uranyl hydrolysis in aqueous solution proceeds via eq 1 and governs the formation of oligomeric/polymeric SBUs.

$$m{UO_2}^{2+} + n{H_2O} \leftrightarrows (UO_2)_m(OH)_n^{2m-n} + n{H^+} \quad (1)$$

Metal cation hydrolysis can lead to oligomerization products through the creation of a point-shared hydroxyl group (olation) or thorough a two-step process that results in an oxo bridge (oxolation).[13, 14] Hydrolysis of the uranyl cation can be influenced by $[UO_2]^{2+}$ concentration and pH with oligomeric species more prevalent at pH values above 4.5.[15] Combined with a rich portfolio of ligands with a strong tendency to coordinate to the

uranyl cation (e.g. carboxylates and phosphonates) the literature is rich in both SBUs and extended assembly thereof.[5, 8, 16-19] Subsequently, the cumulative effects of both ligand contribution and metal-ion hydrolysis make the synthesis of materials with desired (or at least predictable) topologies rather challenging. While the rich diversity of uranyl materials have proven fruitful for structural characterization, the tuning of the electronic properties of the uranyl ion[6, 20, 21] remains challenging and thus an understanding of how to direct structure-property relationships in uranyl materials remains elusive.[4, 22, 23] As metal-ion hydrolysis prevents predictable construction of uranyl hybrid materials we turn to the molecular solid-state and supramolecular chemistry, as is the focus of this issue.

Supramolecular assembly of materials via attractive noncovalent interactions provides a platform to circumvent hydrolysis related synthetic challenges. A combination of chelating and linking ligands allows for the directed assembly of molecules into crystalline architectures.[24] Applications of supramolecular assembly in solid-state materials are broad and continue to expand, yet at present include drug design,[25, 26] catalysis,[27, 28] nanomaterials[29, 30] and organic materials design.[31, 32] Braga described crystal engineering as "making crystals by design,"[33] and by utilizing an understanding of intermolecular interactions in the context of crystal packing and metal-ligand coordination, one can address some of the challenges that stem from a diverse speciation profile. This is a concept that has been explored for transition metal chemistry[34] and that has more recently been extended to the actinide series, yet the area remains underexplored.[7, 35] To take a directed approach to assembly in a U(VI) system, one must find a way to restrict or "shut down" hydrolysis in order to end up with predictable molecular units (or tectons). Previous work in our group has demonstrated that synthesis

of $[UO_2]^{2+}$ materials in highly acidic and high halide media will limit uranyl hydrolysis to yield the $[UO_2X_4]^{2-}$ species (where X=Cl, Br)[36-38] or the analogous halide-nitrate ($[UO_2Cl_3NO_3]^{2-}$)[39] almost exclusively, which can then be assembled via the use of supramolecular (hydrogen- and halogen bonding) synthons. More recently, it has been shown that the use of acidic pseudo-halogens (SCN^-)[40, 41] is also quite effective in limiting uranyl speciation and producing anionic discrete building units that can be assembled via a diverse array of supramolecular interactions.

The formation of molecular $[UO_2]^{2+}$ materials does not exclusively require the use of harsh acidic conditions and indeed the literature is rich with a wide variety of uranyl molecular species.[16, 42-45] This has been highlighted by Forbes *et. al.* in the synthesis of uranyl hybrid materials containing carboxylates and amino acids that can be assembled via hydrogen bonding interactions.[46, 47] Previous work from our group has also shown that a combination of coordination chemistry principles with a series of halogen functionalized benzoic acids can yield discrete uranyl materials which utilize halogen-halogen interactions for assembly.[48] In that study, we relied on pH as a method for trying to control uranyl hydrolysis, which while effective, outcomes remain unpredictable. An approach to thwarting hydrolysis via coordination chemistry that does not require acidic media may be realized via the use of a chelating ligand to force *selection* of a single species with an inherent affinity for forming a specific coordination geometry about the $[UO_2]^{2+}$ cation. Due to their preorganization and relatively large binding affinities for f-element ions (specifically the $[UO_2]^{2+}$ cation),[49] chelating N-donors such as 1,10-phenanthroline (phen) and 2,2':6',2"-terpyridine (TPY) (and it's derivatives) have been explored as 'capping' ligands in the synthesis uranyl coordination polymers,[21, 50] uranyl

molecular materials[51] and the formation lanthanide molecular materials that also contain halogen functionalized benzoic acids.[52, 53]

Drawing inspiration from our previous work on uranyl coordination[21] and lanthanide supramolecular assembly,[52, 53] as well as the work of Loiseau and colleagues on uranyl molecular units with TPY,[54] we set out to explore a system that features both a halogen functionalized benzoic acid ligand and a chelating N-donor ligand (phen, TPY, Cl-TPY) used for the purpose of controlling hydrolysis and tailoring assembly of the uranyl tectons. Changes in ligand geometry and adjusting pH yield a rich array of molecular tectons containing a diverse array of supramolecular synthons sites (i.e. Br-O halogen bonds, Br-Br and Br-Cl halogen-halogen interactions, Br-π interactions, π-π interactions and hydrogen bonding interactions) that lie at the edge of the immediate coordination sphere. Herein we report the synthesis, crystal structures and modes of supramolecular assembly for a family of twelve new uranyl-bromo benzoic acid-N-donor materials. Additionally, the materials described herein have great potential for developing uranyl supramolecular assembly criteria based on the observed acceptor-donor pairings. As this is a *Frontiers* special issue we offer our first of many studies that will explore our motivation to establish a set of comprehensive criteria for supramolecular assembly of actinide species.

Experimental Section

Materials and Methods

Caution: Whereas the uranium oxyacetate dihydrate ($UO_2(CH_3COO)_2 \bullet 2H_2O$) used in this study consists of depleted U, standard precautions for handling radioactive and toxic substances should be followed.

All materials, including the various bromobenzoic acids (*m*-bromobenzoic acid, *p*-bromobenzoic acid and 3,5-dibromobenzoic acid) and chelating N-donors (1,10-phenanthroline, 2,2':6',2"-terpyridine and 4'-chloro-2,2':6',2"-terpyridine) were purchased and used without further purification.

Synthesis

All complexes discussed herein were synthesized via hydrothermal methods at autogeneous pressure in a 23 mL Teflon-lined Parr bomb at an oven temperature of 120 ˚C for 72 hours. A molar ratio of (1:2:2:667—UO_2^{2+}:benzoic acid:phen:water) was used for complexes **1**-**4**, while for complexes **5**-**12** a molar ratio of (1:2:1:667-- UO_2^{2+}:benzoic acid:terpy/Cl-terpy:water) was optimal for single crystal growth (Table 1). Complexes **4, 8** and **12** could only be produced after the synthesis pH was adjusted via the addition of 25 μL 5M NaOH. A comprehensive set of synthetic conditions for the UO_2^{2+}-bromo-benzoic acid-N-donor series are provided in Table 1.

Table 1: A summary of the conditions used to synthesize complexes **1-12**. Numbers in **bold** represent pH dependent syntheses.

	Unadjusted pH			**Adjusted pH**		
	m-bromo	*p*-bromo	3,5-dibromo	*m*-bromo	*p*-bromo	3,5-dibromo
phen	1 pH_f=2.5	**2** pH_f=3.0	3 pH_f=2.7	1 pH_f=5.2	**4** pH_f=5.8	3 pH_f=5.5
terpy	5 pH_f=2.9	**6** pH_f=2.8	7 pH_f=2.9	5 pH_f=5.2	**8** pH_f=5.8	7 pH_f=5.6
Cl-terpy	9 pH_f=2.6	**10** pH_f=2.8	11 pH_f=2.7	9 pH_f=5.4	**12** pH_f=5.5	11 pH_f=5.8

Characterization

X-Ray Structure Determination

Single crystals from each bulk sample were isolated and mounted on MiTeGen micromounts. Structure determination for each of the single crystals was achieved by collecting reflections using 0.5˚ ω scans on a Bruker SMART diffractometer furnished with an APEX II CCD detector using MoKα (λ=0.71073 Å) radiation at 100K (**1, 3, 7** and **11)** and (293 K) (**2, 4**-**6, 8**-**10** and **12)**. The data were integrated using the SAINT software package[55] contained within the APEX II software suite[56] and an absorption correction was performed using *SADABS*.[57] The crystal selected from the bulk product of complex **4** was a two component non-merohedral twin (77% of reflections in domain 1) that was accounted for using *TWINABS*.[58] Complexes **1, 2,** and **7**-**11** were solved via direct methods using SIR 92[59] and complexes **3**-**6** and **12** were solved via Direct Methods (SHELXS-2013).[60] All twelve complexes were refined using SHELXL-2013[60] contained within the WinGX[61] software suite. In each structure, all non-hydrogen atoms were located via difference Fourier maps and refined anisotropically. Aromatic hydrogen atoms were located via difference Fourier map, yet were placed at their idealized positions and allowed to ride on the coordinates of their parent carbon atom ((U_{iso}) fixed at 1.2U_{eq}). The hydrogen atoms on the bound water molecule in complex **4** were located via the difference Fourier map and refined isotropically. Structures **3**-**5, 8**, and **12** contain lattice water molecules and the hydrogen atoms on these molecules could not be located via difference Fourier maps and were not modeled. Hydrogen atoms on bridging hydroxide groups, identified via bond-valence summations (Tables S4-S9, Supporting Information), in **4**-**5, 8**-**9**, and **11**-**12** were not located via difference Fourier map and therefore could not be modeled via HFIX83 commands. Methyl hydrogen atoms on the bridging acetate group in **4** were placed in their idealized positions (HFIX137) and

allowed to ride on the coordinates of the parent atom ((U_{iso}) fixed at 1.5U_{eq}). Positional disorder in 3,5-dibromobenzoic acid ligands in complexes **3** (C14 and C18) and **11** (C1, C11 and C19) and in the *p*-bromobenzoic acid ligands in complex **8** (C11) was restrained via the ISOR command with uncertainty values ranging from 0.01 to 0.001 used depending on the extent of the disorder. All figures were prepared with CrystalMaker.[62] Data collection and refinement details for complexes **1-12** are included in Table 2.

Powder X-ray Diffraction

Powder X-ray diffraction (PXRD) data on the bulk reaction product of complexes **1-12** (Figures S5-S16, Supporting Information) were used to examine the bulk purity of each sample. All data were collected on a Rigaku Miniflex (Cu Kα, 2θ=3-60˚) and were analyzed using the JADE software program.[63] The bulk products of complexes **2-3, 6-7** and **9-11** contain multiple solid-state phases. Attempts were made to identify the impurities (SI) but the synthesis procedure described above was not optimized for phase purity and is thus a limitation of the presented study.

Table 2: Crystallographic Data for Compound **1-12**

	1	**2**	**3**	**4**
chem formula	$C_{26}H_{16}Br_2N_2O_6U$	$C_{26}H_{16}Br_2N_2O_6U$	$C_{26}H_{16}Br_4N_2O_7U$	$C_{28}H_{32}N_4O_{20}U_4$
formula weight	850.26	850.26	1026.08	1696.69
crystal system	triclinic	monoclinic	monoclinic	monoclinic
space group	P-1	$P2_1/c$	$P2_1/m$	$P2_1/n$
a (Å)	8.9104(8)	12.4466(8)	14.2282(8)	7.576(6)
b (Å)	12.1555(10)	21.6789(13)	6.5817(4)	15.177(6)

c (Å)	13.0201(11)	9.4110(6)	16.1780(9)	16.860(7)
α (deg)	63.614(4)	90	90	90
β (deg)	76.124(4)	95.249(4)	115.259(5)	102.094(6)
γ (deg)	84.538(3)	90	90	90
V (Å^3)	1226.32(19)	2528.7(3)	1370.15(15)	1895.6(19)
Z	2	4	2	2
T (K)	100	293	100	293
λ (Mo Kα)	0.71073	0.71073	0.71073	0.71073
D_{calc} (g cm^{-3})	2.303	2.233	2.487	2.941
μ (mm^{-1})	9.923	9.624	11.805	17.118
R_{int}	0.0375	0.0481	0.0622	0.0296
R1 [I>2σ(I)]	0.0255	0.0311	0.0279	0.0204
wR2 [I>2σ(I)]	0.0496	0.0623	0.0543	0.0453
	5	**6**	**7**	**8**
chem formula	$C_{36}H_{26}Br_3N_3O_{12}U_2$	$C_{26}H_{19}Br_2N_3O_6U$	$C_{29}H_{17}Br_4N_3O_6U$	$C_{36}H_{26}Br_3N_3O_{12}U_2$
formula weight	1408.39	903.32	1061.12	1408.39
crystal system	triclinic	triclinic	monoclinic	monoclinic
space group	P-1	P-1	$P2_1/c$	$P2_1/n$
a (Å)	8.1393(3)	8.7005(4)	13.8471(10)	20.6384(9)
b (Å)	14.2487(4)	10.3737(5)	17.0590(12)	7.4578(3)
c (Å)	17.1933(5)	16.6960(8)	14.0709(10)	26.5728(12)
α (deg)	91.870(3)	107.848(4)	90	90

β (deg)	97.985(2)	95.093(4)	115.488(1)	105.647(6)
γ (deg)	98.728(2)	95.359(3)	90	90
V (Å^3)	1948.84(11)	1417.13(12)	3000.3(4)	3938.4(3)
Z	2	2	4	4
T (K)	293	293	100	293
λ (Mo Kα)	0.71073	0.71073	0.71073	0.71073
D_{calc} (g cm^{-3})	2.400	2.117	2.349	2.375
μ (mm^{-1})	11.441	8.595	10.785	11.322
R_{int}	0.0389	0.0321	0.0600	0.0671
R1 [I>2σ(I)]	0.0322	0.0318	0.0273	0.0499
wR2 [I>2σ(I)]	0.0724	0.0695	0.0538	0.1350
	9	**10**	**11**	**12**
chem formula	$C_{36}H_{23}Br_3N_3Cl O_{11}U_2$	$C_{29}H_{18}Br_2N_3Cl O_6U$	$C_{36}H_{20}Br_6N_3Cl O_{11}U_2$	$C_{36}H_{25}Br_3N_3Cl O_{12}U_2$
formula weight	1424.81	937.76	1661.52	1442.83
crystal system	monoclinic	triclinic	monoclinic	monoclinic
space group	$P2_1/n$	P-1	$P2_1/c$	$P2_1/n$
a (Å)	20.7772(8)	8.9940(3)	18.8629(13)	20.7962(8)
b (Å)	7.9807(3)	10.4251(4)	8.6591(6)	7.5283(3)
c (Å)	25.7089(10)	16.3687(6)	26.9328(19)	26.7408(11)
α (deg)	90	104.094(1)	90	90
β (deg)	110.925(1)	94.879(1)	107.231(3)	106.168(5)
γ (deg)	90	96.417(2)	90	90

V (Å^3)	3981.8(3)	1469.19(9)	4201.6(5)	4021.0(3)
Z	4	2	4	4
T (K)	293	293	100	293
λ (Mo Kα)	0.71073	0.71073	0.71073	0.71073
D_{calc} (g cm^{-3})	2.377	2.120	2.627	2.383
μ (mm^{-1})	11.263	8.382	13.530	11.157
R_{int}	0.0438	0.0468	0.0790	0.0711
R1 [I>2σ(I)]	0.0300	0.0383	0.0374	0.0390
wR2 [I>2σ(I)]	0.0664	0.0859	0.0715	0.0769

Description of Structures

Single crystal X-ray crystallography analyses revealed three unique building units in this family of molecular complexes: monomers (one unique UO_2^{2+} cation) (**1**-**3, 6**-**7** and **10**), dimers (two unique UO_2^{2+} cations) (**5**, **8**-**9** and **11**-**12**) and a tetramer (two unique UO_2^{2+} cations) (**4**). Local structures are described in detail for complexes **1**-**6** only as they represent each of the unique observed coordination environments. Modes of supramolecular assembly are described for all complexes however as they are affected by systematic changes in the location of the bromine atoms on the benzoic acid groups and by the nature of the chelating N-donor ligands.

Complex **1**, $[UO_2(C_{12}H_8N_2)(C_7H_4BrO_2)_2]$, crystallizes in the space group P-1 and features an asymmetric unit that contains a uranyl monomer with pentagonal bipyramidal coordination geometry. The $[UO_2]^{2+}$ cation is chelated by a bidentate phen molecule and further coordinated to bidentate and monodentate *m*-bromobenzoic acid ligands (Figure

1). U1-O bond distances to the bidentate *m*-bromobenzoic acid (O3 and O4) are 2.405(2) Å and 2.442(2) Å respectively. The monodentate *m*-bromobenzoic acid is bound through O5 and is at a distance of 2.225(3) Å from the uranium center and the bromine atom (Br2) of this ligand facilitates intermolecular Br-O interactions that will be discussed in more detail in the following paragraph. Completing the equatorial coordination sphere of the uranyl ion is the bidentate phen molecule (N1 and N2) and the U1-N distances are 2.552(3) Å and 2.442(2) Å, respectively.

The uranyl monomers of **1** are assembled to form molecular dimers via halogen bonds between the axial uranyl oxygen atom (O2) on one unit and the bromine from an *m*-bromobenzoic acid ligand (Br2) of an adjacent monomer (Figure 1). The corresponding Br-O interaction distance and angle are 3.271(3) Å and ∠C-Br-O 162.82(14)º. Oxo-fuctionalization of the uranyl is known in some systems,[64-67] yet the uranyl oxygens are typically terminal in most hybrid materials (hence the bipyramidal building units). Some interactions involving the "yl" oxygen atoms are known (i.e cation-cation interactions (CCIs),[50, 68-73] yet these are observed much more frequently for the $[NpO_2]^+$ cation.[74] Efforts to 'activate' the "yl" oxygen atoms in molecular chemistry have primarily relied on the "yl" oxygen atoms ability to act as hydrogen bond acceptors.[75, 76] We have shown that the axial of the uranyl ion can act as a halogen bond acceptor with the $[UO_2(NCS)_4(H_2O)]^{2-}$ anion and the 4-chloropyridine cation[41] and in **1** we have the first of four examples where the "yl" oxygen atoms adopts the same function.

The dimers in **1** are assembled into an infinite 2D chain that propagates in the [100] direction via slightly offset π-π stacking interactions[77] between phenanthroline ligands on neighboring units. These non-covalent interactions are between the centroid (a

calculated centroid, Cg, corresponds to the center of the aromatic ring) of the phen moiety on one unit with the edge of the phen ring on the neighboring unit. Centroids were calculated in the center of the aromatic phen rings participating in these interactions in order to obtain the linear distance (Cg···Cg) between the centroids as well as displacement perpendicular to the plane of the phen rings for each of the unique π-stacks (Cg⊥···Cg⊥). Additionally, the angle (β) formed by the intersection of the line between centroids and the displacement perpendicular to the plane of the phen rings was determined. As such, the relevant distances and angles for these interactions are: Cg···Cg 3.803(2) Å; Cg⊥···Cg⊥ 3.3542(14) Å; β=27.81°.

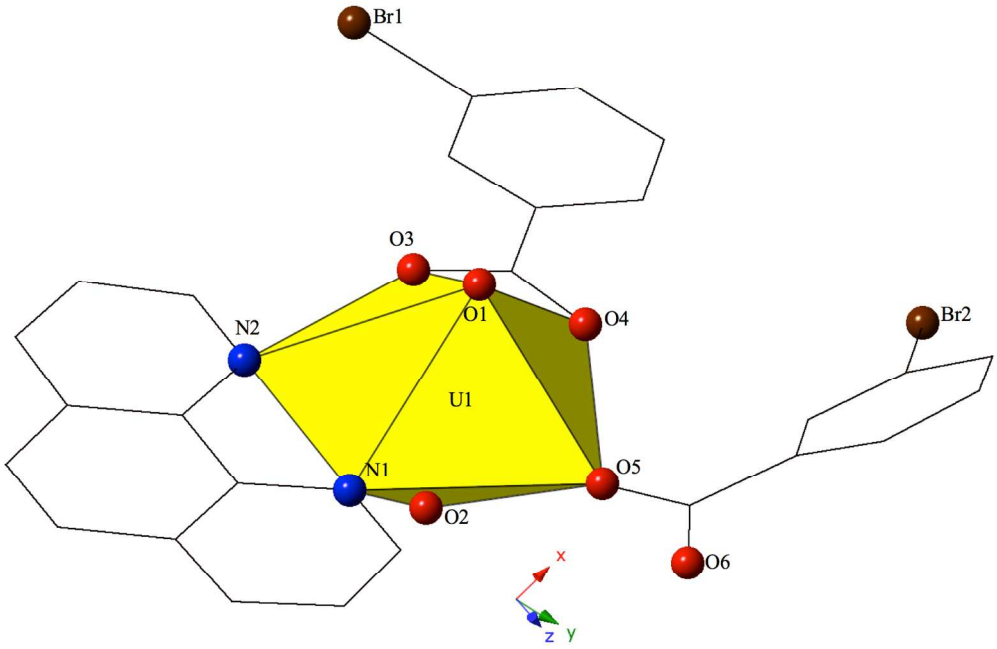

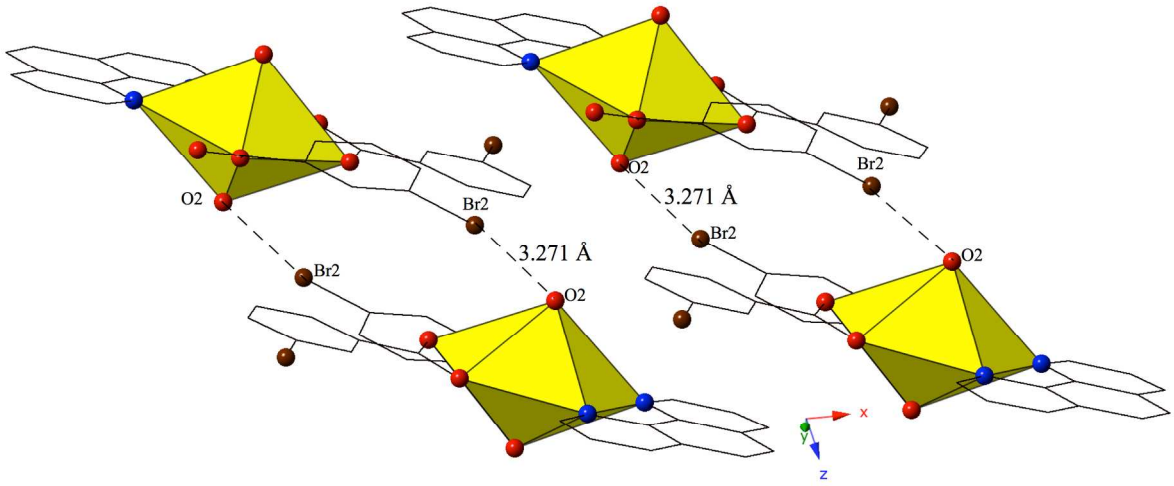

Figure 1 (Top) Polyhedral representation of asymmetric unit of **1**. Yellow polyhedra represent uranium metal centers, whereas spheres represent bromine (brown), nitrogen (blue) and oxygen (red). All H atoms have been omitted for clarity. **(Bottom)** Complex **1** viewed in the (101) plane highlighting the Br-O halogen bonding interactions between uranyl monomers.

Changing the position of the bromine from the *ortho*- to the *para*- position on the benzoic acid ligand yields complex **2**, $[UO_2(C_{12}H_8N_2)(C_7H_4BrO_2)_2]$, which crystallizes in the space group $P2_1/c$. The asymmetric unit of **2** contains a uranyl monomer with distorted hexagonal bipyramidal coordination geometry. The $[UO_2]^{2+}$ cation is chelated by a bidentate phen molecule along with two bidentate *p*-bromobenzoic acid ligands (Figure 2). U1-O bond distances to the two *p*-bromobenzoic acid ligands (O3, O4, O5 and O6) are at an average distance of 2.466 Å. U1-N distances to the bidentate phen molecule (N1 and N2) are 2.664(4) Å and 2.705 Å respectively and these values are consistent with expected distances for U-N bonds.[78, 79]

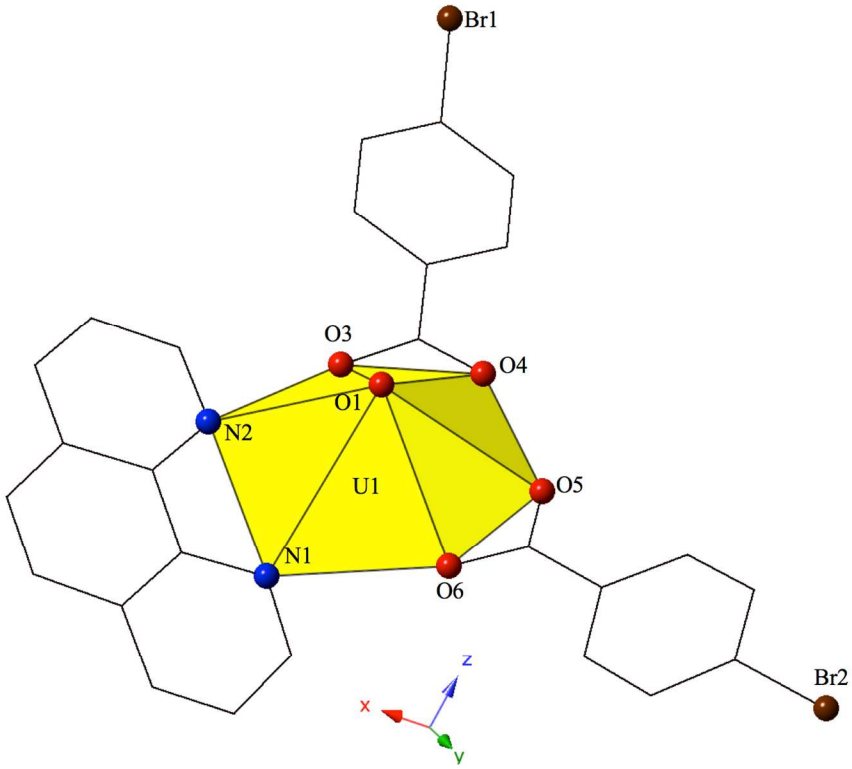

Figure 2 The local coordination geometry of **2** is shown. All H atoms have been omitted for clarity

Complex **3**, $[UO_2(C_{12}H_8N_2)(C_7H_3Br_2O_2)]\bullet H_2O$, crystallizes in the space group $P2_1/m$ and consists of uranyl monomers with a pentagonal bipyramidal coordination geometry. Each $[UO_2]^{2+}$ cation is chelated by a bidentate phen molecule and further coordinated to bidentate and monodentate 3,5-dibromobenzoic acid ligands (Figure 3). U1-O bond distances to the bidentate 3,5-dibromobenzoic acid (O2 and O3) are each 2.438(4) Å. The monodentate 3,5-dibromobenzoic acid is bound through O4 and is at a distance of 2.235(4) Å from the uranium center. U1-N distances to the bidentate phen molecule (N1 and N2) are 2.561(5) Å and 2.540(5) Å, respectively. The asymmetric unit further contains a lattice water molecule, OW1, which facilitates the supramolecular assembly of the uranyl monomers of **3** into infinite 1D chains.

Offset π-π stacking interactions between 3,5-dibromobenzoic acid ligands on adjacent units link monomers of **3** to form a 1D chain, which propagates infinitely in the [010] direction. The relevant distances and angles for these interactions are Cg···Cg 3.5832(14) Å; Cg⊥···Cg⊥ 3.2909(10) Å; β=23.30° (Figure 3). A bifurcated hydrogen bonding interaction from the lattice water, OW1, occurs with the uranyl axial oxygen atom (O1) and its symmetry equivalent (O1') and decorates the periphery of the chain (Figure S1, Supporting Information). Interaction distances from OW1 to O1 and O1' are equivalent at 3.234(5) Å.

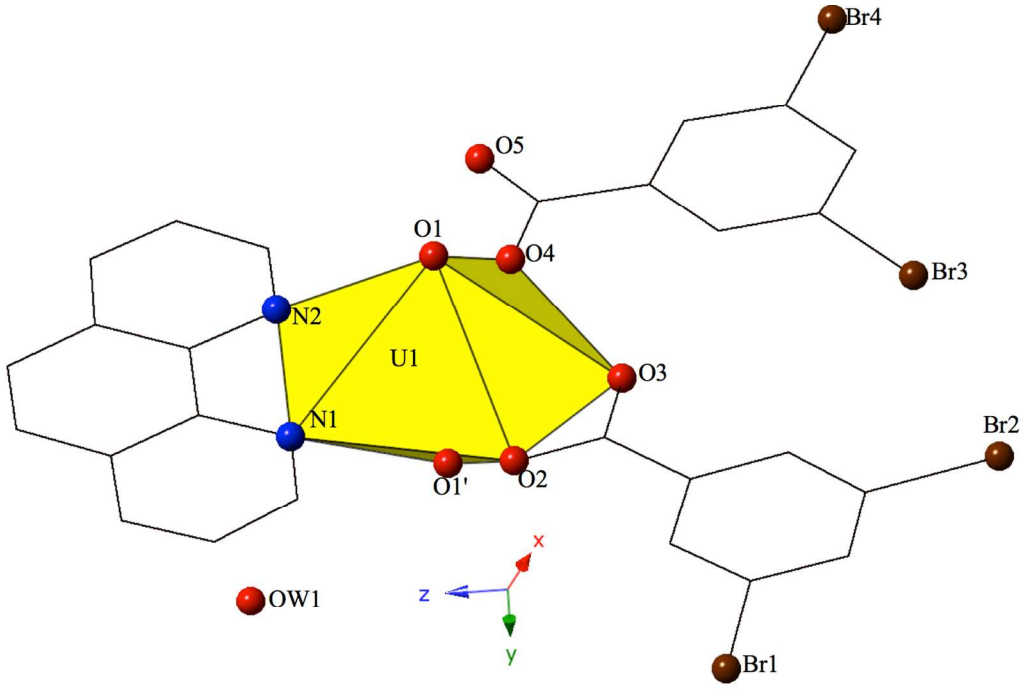

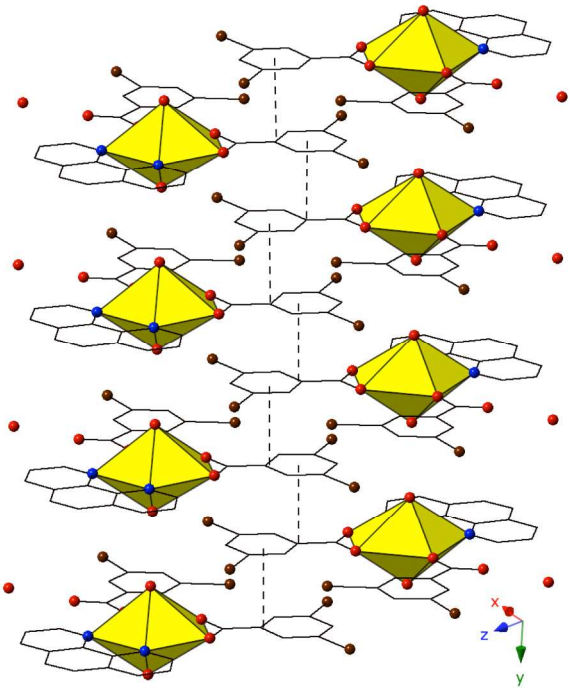

Figure 3 (Top) Polyhedral representation of local structure of **3**. All H atoms have been omitted for clarity. (**Bottom)** Complex **3** viewed down the [010] direction. π-π interactions between 3,5-dibromobenzoic acid ligands that assemble 1D chains of **3** are shown.

Complex **4,** $[(UO_2)_2(OH)(O)(C_{12}H_8N_2)(CH_3COO)(H_2O)]_2 \bullet 2H_2O$, is the first phase described herein to form exclusively at adjusted pH values (approximately 5-6) and crystallizes in the space group $P2_1/c$. The asymmetric unit of **4** consists of uranyl tetramer where two unique $[UO_2]^{2+}$ cations, and their symmetry equivalents, have adopted pentagonal bipyramidal coordination geometries (Figure 4). Both unique uranyl cations are bridged via a point-sharing μ_2-OH group (O5) with U-O bond distances of 2.320(3) Å (U1-O5) and 2.355(3) Å (U2-O5) (Confirmed via bond valence calculations, Table S4, Supporting Information). Oxolation yielded a μ_3-O bridge (O6) that connects U1, U2 and U2' with an average U-O bond distance of 2.264 Å. A third bridging interaction occurs through the coordinated acetate group (O8, O9) and this links U2 with

U1' to complete the tetramer. The corresponding U-O bond distances for the acetate group are 2.359(3) Å (U1'-O9) and 2.376(3) Å (U2-O8), respectively. Bidentate phen groups decorate the periphery of the uranyl tetramer in **4** and complete the equatorial coordination sphere of U1. U1-N distances are 2.673(4) Å (U1-N1) and 2.663(4) Å (U1-N2) which are consistent with the bond lengths observed in complexes **1-3.** A bound water molecule (OW1) lies at the apex of pentagonal bipyramid equatorial geometry of U2 at a distance 2.595(4) Å and the asymmetric unit of **4** further contains a lattice water molecule, OW2, which facilitates additional intermolecular interactions that will be discussed below. Despite its inclusion in the initial synthesis, the *p*-bromobenzoic acid ligand did not incorporate into the final structure of **4** nor was its presence as an impurity detected via PXRD. (Figure S8)

Looking at the global structure of **4**, the uranyl tetramers are assembled via offset π-π stacking interactions into a staggered 1D chain that propagates in approximately the [100] direction. (Figure 4). These non-covalent interactions are between the centroid of the phen moiety on one unit with the edge of the phen ring on the neighboring unit. The relevant distances and angles for these interactions are: Cg···Cg 3.667(4) Å; Cg⊥···Cg⊥ 3.4082(19) Å; β=21.67°. A bifurcated hydrogen bonding interaction from the lattice water, OW2, occurs with the axial uranyl oxygen atom (O3) of one tetramer and the bound water molecule (OW1) on the tetramer directly below. Interaction distances from OW2 are 2.817(5) Å to O3 and 2.798(6) Å to OW1 and the bifurcated interaction leads to the formation of a 2D sheet in approximately the (101) plane.

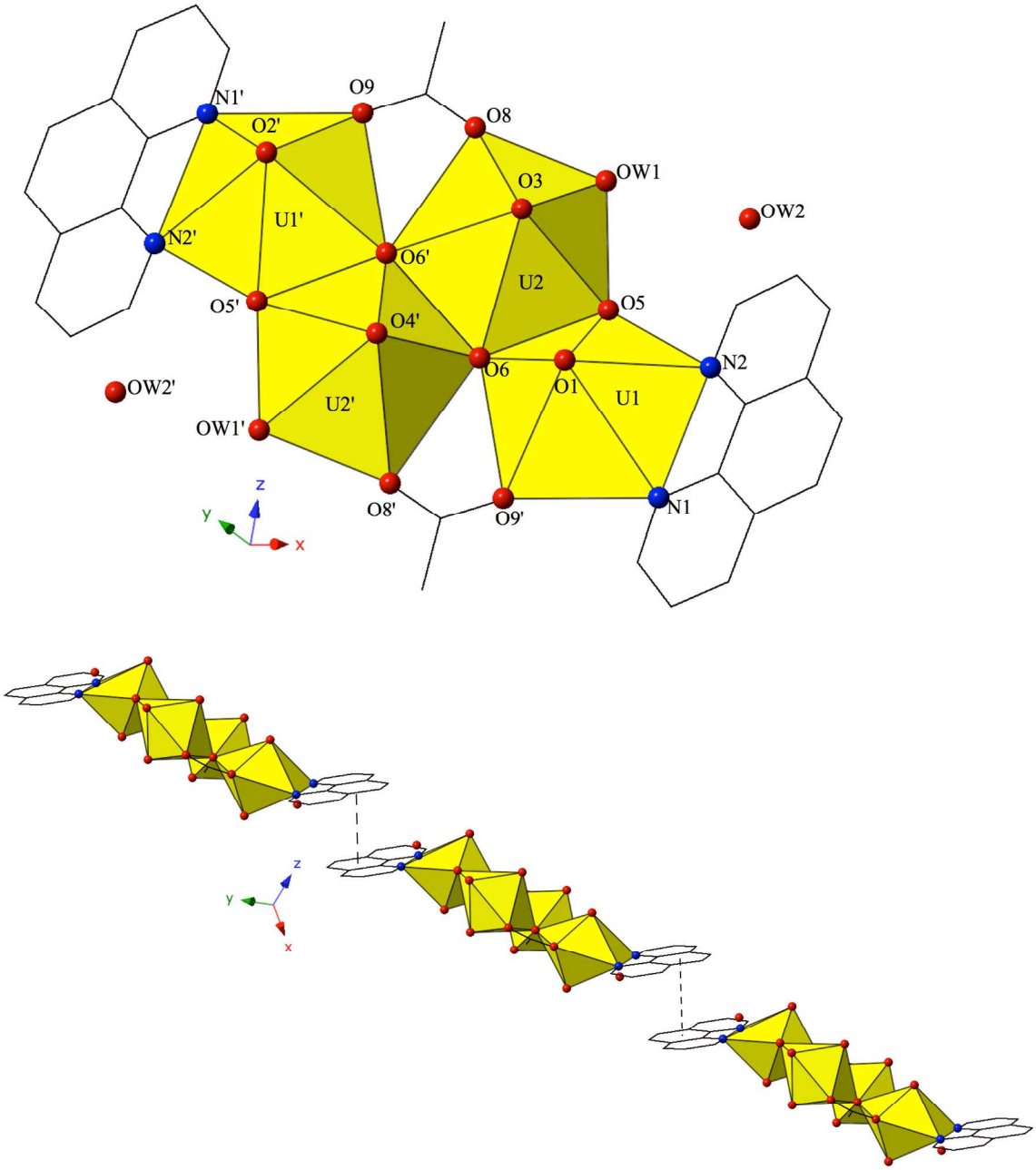

Figure 4 (Top) Polyhedral representation of local structure of **4**. All H atoms have been omitted for clarity. **(Bottom)** Complex **4** viewed down approximately the [101] direction. π-π interactions that stitch together the 1D chains of uranyl tetramers are highlighted.

The introduction of terpy as a chelating ligand yields complex **5**, $[(UO_2)_2(OH)(C_{15}H_{11}N_3)(C_7H_4BrO_2)_3]\bullet H_2O$, which crystallizes in the space group P-1. The asymmetric unit of **5** consists of a uranyl dimer where both $[UO_2]^{2+}$ cations display

pentagonal bipyramidal local coordination geometries (Figure 5). The two uranyl cations are linked via a bridging bidentate *m*-bromobenzoic acid ligand (O6 and O7) as well as a point-sharing μ_2-OH group (confirmed via bond valence calculations, Table S5, Supporting Information). Equatorial uranium-oxygen bond distances are 2.398(3) Å (U1-O6) and 2.341(4) Å (U2-O7) for the bridging *m*-bromobenzoic acid and 2.255(3) Å (U1-O5) and 2.374(3) Å (U2-O5) for the bridging hydroxide. The coordination sphere of U1 is completed by a tridentate terpy molecule bound through its three nitrogen atoms (N1, N2 and N3), with an average U1-N bond distance of 2.587 Å. Two additional *m*-bromobenzoic acid ligands decorate the U2 metal center and exhibit bidentate and monodentate coordination modes. U2-O bond distances to the bidentate *m*-bromobenzoic acid ligand (O8 and O9) are 2.453(4) Å and 2.548(3) respectively and the U2-O10 bond distance for the monodentate *m*-bromobenzoic acid is 2.276(3) Å. A lattice water molecule, OW1, which interacts with carboxylate oxygen (O11) via hydrogen bonding, completes the asymmetric unit.

Looking at the global structure of **5**, we see our first example of the halogen-halogen interaction as the uranyl dimers are linked via bromine atoms on adjacent units (Figure 5). Halogen-halogen interactions tend to adopt one of two geometries in order to minimize the overlap of regions of negative charge density.[80, 81] The interactions in complex **5** (Br3-Br3') meet the criteria described by Desiraju *et. al.*[82, 83] for a Type I halogen-halogen interaction with a distance of 3.4397(13) Å (93.0% vdW) and angles (θ_1,θ_2) equal to 139.00(19)°. The uranyl dimers of complex **5** propagate as infinite 1D chains via hydrogen bonds in approximately the [100] direction with the lattice water molecule, OW1, interacting with the point sharing hydroxide group, O5, of one dimer

directly above and the carboxylate oxygen, O9, of the dimer lying directly below at distances of 2.721(5) Å and 2.808(5) Å, respectively.

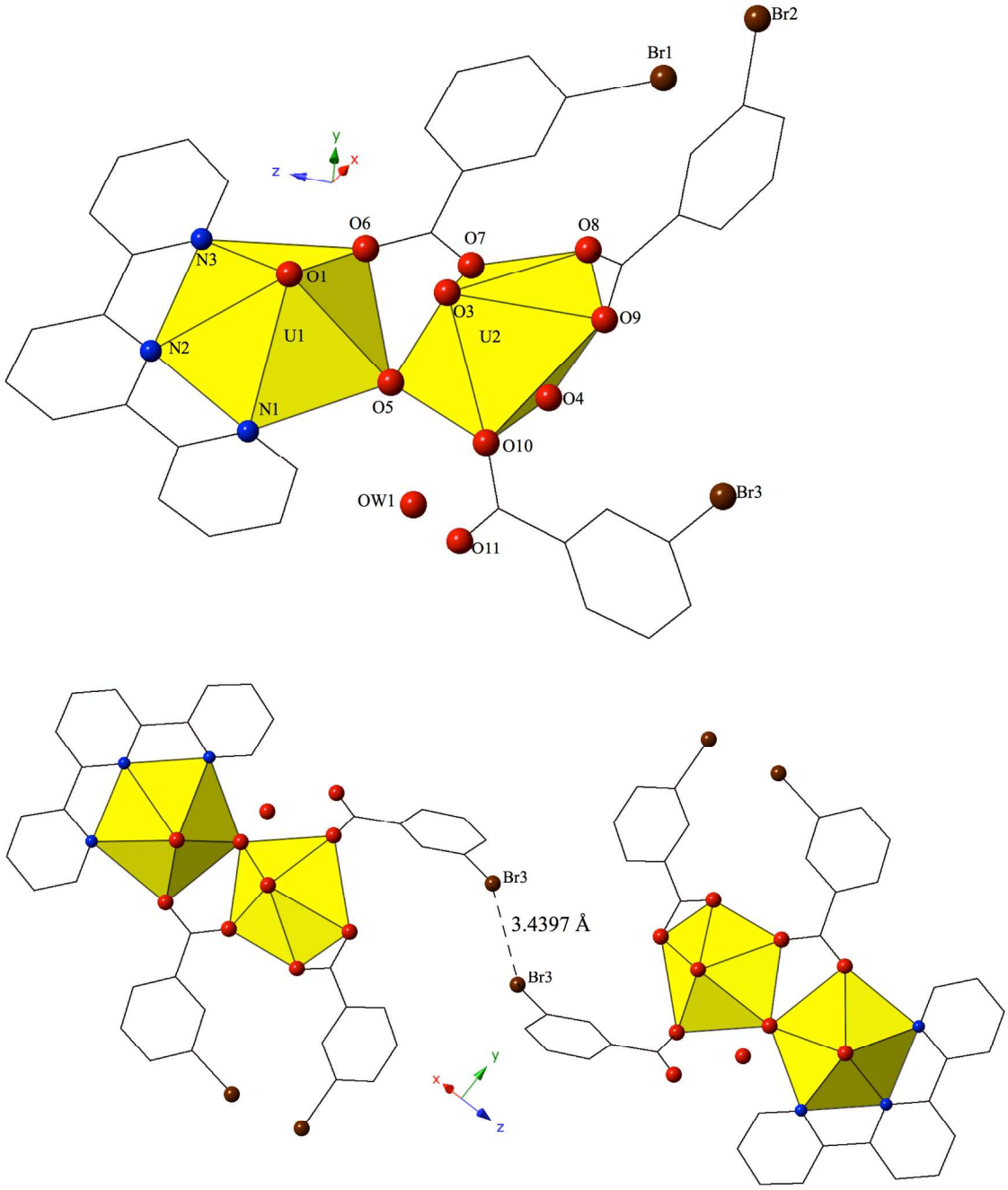

Figure 5 (Top) Polyhedral representation of asymmetric unit of **5**. All H atoms have been omitted for clarity. **(Bottom)** Complex **5** viewed down approximately the [011] direction featuring a Type I Br-Br interaction that links the adjacent uranyl dimers.

Complex **6**, $[UO_2(C_{15}H_{11}N_3)(C_7H_4BrO_2)_2]$, crystallizes in the space group P-1 and features an asymmetric unit that contains one pentagonal bipyramidal uranyl PBU. Each $[UO_2]^{2+}$ cation is chelated by a tridentate terpy molecule and coordinated by two monodentate *p*-bromobenzoic acid ligands (Figure 6). U1-O bond distances to the monodentate *p*-bromobenzoic acid ligands (O3 and O5) are 2.230(3) Å and 2.285(3) Å, respectively. The tridentate terpy molecule (N1, N2 and N3) caps the uranyl coordination sphere and the average U1-N distance is 2.582 Å.

The uranyl monomers of **6** form molecular dimers via halogen bonding interactions between the axial uranyl oxygen atom (O1) on one unit and the bromine from a *p*-bromobenzoic acid ligand (Br1) on the neighboring monomer (Figure 6). The corresponding Br-O interaction distance and angle are 3.320(3) Å and ∠C-Br-O 144.52(17)º. Additional supramolecular connectivity in **6** is achieved through a series a series of weak hydrogen bonding interactions.

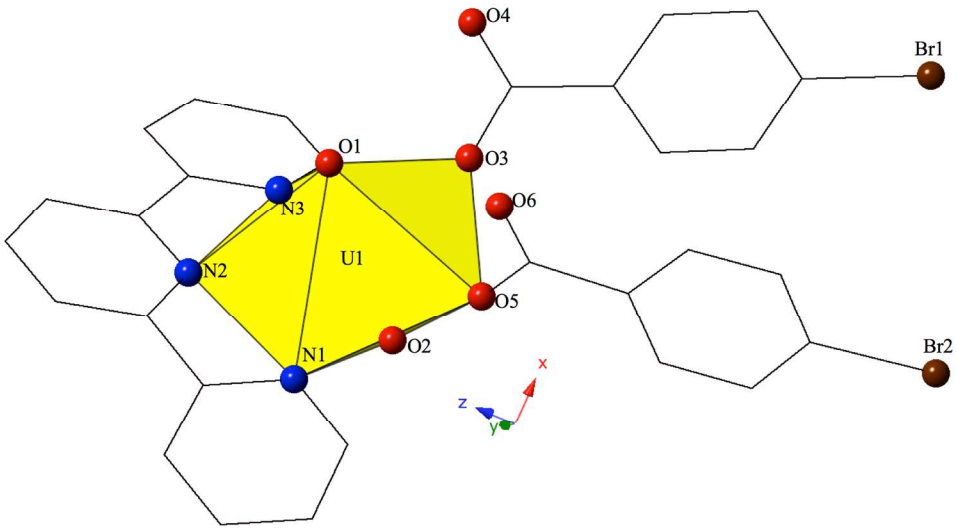

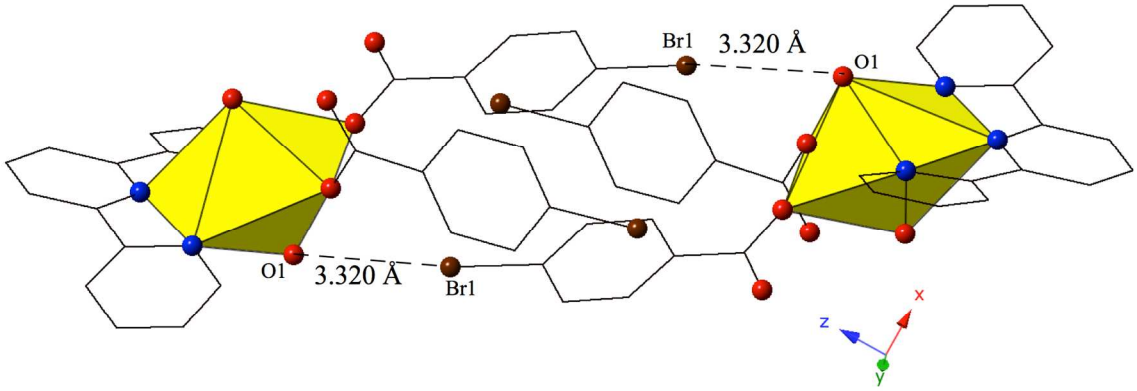

Figure 6 (Top) Polyhedral representation of asymmetric unit of **6**. All H atoms have been omitted for clarity. **(Bottom)** Complex **6** viewed down approximately the [001] direction highlighting Br-O halogen bonding interactions that assemble uranyl monomers into molecular dimers.

The combination of terpy and the 3,5-dibromobenzoic acid ligand yields complex **7**, $[UO_2(C_{15}H_{11}N_3)(C_7H_3Br_2O_2)]$, which crystallizes in the space group $P2_1/c$. Complex **7** features nearly identical uranyl coordination geometry to **6**, and thus will not be described in detail. The modes of supramolecular assembly appear to be similar when comparing **6** and **7**, yet a detailed look reveals significant differences. Similar to **6**, uranyl monomers of **7** are tethered to form molecular dimers via halogen bonding interactions between the axial uranyl oxygen atom (O1) on one unit and the bromine from a 3,5-dibromobenzoic acid ligand (Br1) on the neighboring monomer (Figure 7). The corresponding Br-O interaction distance and angle are 3.246(3) Å and ∠C-Br-O 152.80(13)º. Whereas additional dimensionality in **6** was achieved via weak hydrogen bonding interactions, the supramolecular dimers of **7** are assembled into a zigzag 1D chain via a pair of moderately strong[84] localized Br-π (Br2-C7) and (Br4-C3) interactions[85] between two 3,5-dibromobenzoic acid ligands on the same uranyl unit with the periphery of the terpyridine moiety on a neighboring unit (Figure S2, Supporting Information). Halogen-π interactions are defined as either moderate or strong lone pair-π interactions by Reedijk

and colleagues[84] based on whether the interaction distance is less than equal to the corresponding sum of the van der Waals radii (3.550 Å for bromine and carbon). The halogen-π interactions of **7** are at distances of 3.441(4) Å (Br2-C7) and 3.315(4) Å (Br4-C3) respectively and as both of these interactions are well within the sum of the corresponding vdW radii of bromine and carbon this is suggestive that the vdW overlap of the bromine atoms (Br2 and Br4) of the 3,5-dibromobenzoic acid ligands and the aromatic rings of the terpyridine molecules in **7** are significant.

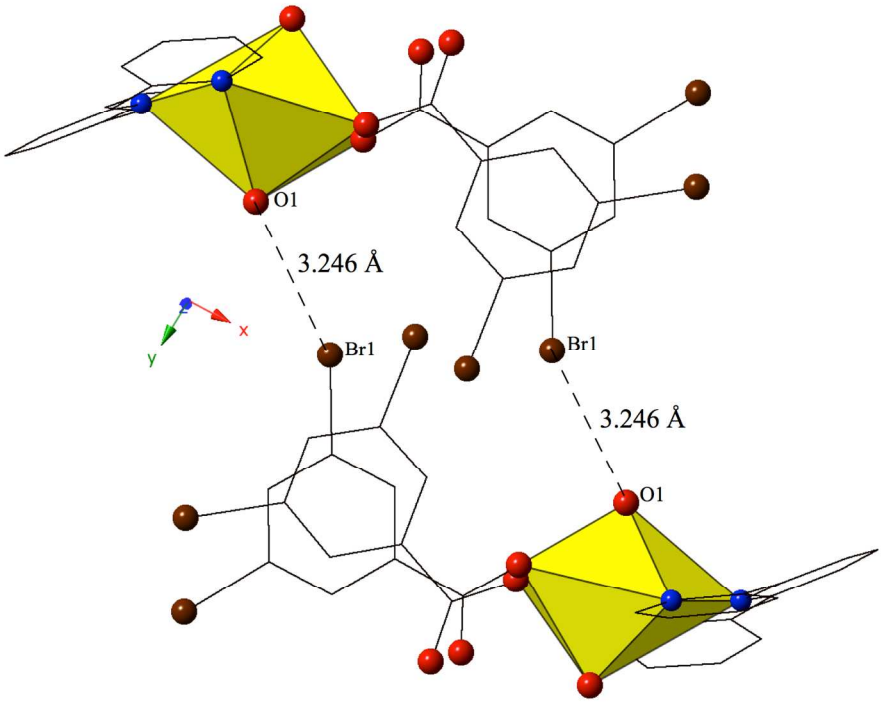

Figure 7 Complex **7** viewed down approximately the [010] direction showing the Br-O halogen bonding interactions that stitch together neighboring uranyl monomers.

Complex **8**, $[(UO_2)_2(OH)(C_{15}H_{11}N_3)(C_7H_4BrO_2)_3]$, forms at adjusted pH values (5-6) and crystallizes in the space group $P2_1/n$. Although the *p*-bromobenzoic acid is used in the synthesis of **8**, the local coordination geometry is similar to **5** and will not be described in detail. The structure of **8** contains uranyl dimers that are linked via localized

Br-π interactions, stemming from the bromine of a *p*-bromobenzoic acid ligand on one unit (Br1) and the periphery of a benzoic acid ring on the neighboring uranyl unit (C31) (Figure 8). The chains formed from these Br-π interactions propagate in approximately the [101] direction with Br1-C31 interaction distances of 3.315(12) Å. Additionally, a lattice water molecule is absent in **8**, which represents a slight variation from the asymmetric unit of **5**.

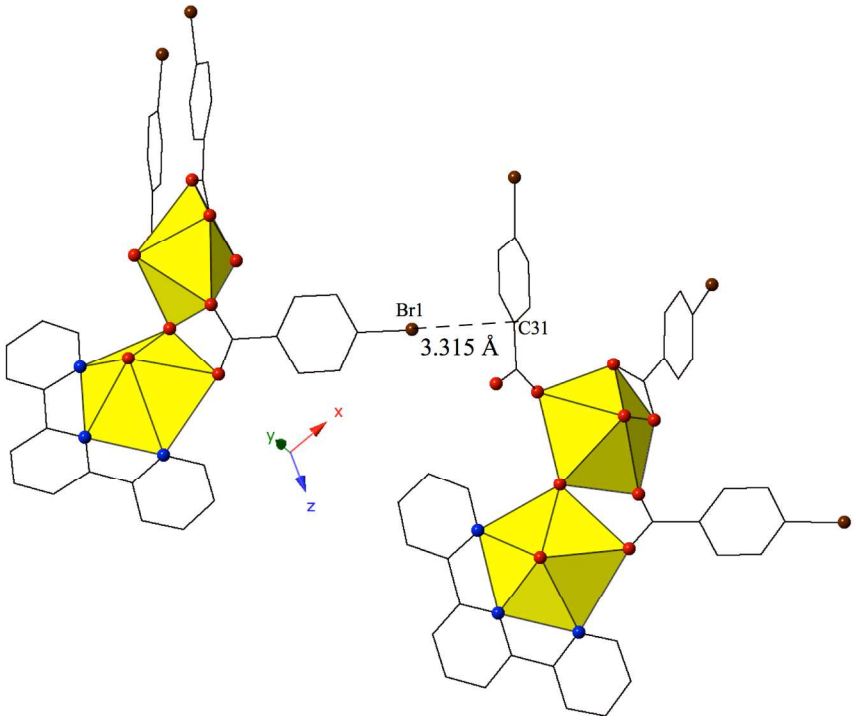

Figure 8 Complex **8** viewed down approximately the [101] direction highlighting the localized Br-π interaction that ties together neighboring uranyl dimers.

Complex **9**, $[(UO_2)_2(OH)(C_{15}H_{10}ClN_3)(C_7H_4BrO_2)_3]$, crystallizes in the space group $P2_1/n$. Beyond the introduction of Cl-terpy as a capping ligand, **9** features a nearly identical local coordination geometry to **5** so it will not be described in detail. The only changes from **5** to **9** are the absence of a crystallized lattice water molecule and the addition of a chlorine atom at the 4'-position of the terpy molecule in **9**. Whereas these

changes may seem insignificant, the resulting supramolecular interactions in **9** have changed dramatically. A bifurcated halogen-halogen interaction (Br3-Cl1 and Br3-Br1) where the bromine atom of one *m*-bromobenzoic acid ligand (Br3) acts as a halogen bond donor links together the uranyl dimers of **9** into a 1D chain that propagates in the [100] direction (Figure 9). The bifurcated interaction is made up of a type II[83] interaction between the halogen bond donor Br3 and a chlorine (Cl1) at the 4'-position of the terpyridine moiety on an adjacent uranyl unit. The Br3-Cl1 distance is 3.550(2) Å, which is 98.6% of the sum of the van der Waals radii, and the θ_1 and θ_2 angles are very near type II geometry (θ_1=180º, θ_2=90º) at 174.5(2)º and 83.4(2)º respectively. Completing the bifurcated halogen-halogen interaction is a quasi-type I interaction[83] between the halogen bond donor Br3 and a bromine (Br1) from an *m*-bromobenzoic acid ligand on a different neighboring unit. The Br1-Br3 distance is 3.4661(14) Å (93.7% of the sum of the vdW radii) and the θ_1 (C19-Br1-Br3) and θ_2 (C33-Br3-Br1) values are 163.6(3)º and 148.2(2)º, respectively.

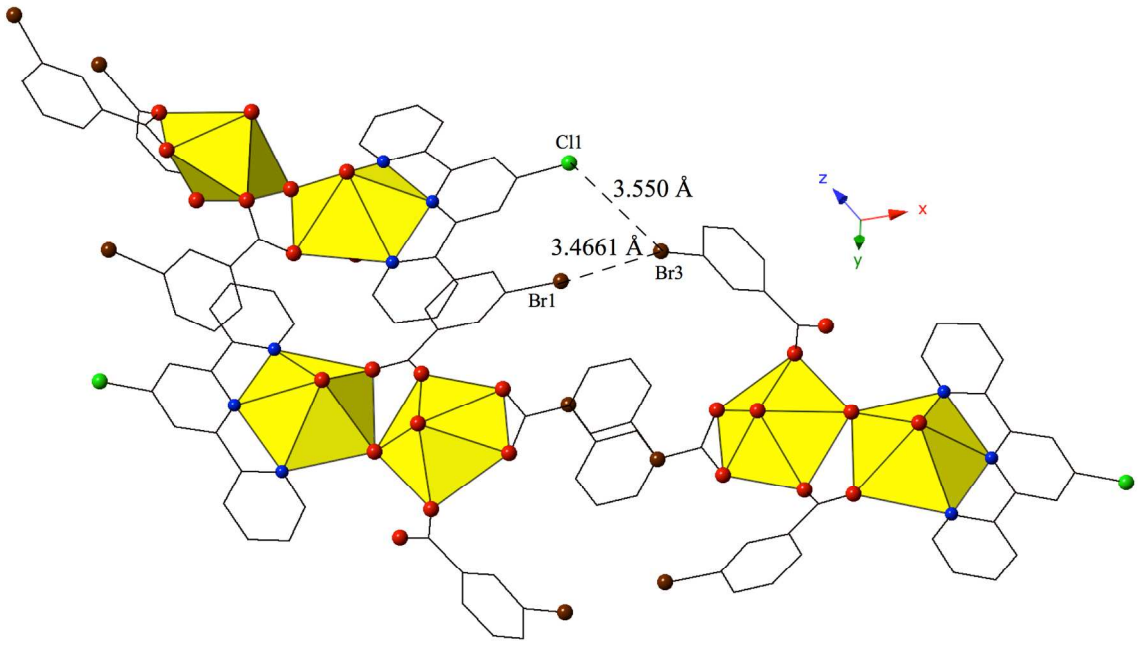

Figure 9 Polyhedral representation of complex **9** viewed down the [100] direction. Green spheres represent chlorine. The bifurcated halogen bonding interaction that connects three neighboring uranyl dimers is highlighted.

Complex **10**, $[UO_2(C_{15}H_{10}ClN_3)(C_7H_4BrO_2)_2]$, crystallizes in the space group P-1 and features nearly identical local coordination geometry to **6** so it will not be described here in detail. The only change from **6** to **10** is the addition of a chlorine atom at the 4' position of the terpy molecule in **10**, which once again results in significant changes in the modes of supramolecular assembly. The uranyl monomers of **10** are assembled into an infinite 1D chain extending approximately along the [011] direction via cooperative Br-O halogen bonding and Br-Cl halogen-halogen interactions (Figure 10, Figure S3, Supporting Information). Halogen bonding interactions between the axial uranyl oxygen of one uranyl monomer (O1) and the bromine of a *p*-bromobenzoic acid ligand (Br2) on the neighboring unit are similar to those observed in **6** with corresponding interaction distances and angles of 3.319(3) Å and 148.9(2)°, respectively (Figure 10). In addition, **10** features a type I halogen-halogen interaction[83] between the bromine of the *p*-bromobenzoic acid ligand (Br1) of the uranyl monomer and the chlorine at the 4'-position of the terpy on an adjacent unit. The Br1-Cl1 interaction distance is 3.588(2) Å (99.6% vdW) with a θ_1 value of 120.7(2)° and a θ_2 value of 118.4(2). (Figure S3, Supporting Information)

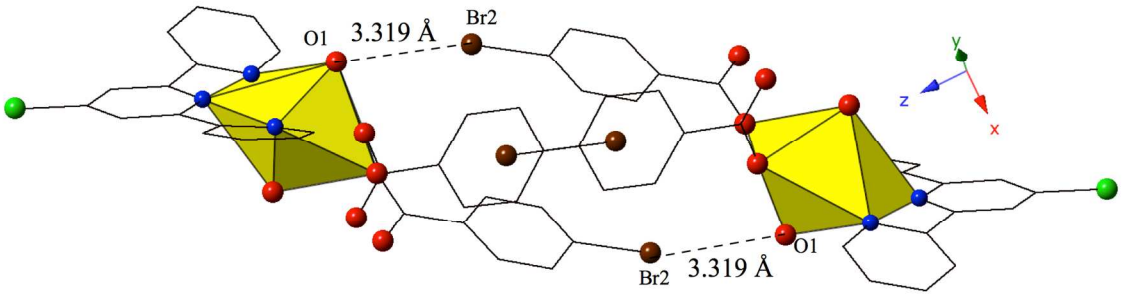

Figure 10 Complex **10** viewed down approximately the [001] direction showing the Br-O halogen bonding interactions that in concert with Br-Cl interactions link neighboring uranyl monomers.

Complex **11**, $[(UO_2)_2(OH)(C_{15}H_{10}ClN_3)(C_7H_3Br_2O_2)_3]$, crystallizes in the space group $P2_1/c$ and has nearly identical local coordination geometry to **5,** so it will not be described here in detail. Similar to **9**, **11** lacks a lattice water molecule and features the addition of a chlorine atom at the 4'-position of the terpy molecule as well as the use of 3,5-dibromobenzoic acid ligand in place of the *m*-bromobenzoic acid ligand used in **5**. These changes in ligand geometry yield a global structure that is unlike those observed for complexes **1**-**10.** The major mode of supramolecular assembly is a trifurcated halogen-halogen interaction originating from the chlorine atom at the 4'-position of the TPY molecule, which is acting as both a halogen bond acceptor and donor in **11** (Figure 11). Generally it is the heavier, more polarizable halogens that behave as halogen bond donors (i.e iodine)[86] but here we observe both a bromine (Br5) and a chlorine (Cl1) atom adopting the role. All three halogen-halogen interactions involving Cl1 (Cl1-Br4, Cl1-Br5 and Cl1-Br6) meet the criteria for type II halogen-halogen interactions ($|\theta_1-\theta_2| > 30^o$) described by Desiraju *et. al.*[83] and feature interaction distances of 3.347(2) Å (Cl1-Br4, 93.0% vdW), 3.415(2) Å (Cl1-Br5, 94.9% vdW) and 3.512(2) Å (Cl1-Br6, 97.6 % vdW), respectively. Increased connectivity in the structure of **11** is achieved via further supramolecular interactions in the form of a fourth halogen-halogen interaction and a localized Cl-π interaction between Cl1 and the periphery of a 3,5-dibromobenzoic acid ligand on a fourth neighboring unit. The additional halogen-halogen interaction (Br3-Br5) also adopts a type II orientation with an interaction distance of 3.6893(13) Å (99.7 vdW) and θ_1 and θ_2 values of 150.7(2)º and 68.03(2)º, respectively. The moderate,[84] localized Cl-π interaction (Cl1-C20) is at an interaction distance 3.423(7) Å (99.2% of

the sum of the vdW radii of chlorine and carbon) and is suggestive of some vdW overlap between the chlorine atom and the benzoic acid ring of the 3,5-dibromobenzoic acid ligand.

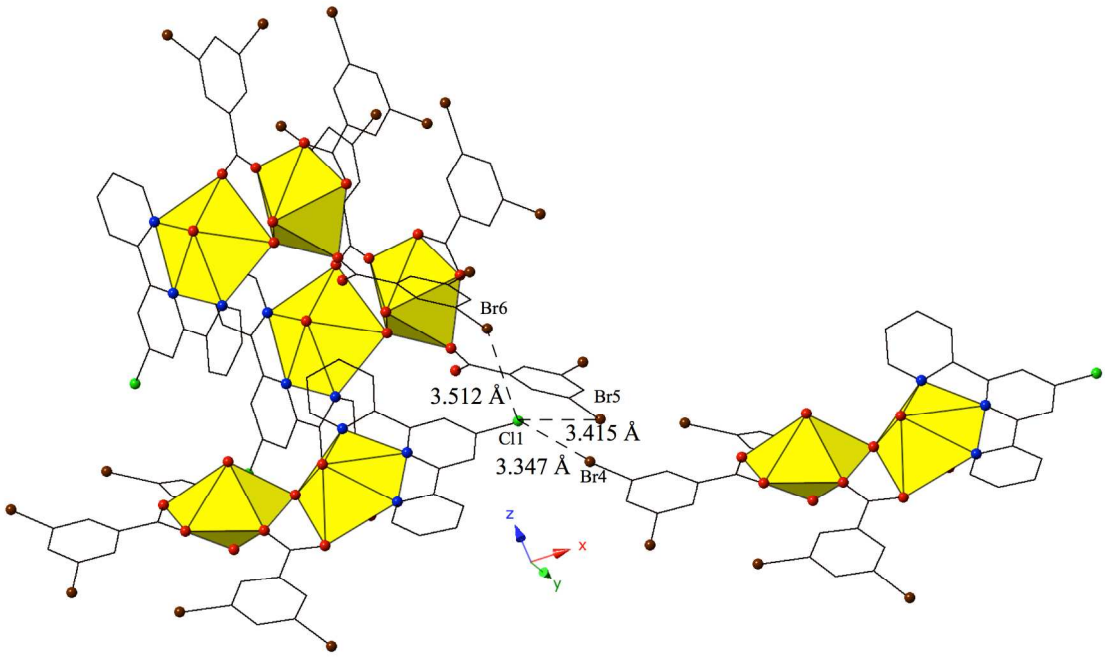

Figure 11 Complex **11** viewed in the (110) plane illustrating the trifurcated halogen-halogen interaction that links together four neighboring uranyl dimers.

Complex **12**, $[(UO_2)_2(OH)(C_{15}H_{10}ClN_3)(C_7H_4BrO_2)_3]$, is the third phase (along with **4** and **8**) that forms only at adjusted pH values (5-6) and crystallizes in the space group $P2_1/n$. **12** features nearly identical local coordination geometry to **5** and is isostructural with complex **9**, and thus will not be described in detail. Whereas at unadjusted pH with the *p*-bromobenzoic acid and Cl-TPY ligands we observed a uranyl monomer (**10**), **12** is a uranyl dimer where the two unique $[UO_2]^{2+}$ cations are bridged by a *p*-bromobenzoic acid ligand and a point sharing hydroxyl group that is a result of olation.

Similar to **9, 12** features halogen-halogen interactions that assemble the uranyl dimers in approximately the [101] direction (Figure 12). The interactions between the chlorine at the 4'-position of the TPY molecule (Cl1) and the bromine from the monodentate *p*-bromobenzoic acid ligand on the neighboring dimer (Br3) can be classified as a type II interaction[83] and feature a Cl1-Br3 interaction distance of 3.485(3) Å (96.8% of the sum of the vdW radii) and θ_1 and θ_2 values of 155.4(5)º and 108.6(3)º, respectively. Further assembly is the result of localized Cl-π interactions between the chlorine at the 4'-position of the TPY molecule and the periphery of an adjacent *p*-bromobenzoic ligand (C32) (Figure S4, Supporting Information). These strong[84] Cl-π interactions are at distance of 3.296(9) Å (95.5% vdW) and originate from the same chlorine atoms that are also participating in halogen-halogen interactions described above.

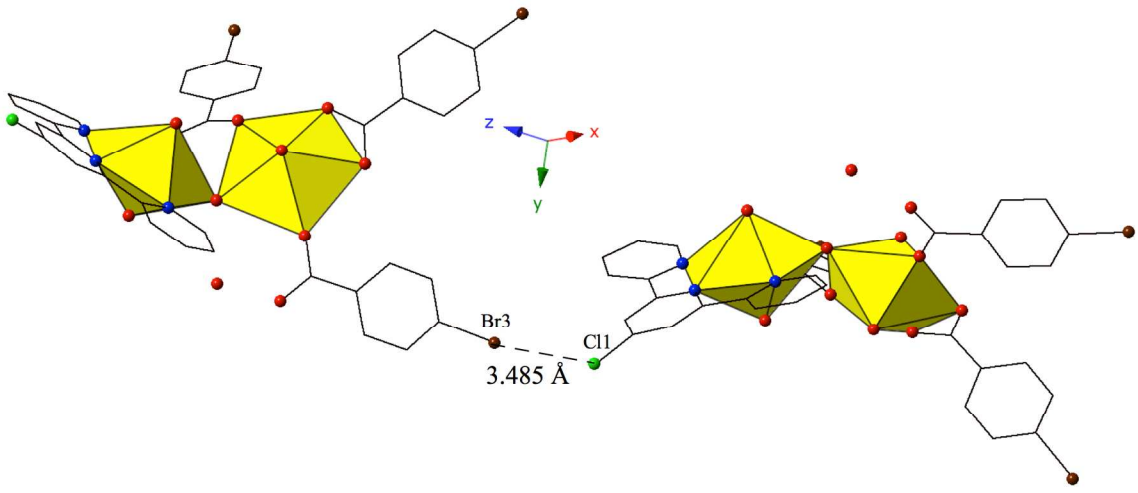

Figure 12 Complex **12** shown in approximately the [101] direction highlighting the Type II Br-Cl interaction that assembles neighboring uranyl dimers.

Structural Discussion

As structures **1**-**12** were synthesized from similar reaction conditions, the resulting structure types and supramolecular synthons provide an opportunity to assess

the influence of ligand sterics, the selected chelating N-donor and to a lesser extent hydrolysis on supramolecular assembly. (Table 3)

Table 3: A Summary of the Observed Supramolecular Synthons in Complex **1**-**12**

Complex	Observed Synthons	Benzoic Acid Ligand	Chelating Ligand
1	Br-O	*m*-BrBA	Phen
2	N/A	*p*-BrBA	Phen
3	H-Bonding, π-π	3,5-diBrBA	Phen
4	H-Bonding, π-π	*p*-BrBA* (did not incorporate into final structure)	Phen
5	Br-Br	*m*-BrBA	Terpy
6	Br-O	*p*-BrBA	Terpy
7	Br-O, Br-π	3,5-diBrBA	Terpy
8	Br-π	*p*-BrBA	Terpy
9	Br-Br, Br-Cl	*m*-BrBA	Cl-terpy
10	Br-Cl, Br-O	*p*-BrBA	Cl-terpy
11	Br-Cl (x3), Br-Br, Cl-π	3,5-diBrBA	Cl-terpy
12	Br-Cl, Cl-π	*p*-BrBA	Cl-terpy

m-BrBA=*m*-bromobenzoic acid, *p*-BrBA=*p*-bromobenzoic acid, 3,5-diBrBA=3,5-dibromobenzoic acid

Family 1: Complexes with Phen (1-4)

Compounds **1**-**4** feature a uranyl cation capped by the chelating N-donor phen and further coordinated by bromo-fuctionalized benzoic acid ligands, except in the case of **4** where the *p*-bromobenzoic acid ligand did not incorporate into the final structure. In **1** and **3** we observe uranyl monomers that adopt pentagonal bipyramidal coordination

geometry whereas in the case of **2,** we have our only example of a hexagonal bipyramidal coordination geometry**.** The two unique uranyl cations in the tetramer of **4** also adopt the pentagonal bipyramidal geometries seen in **1** and **3.** In this family of phen complexes, supramolecular interactions are observed for complexes **1**, **3** and **4**, but not complex **2** as hexagonal bipyramidal uranyl geometry does not facilitate additional assembly. These results suggest that uranyl coordination geometry may play some role in supramolecular assembly, yet this was not explored systematically. Complex **1** features uranyl monomers assembled into molecular dimers via halogen bonding interactions between *m*-bromobenzoic acid ligands and uranyl axial oxygen atoms. In complex **3**, where the larger 3,5-dibromobenzoic acid ligand is incorporated, halogens are not involved in supramolecular assembly and the monomers are assembled into 1D chains via bifurcated hydrogen bonding interactions. Finally, in complex **4** where the *p*-bromobenzoic acid ligand did not incorporate we observe assembly of the uranyl tetramers into a 2D sheet via a combination of π-π stacking interactions between phen ligands and bifurcated hydrogen bonding interactions similar to those observed in complex **7.**

Family 2: Complexes with TPY (5-8)

In compounds **5**-**8**, the unique uranyl cations are chelated by the tridentate N-donor terpy and then feature additional coordination to bromo-fuctionalized benzoic acid ligands. Complex **5** is a uranyl dimer that features the *m*-bromobenzoic acid ligand and is made at both unadjusted (2.5-3) and adjusted pH (5-6). Complexes **6** and **7** both contain uranyl monomers that incorporate the *p*-bromobenzoic acid and 3,5-dibromobenzoic acid ligands respectively. The former species forms only at unadjusted pH whereas the latter can be made under a range of synthetic conditions. When the pH of the synthesis of **6** is

raised to approximately neutral (pH 5-6) the result is complex **8**, which is a uranyl dimer that also features the *p*-bromobenzoic acid ligand. Looking at the modes of assembly of the molecular species in family 2, we see that the dimers of complex **5** are tethered via symmetrical Type I halogen-halogen interactions, the monomers of complexes **6** and **7** utilize halogen bonding interactions to assemble into dimers and 1D chains respectively and the dimers of complex **8** are also stitched into 1D chains via localized Br-π interactions. Br-π interactions, made possible by the additional bromine atoms on the 3,5-dibromobenzoic acid ligands, are also observed in complex **7** and are utilized to achieve additional supramolecular dimensionality.

Family 3: Complexes with Cl-TPY (9-12)

Compounds **9**-**12** all feature the chelating Cl-terpy ligand and a bromo-fuctionalized benzoic acid ligand. Complex **10**, with the *p*-bromobenzoic acid ligand, is a monomer made at low (~3) pH while all other members of this family are uranyl dimers. **9** and **11** are produced at both unadjusted (2.5-3) and adjusted (5-6) pH while **12** is only produced when utilizing the latter conditions. Whereas in families 1 and 2 we observed some variation in the modes of supramolecular assembly, the addition of the chlorine atom at the 4'-position of the terpy molecule in the complexes of family 3 provided the necessary conditions for halogen-halogen interactions to be the dominant mode of assembly. In all four complexes (**9-12**) we observe at least one unsymmetrical[87] ($X_1 \neq X_2$) Cl-Br interaction between molecular units and in complexes **9** and **11** we observe two and three respectively. These interactions, except in complex **10**, all adopt type II halogen-halogen geometries,[83] which arise from electrophile-nucleophile pairings, and the electrostatic nature of these interactions allows them to be viable at interaction distances

near the sum of the vdW radii. In complex **10**, the Br-Cl interactions adopt the quasi-type I orientation,[83] which is most commonly observed for Cl-Cl contacts,[87] yet is not unknown for unsymmetrical Br-Cl interactions.

From the results in structural families 1-3 we have noted that the use of the *m*-bromobenzoic ligand yields assembly via halogen bonding interactions, either halogen-halogen or halogen-heteroatom, independent of the N-donor. Despite its similarities, the *p*-bromobenzoic acid ligand yields very different results with modes of assembly varying with both the accompanying N-donor and the reaction pH. The sterically larger 3,5-dibromobenzoic acid ligand uses halogen bonding as means of assembly when the N-donor is also of sufficient size (terpy or Cl-terpy). With regards to the chelating N-donors used herein, the bidentate phen was not very useful as crystal engineering tool as it yielded a variety of local coordination modes, yet did not offer much control over the modes of supramolecular assembly. The terpy molecule, however, was able to selectively utilize halogen bonding as means of assembly in all members of family 2, yet there was still some variance in these interactions, whether they were between two halogens, a halogen and a heteroatom or a halogen and a π-system. The Cl-terpy was found to be best tool for crystal engineering the uranyl molecular complexes described herein as all that incorporated the Cl-terpy as a capping ligand were then assembled via unsymmetrical halogen-halogen interactions into extended solid-state structures of varying dimensionalities.

Returning to the participation of the axial uranyl oxygen atoms, the non-covalent coordination observed in **1**, **6**, **7** and **10** are likely not a consequence not be a function of "activation" that has been described previously where careful choice of equatorial ligands

affect Lewis basicity.[64-67] Instead our results suggest that the participation of the weakly Lewis basic uranyl oxo ligands in non-covalent interactions is possibly a function of having an agreeable donor with which to pair—in this case a polarizable bromine atom.

Conclusions

The synthesis and crystal structures of twelve uranyl complexes containing bromine functionalized benzoic acids, *m*-bromobenzoic acid, *p*-bromobenzoic acid and 3,5-dibromobenzoic acid, and the chelating N-donors phen, terpy and Cl-terpy obtained using hydrothermal reaction conditions have been reported, and their resulting means of supramolecular assembly have been investigated. Throughout the series of structurally diverse materials that were characterized herein, we observe that subtle changes in ligand geometry often lead to significant changes in the interactions utilized for supramolecular assembly. In the materials containing the chelating N-donor Cl-terpy, halogen-halogen interactions were always observed as the functionalization of the back-end of the terpy moiety proved to be a consistent method for the generation of halogen-halogen interactions. In four materials we observed oxo-functionalization of the uranyl via halogen bonding interactions and the 'activation' of the uranyl via non-covalent methods is a topic we are continuing to explore. A correlation between the SBU and pH was observed for the materials containing the *p*-bromobenzoic acid ligand, but not for the *m*-bromobenzoic acid or 3,5-dibromobenzoic acid ligands. The mechanism for these seemingly divergent results is under investigation. Follow up studies to investigate changing the character of halogens (more electron withdrawing or more electron donating) on the benzoic acid group can effect the resulting local structures and the corresponding modes for supramolecular assembly. Design of mixed-synthon systems

(Br and NO_2) and modeling efforts to better understand the role of partial charge in supramolecular interaction strength are also ongoing.

Supporting Information Available

X-ray crystallographic files in CIF format, ORTEP figures of all compounds, PXRD spectra of all compounds, tables of selected supramolecular interaction distances and bond lengths, additional figures for complexes **3**, **7**, **10** and **12** and bond valence calculations are all available. CIFs have also been deposited at the Cambridge Crystallographic Database Centre and may be obtained from http://www.ccdc.cam.ac.uk by citing reference numbers 1025739-1025750 for compounds **1**-**12**, respectively.

Author Information

Corresponding Author

*E-mail: cahill@gwu.edu Phone: (202) 994-6959

Notes

The authors declare no competing financial interest.

Acknowledgement

This material was supported by the U. S. Department of Energy—Chemical Sciences, Geosciences and Biosciences Division, Office of Basic Sciences, Office of Science, Heavy Elements Program, under grant number DE-FG02-05ER15736.

References

1. M. Ephritikhine, *Dalton Transactions*, 2006, 2501-2516.
2. C. L. Cahill and L. A. Borkowski, in *Structural Chemistry of Inorganic Actinide Compounds*, eds. S. V. Krivovichev, P. C. Burns and I. G. Tananaev, Elsevier, Amsterdam, 2007.
3. C. L. Cahill, D. T. de Lill and M. Frisch, *CrystEngComm*, 2007, 9, 15-26.
4. K.-X. Wang and J.-S. Chen, *Accounts of Chemical Research*, 2011, 44, 531-540.
5. K. E. Knope and C. L. Cahill, in *Metal Phosphonate Chemistry: From Synthesis to Applications*, eds. A. Clearfield and K. Demadis, Royal Society of Chemistry, London, UK, 2012.
6. L. S. Natrajan, *Coordination Chemistry Reviews*, 2012, 256, 1583-1603.
7. M. B. Andrews and C. L. Cahill, *Chemical Reviews*, 2013, 113, 1121-1136.
8. T. Loiseau, I. Mihalcea, N. Henry and C. Volkringer, *Coordination Chemistry Reviews*, 2014, 266–267, 69-109.
9. P. Thuéry and J. Harrowfield, *Crystal Growth & Design*, 2014, 14, 1314-1323.
10. C. Janiak, *Dalton Transactions*, 2003, 2781-2804.
11. C. E. Rowland and C. L. Cahill, *Inorganic Chemistry*, 2010, 49, 6716-6724.
12. M. B. Andrews and C. L. Cahill, *Angewandte Chemie International Edition*, 2012, 51, 6631-6634.
13. C. F. Baes and R. E. Mesmer, *The Hydrolysis of Cations*, John Wiley and Sons, New York, NY, 1976.
14. K. E. Knope and L. Soderholm, *Chemical Reviews*, 2013, 113, 944-994.
15. I. Grenthe, J. Fuger, R. J. M. Konings, R. J. Lemire, C. Nguyen-Trun and H. Wanner, *Chemical Thermodynamics of Uranium*, Organization for Econmoic Cooperation and Development, Issy-les-Moulineaux, France, 2004.
16. J. Leciejewicz, N. Alcock and T. Kemp, in *Coordination Chemistry*, Springer Berlin Heidelberg, 1995, vol. 82, ch. 2, pp. 43-84.
17. K. E. Knope and C. L. Cahill, *European Journal of Inorganic Chemistry*, 2010, 2010, 1177-1185.
18. W. Yang, T. Tian, H.-Y. Wu, Q.-J. Pan, S. Dang and Z.-M. Sun, *Inorganic Chemistry*, 2013, 52, 2736-2743.
19. B. Monteiro, J. A. Fernandes, C. C. L. Pereira, S. M. F. Vilela, J. P. C. Tome, J. Marcalo and F. A. Almeida Paz, *Acta Crystallographica Section B*, 2014, 70, 28-36.
20. R. G. Denning, *The Journal of Physical Chemistry A*, 2007, 111, 4125-4143.
21. S. G. Thangavelu, M. B. Andrews, S. J. A. Pope and C. L. Cahill, *Inorganic Chemistry*, 2013, 52, 2060-2069.
22. G. Liu, N. P. Deifel, C. L. Cahill, V. V. Zhurov and A. A. Pinkerton, *The Journal of Physical Chemistry A*, 2012, 116, 855-864.
23. G. Liu, L. Rao and G. Tian, *Physical Chemistry Chemical Physics*, 2013, 15, 17487-17495.
24. C. B. Aakeroy, P. D. Chopade, C. Ganser and J. Desper, *Chemical Communications*, 2011, 47, 4688-4690.
25. Y. Lu, T. Shi, Y. Wang, H. Yang, X. Yan, X. Luo, H. Jiang and W. Zhu, *Journal of Medicinal Chemistry*, 2009, 52, 2854-2862.

26. R. Wilcken, M. O. Zimmermann, A. Lange, A. C. Joerger and F. M. Boeckler, *Journal of Medicinal Chemistry*, 2012, 56, 1363-1388.
27. R. R. Knowles and E. N. Jacobsen, *Proceedings of the National Academy of Sciences*, 2010, 107, 20678-20685.
28. W. Tang, S. Johnston, J. A. Iggo, N. G. Berry, M. Phelan, L. Lian, J. Bacsa and J. Xiao, *Angewandte Chemie International Edition*, 2013, 52, 1668-1672.
29. P. H. Dinolfo and J. T. Hupp, *Chemistry of Materials*, 2001, 13, 3113-3125.
30. T. Kudernac, S. Lei, J. A. A. W. Elemans and S. De Feyter, *Chemical Society Reviews*, 2009, 38, 402-421.
31. S. I. Stupp and L. C. Palmer, *Chemistry of Materials*, 2014, 26, 507-518.
32. D. Wang, G. Tong, R. Dong, Y. Zhou, J. Shen and X. Zhu, *Chemical Communications*, 2014, 50, 11994-12017.
33. D. Braga, *Chemical Communications*, 2003, 2751-2754.
34. Y. E. Alexeev, B. I. Kharisov, T. C. H. García and A. D. Garnovskii, *Coordination Chemistry Reviews*, 2010, 254, 794-831.
35. R. J. Baker, *Chemistry – A European Journal*, 2012, 18, 16258-16271.
36. N. P. Deifel and C. L. Cahill, *CrystEngComm*, 2009, 11, 2739-2744.
37. N. P. Deifel and C. L. Cahill, *Comptes Rendus Chimie*, 2010, 13, 747-754.
38. M. B. Andrews and C. L. Cahill, *Dalton Transactions*, 2012, 41, 3911-3914.
39. M. B. Andrews and C. L. Cahill, *CrystEngComm*, 2013, 15, 3082-3086.
40. C. E. Rowland, M. G. Kanatzidis and L. Soderholm, *Inorganic Chemistry*, 2012, 51, 11798-11804.
41. R. G. Surbella III and C. L. Cahill, *CrystEngComm*, 2014, 16, 2352-2364.
42. N. W. Alcock, D. J. Flanders and D. Brown, *Journal of the Chemical Society, Dalton Transactions*, 1985, 1001-1007.
43. J.-C. Berthet, M. Nierlich and M. Ephritikhine, *Dalton Transactions*, 2004, 2814-2821.
44. P. Thuéry, *Inorganic Chemistry*, 2012, 52, 435-447.
45. X.-S. Zhai, Y.-Q. Zheng, J.-L. Lin and W. Xu, *Inorganica Chimica Acta*, 2014, 423, Part A, 1-10.
46. D. K. Unruh, K. Gojdas, E. Flores, A. Libo and T. Z. Forbes, *Inorganic Chemistry*, 2013, 52, 10191-10198.
47. J. de Groot, K. Gojdas, D. K. Unruh and T. Z. Forbes, *Crystal Growth & Design*, 2014, 14, 1357-1365.
48. N. P. Deifel and C. L. Cahill, *Chemical Communications*, 2011, 47, 6114-6116.
49. R. D. Hancock, *Chemical Society Reviews*, 2013, 42, 1500-1524.
50. P. O. Adelani and P. C. Burns, *Inorganic Chemistry*, 2012, 51, 11177-11183.
51. P. Thuéry, *European Journal of Inorganic Chemistry*, 2013, 2013, 4563-4573.
52. K. P. Carter, S. J. A. Pope and C. L. Cahill, *CrystEngComm*, 2014, 16, 1873-1884.
53. K. P. Carter, C. H. F. Zulato and C. L. Cahill, *CrystEngComm*, 2014, 16, 10189-10202.
54. J. Lhoste, N. Henry, T. Loiseau, Y. Guyot and F. Abraham, *Polyhedron*, 2013, 50, 321-327.
55. *SAINT*, Bruker AXS Inc., Madison, Wisconsin, USA, 2007.
56. *APEX2*, Bruker AXS Inc. , Madison, Wisconsin, USA, 2008.
57. *SADABS*, Bruker AXS, Madison, Wisconsin, USA, 2008.

58. *TWINABS*, Bruker AXS, Madison, Wisconsin, USA, 2008.
59. A. Altomare, G. Cascarano, C. Giacovazzo, A. Guagliardi, M. C. Burla, G. Polidori and M. Camalli, *Journal of Applied Crystallography*, 1994, 27, 435-435.
60. G. Sheldrick, *Acta Crystallographica Section A*, 2008, 64, 112-122.
61. L. Farrugia, *Journal of Applied Crystallography*, 2012, 45, 849-854.
62. *Crystal Maker*, Crystal Maker Software Limited, Bicester, England, 2009.
63. *JADE*, Materials Data Inc., Livermore, California, USA, 2003.
64. M. J. Sarsfield and M. Helliwell, *Journal of the American Chemical Society*, 2004, 126, 1036-1037.
65. S. Fortier and T. W. Hayton, *Coordination Chemistry Reviews*, 2010, 254, 197-214.
66. P. L. Arnold, A.-F. Pécharman, E. Hollis, A. Yahia, L. Maron, S. Parsons and J. B. Love, *Nat Chem*, 2010, 2, 1056-1061.
67. A. J. Lewis, H. Yin, P. J. Carroll and E. J. Schelter, *Dalton Transactions*, 2014, 43, 10844-10851.
68. P. Thuéry, M. Nierlich, B. Souley, Z. Asfari and J. Vicens, *Journal of the Chemical Society, Dalton Transactions*, 1999, 2589-2594.
69. Y. Li, C. L. Cahill and P. C. Burns, *Chemistry of Materials*, 2001, 13, 4026-4031.
70. K.-A. Kubatko and P. C. Burns, *Inorganic Chemistry*, 2006, 45, 10277-10281.
71. J. Lhoste, N. Henry, P. Roussel, T. Loiseau and F. Abraham, *Dalton Transactions*, 2011, 40, 2422-2424.
72. R. C. Severance, M. D. Smith and H.-C. zur Loye, *Inorganic Chemistry*, 2011, 50, 7931-7933.
73. V. N. Serezhkin, G. V. Sidorenko, D. V. Pushkin and L. B. Serezhkina, *Radiochemistry*, 2014, 56, 115-133.
74. N. N. Krot and M. S. Grigoriev, *Russian Chemical Reviews*, 2004, 73, 89-100.
75. D. L. Clark, S. D. Conradson, R. J. Donohoe, D. W. Keogh, D. E. Morris, P. D. Palmer, R. D. Rogers and C. D. Tait, *Inorganic Chemistry*, 1999, 38, 1456-1466.
76. L. A. Watson and B. P. Hay, *Inorganic Chemistry*, 2011, 50, 2599-2605.
77. C. Janiak, *Journal of the Chemical Society, Dalton Transactions*, 2000, 3885-3896.
78. N. W. Alcock, D. J. Flanders, M. Pennington and D. Brown, *Acta Crystallographica Section C*, 1988, 44, 247-250.
79. J.-C. Berthet, M. Nierlich and M. Ephritikhine, *Chemical Communications*, 2003, 1660-1661.
80. F. F. Awwadi, R. D. Willett, K. A. Peterson and B. Twamley, *Chemistry – A European Journal*, 2006, 12, 8952-8960.
81. L. Brammer, G. Minguez Espallargas and S. Libri, *CrystEngComm*, 2008, 10, 1712-1727.
82. G. R. Desiraju and R. Parthasarathy, *Journal of the American Chemical Society*, 1989, 111, 8725-8726.
83. A. Mukherjee, S. Tothadi and G. R. Desiraju, *Accounts of Chemical Research*, 2014, 47, 2514-2524.
84. T. J. Mooibroek, P. Gamez and J. Reedijk, *CrystEngComm*, 2008, 10, 1501-1515.
85. D. Schollmeyer, O. V. Shishkin, T. Ruhl and M. O. Vysotsky, *CrystEngComm*, 2008, 10, 715-723.

86. P. Metrangolo, F. Meyer, T. Pilati, G. Resnati and G. Terraneo, *Chemical Communications*, 2008, 1635-1637.
87. S. Tothadi, S. Joseph and G. R. Desiraju, *Crystal Growth & Design*, 2013, 13, 3242-3254.

Combining coordination and supramolecular chemistry to explore uranyl assembly in the solid state

Korey P. Carter and Christopher L. Cahill*
Department of Chemistry, The George Washington University, 725 21st Street, NW, Washington, D.C. 20052, United States

E-mail:cahill@gwu.edu

Supporting Info Section

I. Additional Figures

II. Powder X-ray Diffraction data

III. Thermal Ellipsoid Plots

IV. Tables of Bond Distances

V. Bond Valence Summations

VI. References

I. Additional Figures

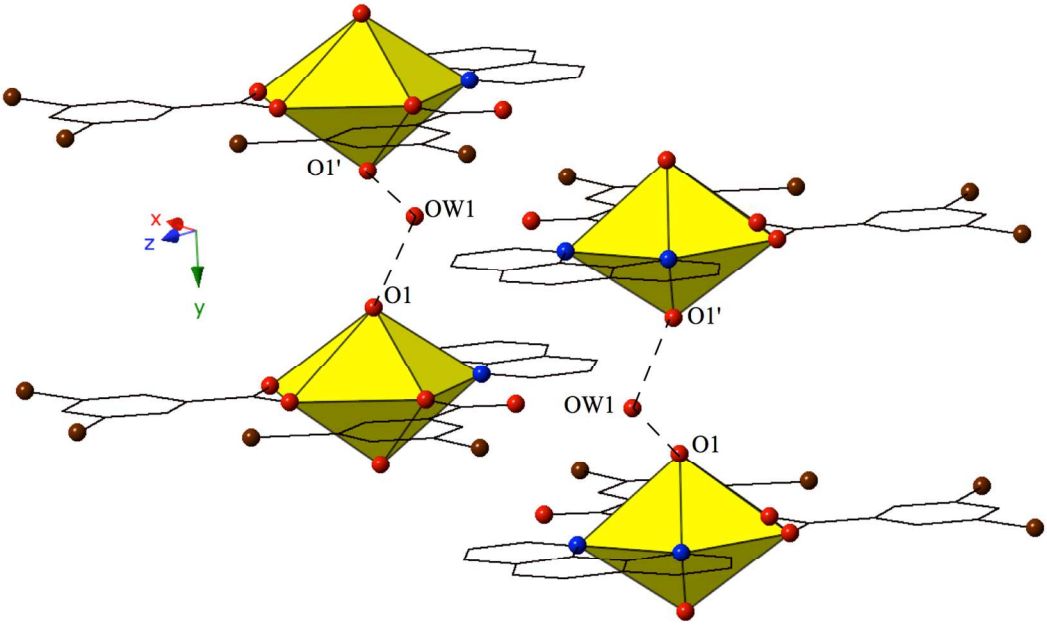

Figure S1: Complex **3** shown down the [010] direction highlighting the hydrogen bonding interactions that decorate the 1D chain of uranyl monomers.

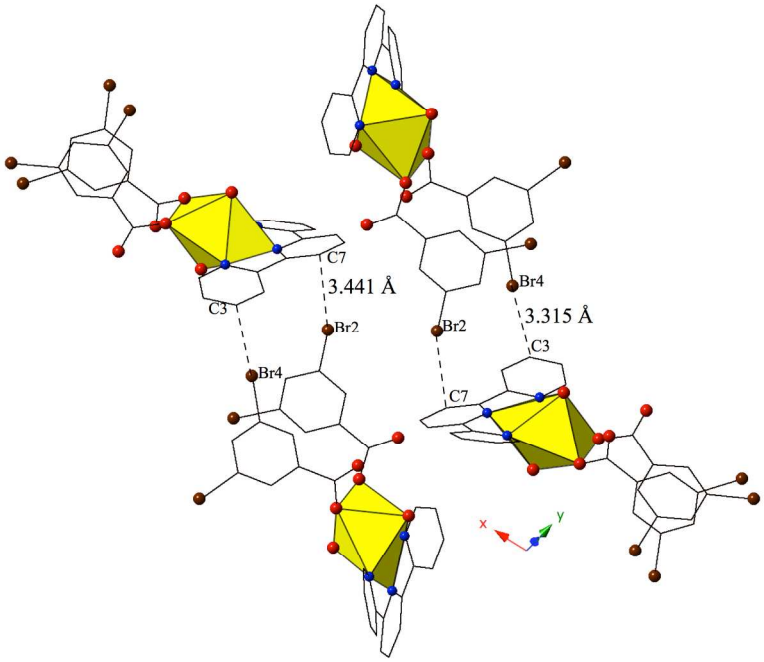

Figure S2: Complex **7** viewed down approximately the [110] direction highlighting the localized Br-π interactions that assemble neighboring uranyl monomers.

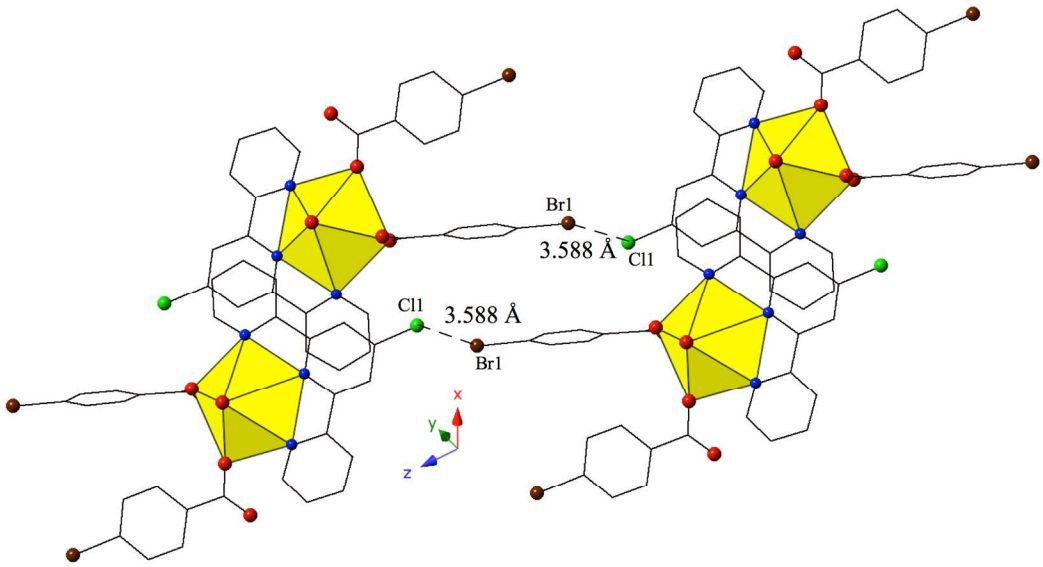

Figure S3: Complex **10** viewed down approximately the [011] direction highlighting the Type I Br-Cl interaction that links neighboring uranyl monomers.

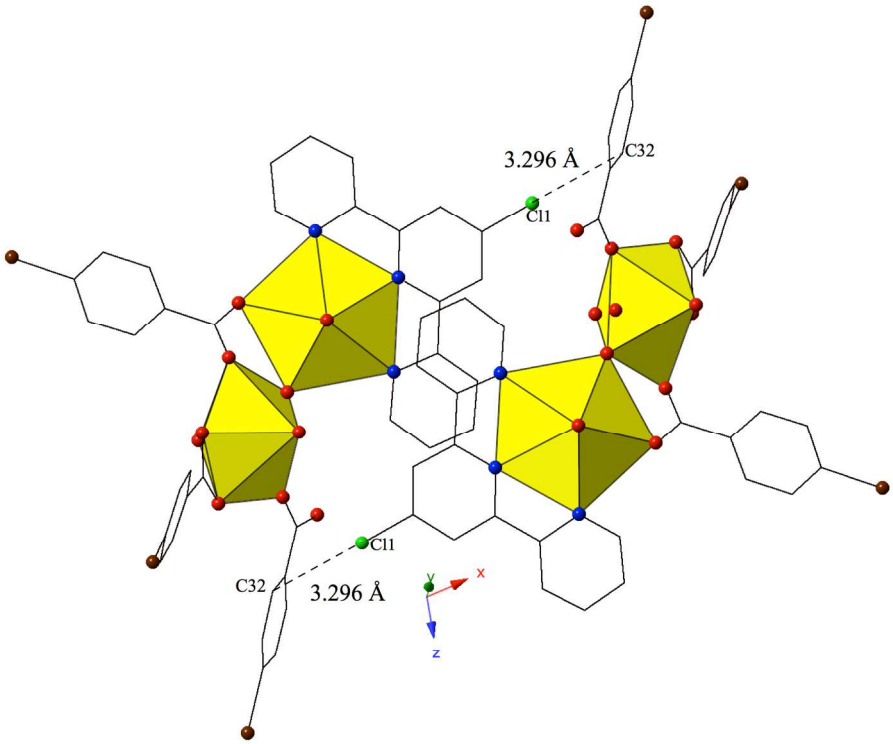

Figure S4: Complex **12** viewed along approximately the [100] direction highlighting the localized Cl-π interaction that links adjacent uranyl dimers.

II. Powder X-ray diffraction data

For the following PXRD spectra it is important to note that calculated patterns are from low temperature (100K) (complexes **1, 3, 7** and **11)** data collections while observed patterns were collected at room temperature (298 K). This difference may result in slight shifts in two-theta values. For complexes **2, 4-6, 8-10** and **12** calculated and observed patterns were both collected a room temperature (298K).

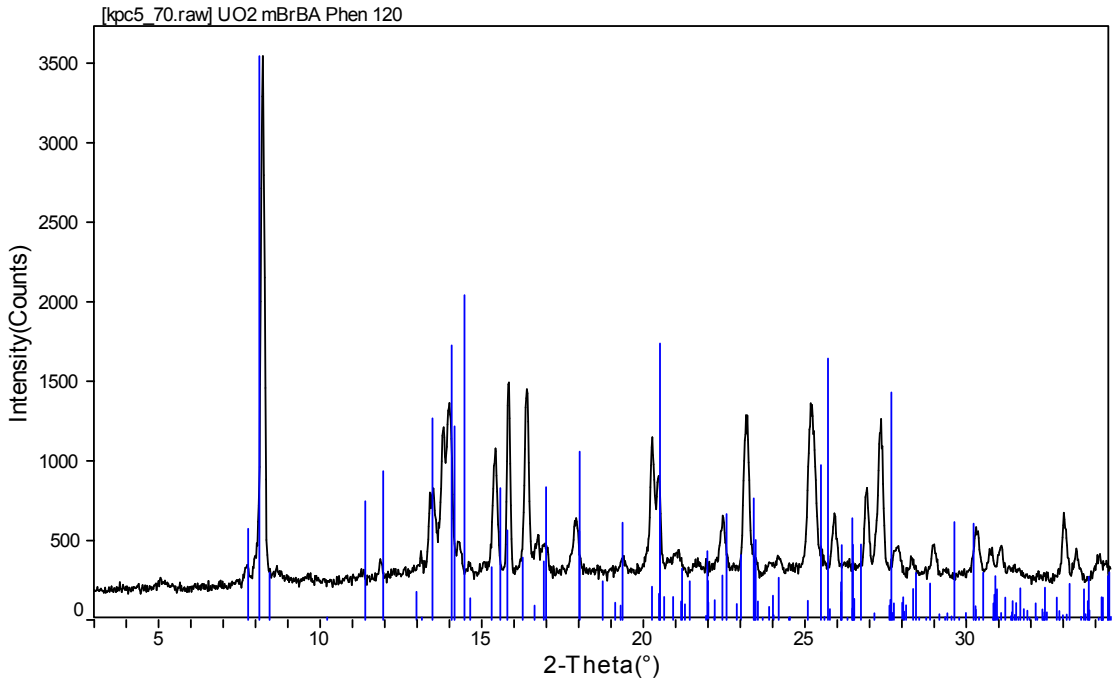

Figure S5: The observed PXRD pattern of structure **1** with calculated pattern overlaid in blue.

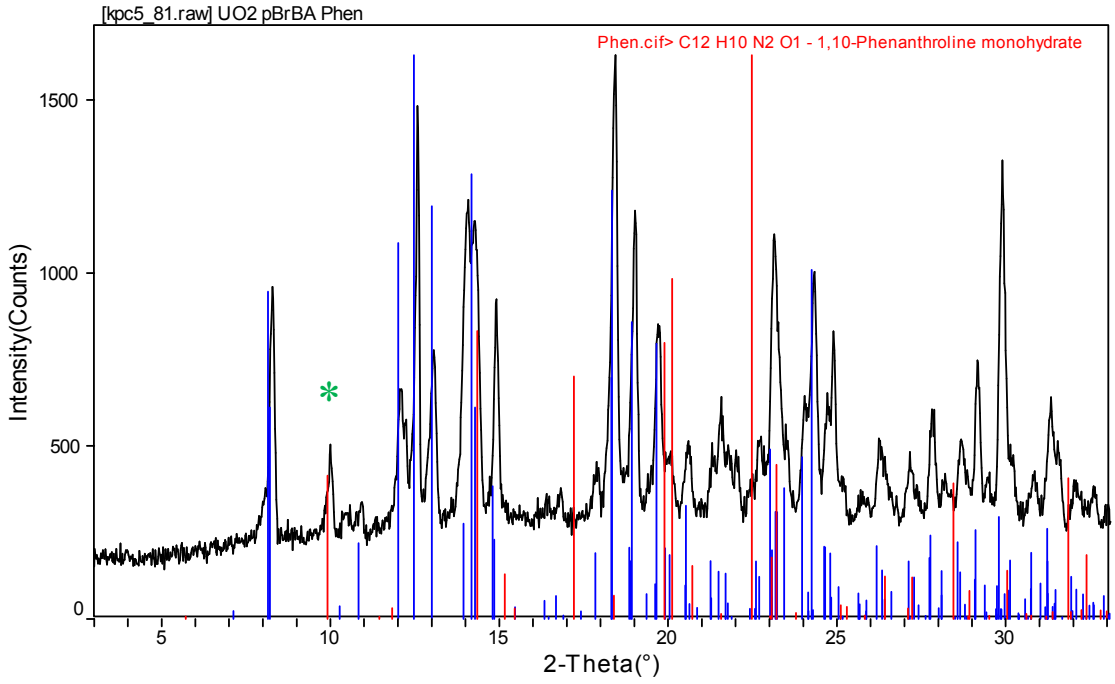

Figure S6: The observed PXRD pattern of structure **2** with calculated pattern overlaid in blue. We acknowledge a minor impurity as indicated with an asterisk and we have identified this impurity as excess 1,10-phenanthroline (calculated CIF overlaid in red).

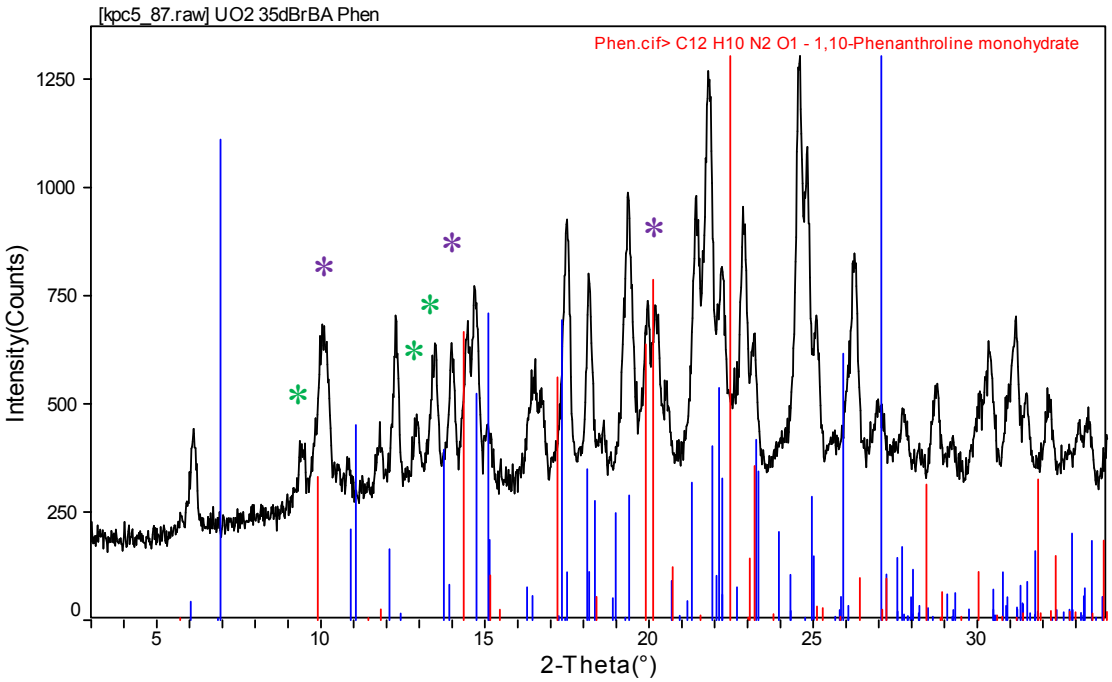

Figure S7: The observed PXRD pattern of structure **3** with calculated pattern overlaid in blue. We acknowledge several impurities in the bulk product. Some of these impurities have been identified as 1,10-phenanthroline (calculated CIF overlaid in red) and these are indicated with purple asterisks. Impurities that could not be identified are indicated with green asterisks.

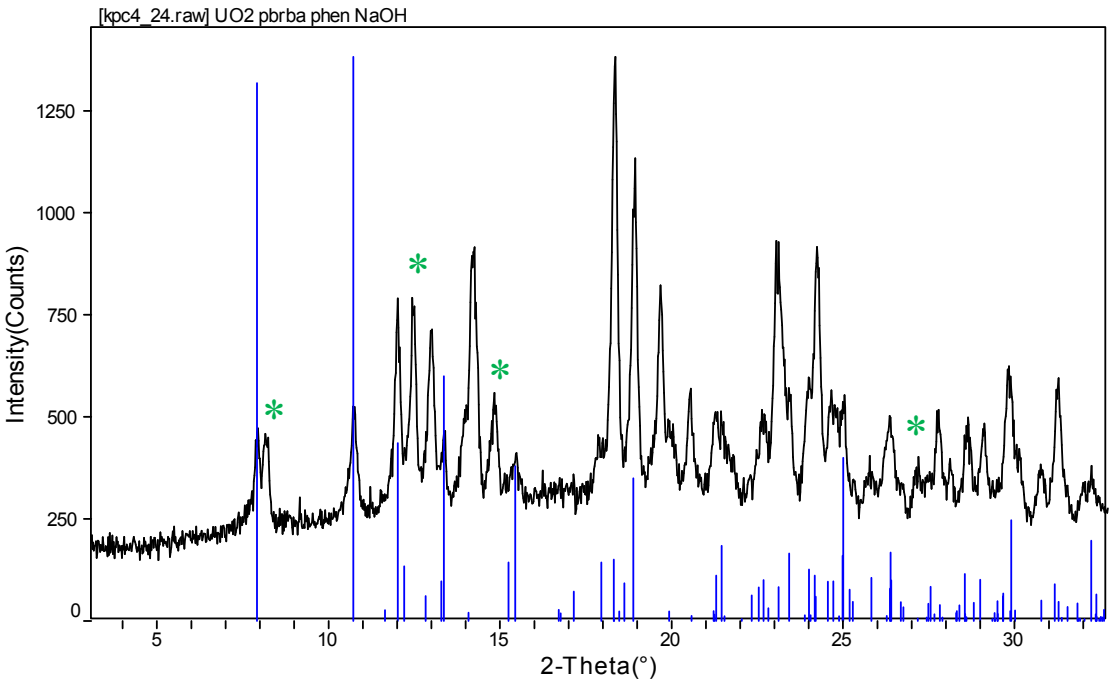

Figure S8: The observed PXRD pattern of structure **4** with calculated pattern overlaid in blue. We acknowledge several impurities as indicated with asterisks.

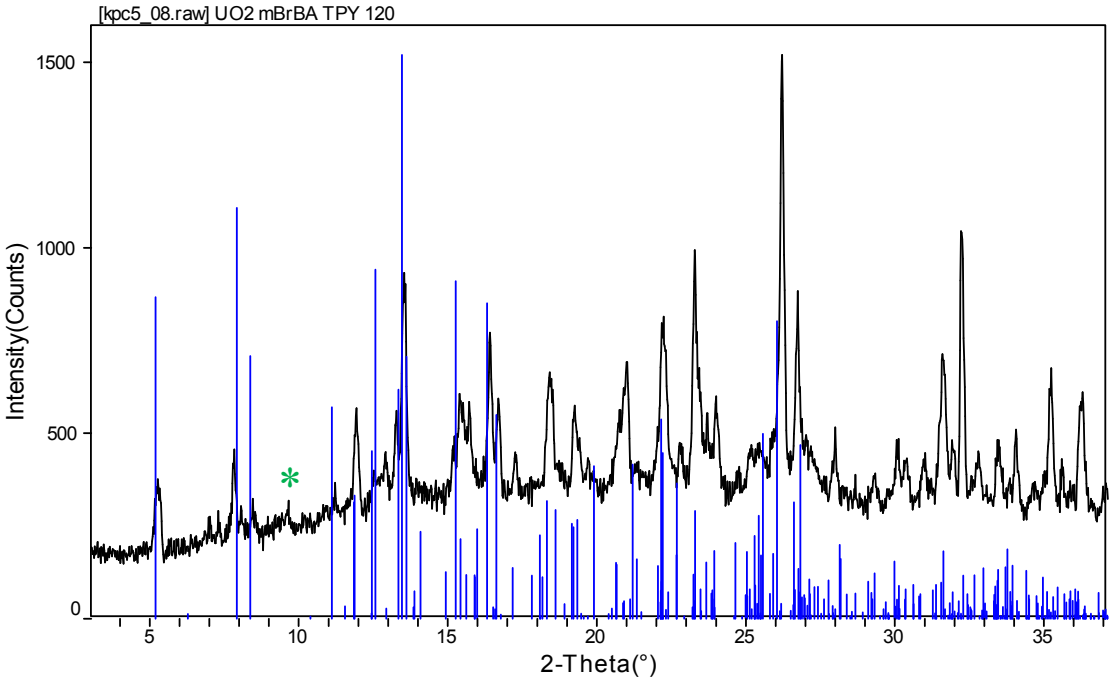

Figure S9: The observed PXRD pattern of structure **5** with calculated pattern overlaid in blue. We acknowledge a minor impurity as indicated with an asterisk.

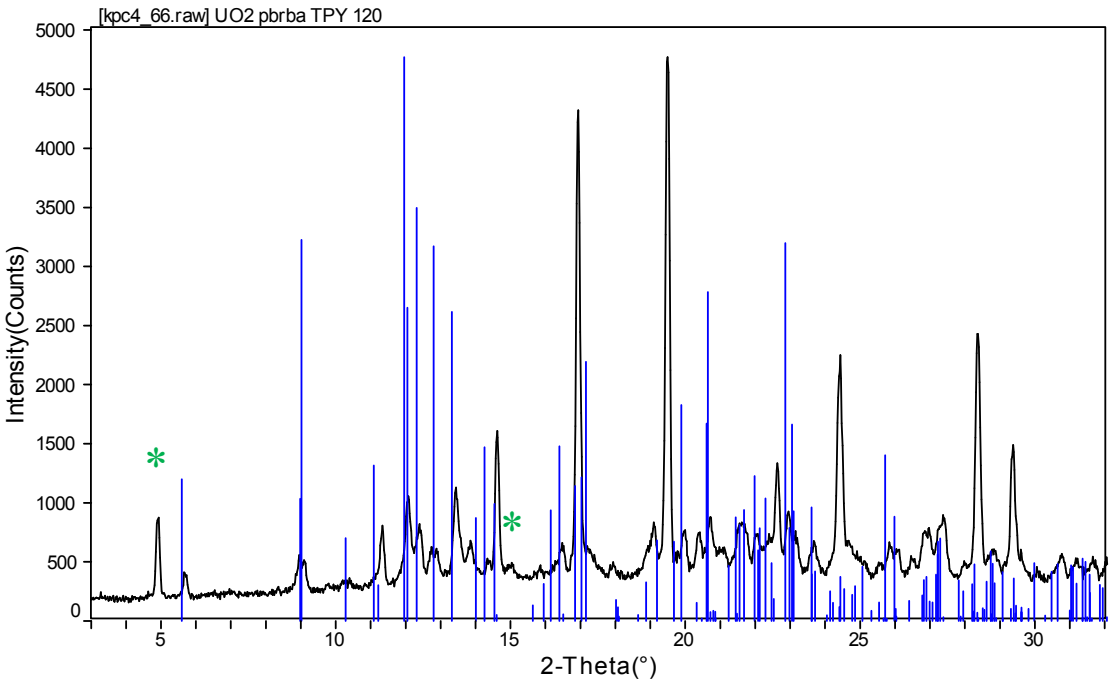

Figure S10: The observed PXRD pattern of structure **6** with calculated pattern overlaid in blue. We acknowledge two minor impurities as indicated with asterisks.

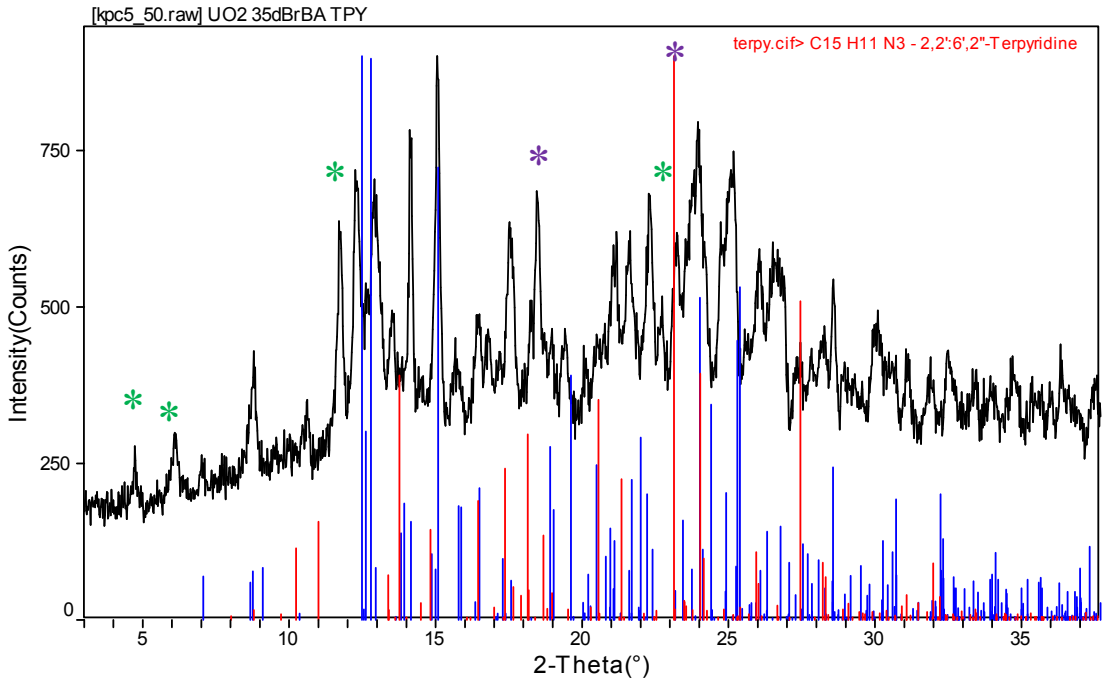

Figure S11: The observed PXRD pattern of structure **7** with calculated pattern overlaid in blue. We acknowledge several impurities in the bulk product. Some of these impurities

have been identified as 2,2':6',2"-terpyridine (calculated CIF overlaid in red) and these are indicated with purple asterisks. Impurities that could not be identified are indicated with green asterisks.

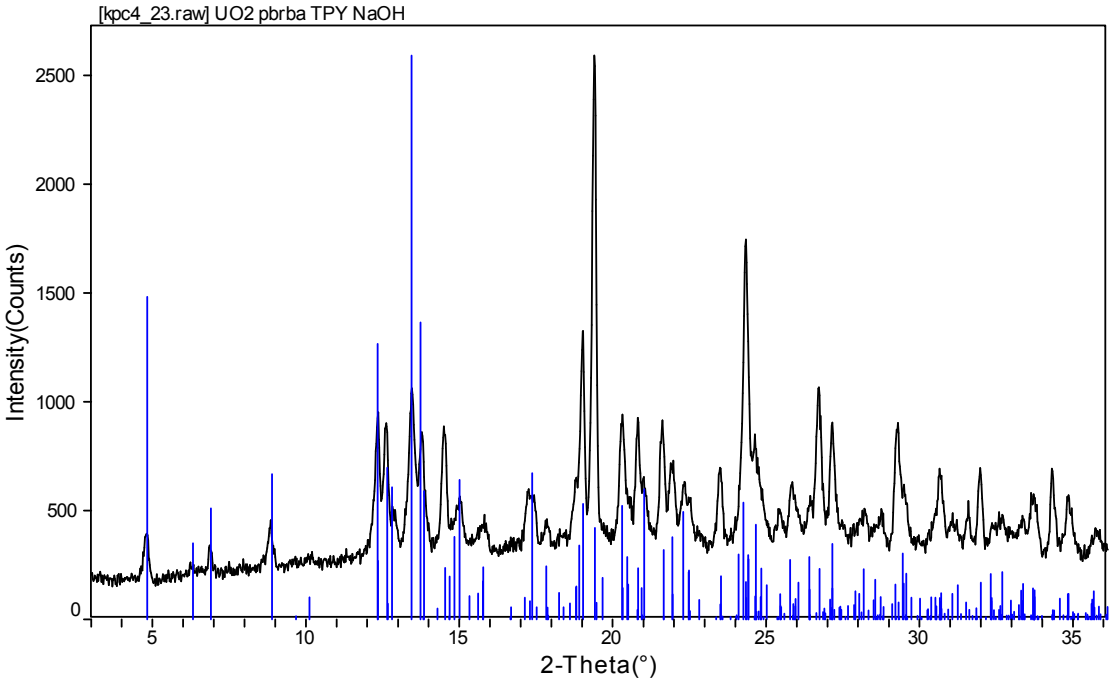

Figure S12: The observed PXRD pattern of structure **8** with calculated pattern overlaid in blue.

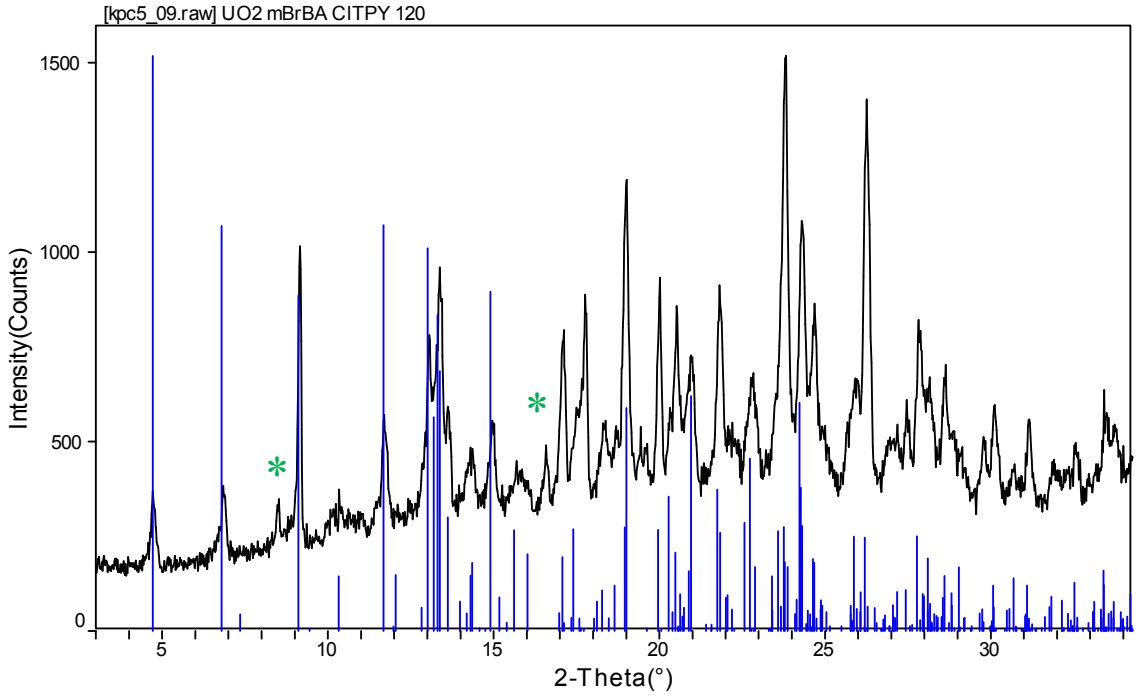

Figure S13: The observed PXRD pattern of structure **9** with calculated pattern overlaid in blue. We acknowledge two minor impurities as indicated with asterisks.

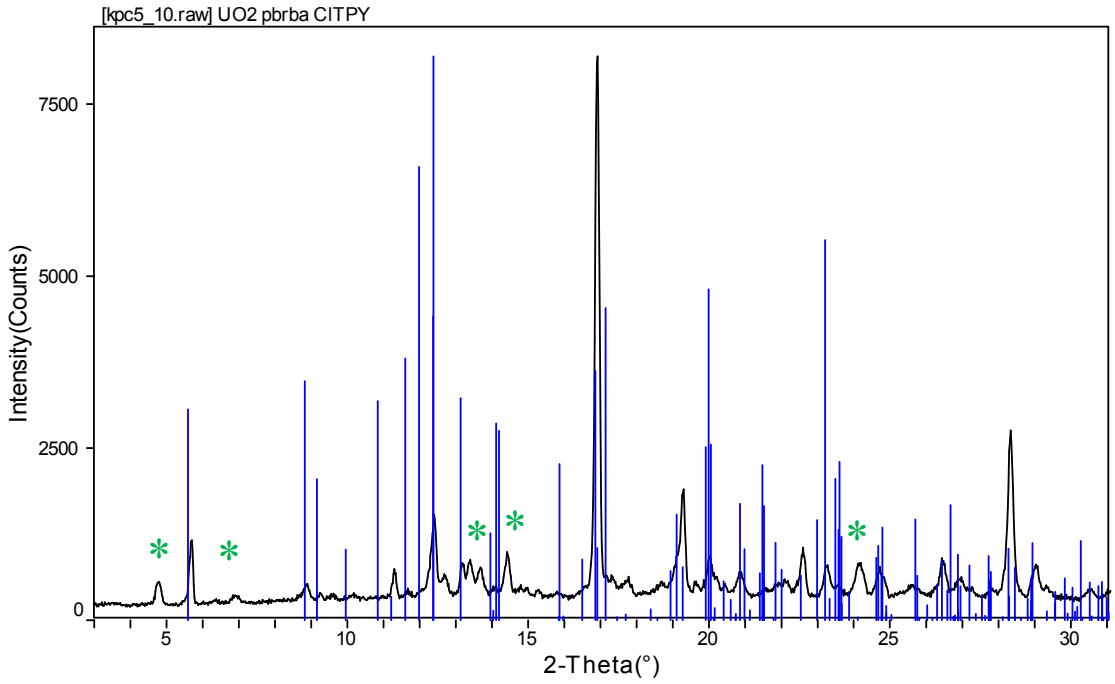

Figure S14: The observed PXRD pattern of structure **10** with calculated pattern overlaid in blue. We acknowledge a number of minor impurities as indicated with asterisks.

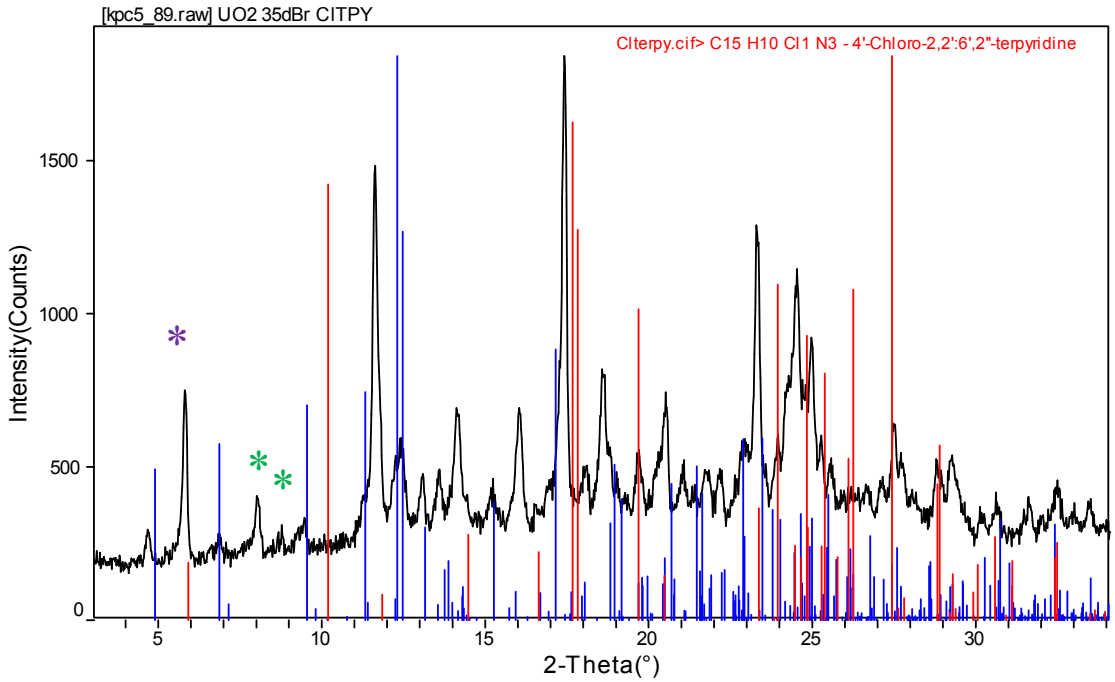

Figure S15: The observed PXRD pattern of structure **11** with calculated pattern overlaid in blue. We acknowledge a couple of minor impurities in the bulk product. One of these impurities was identified as 4'-chloro-2,2':6',2"-terpyridine (calculated CIF overlaid in red) and it is indicated with a purple asterisk. Impurities that could not be identified are indicated with green asterisks.

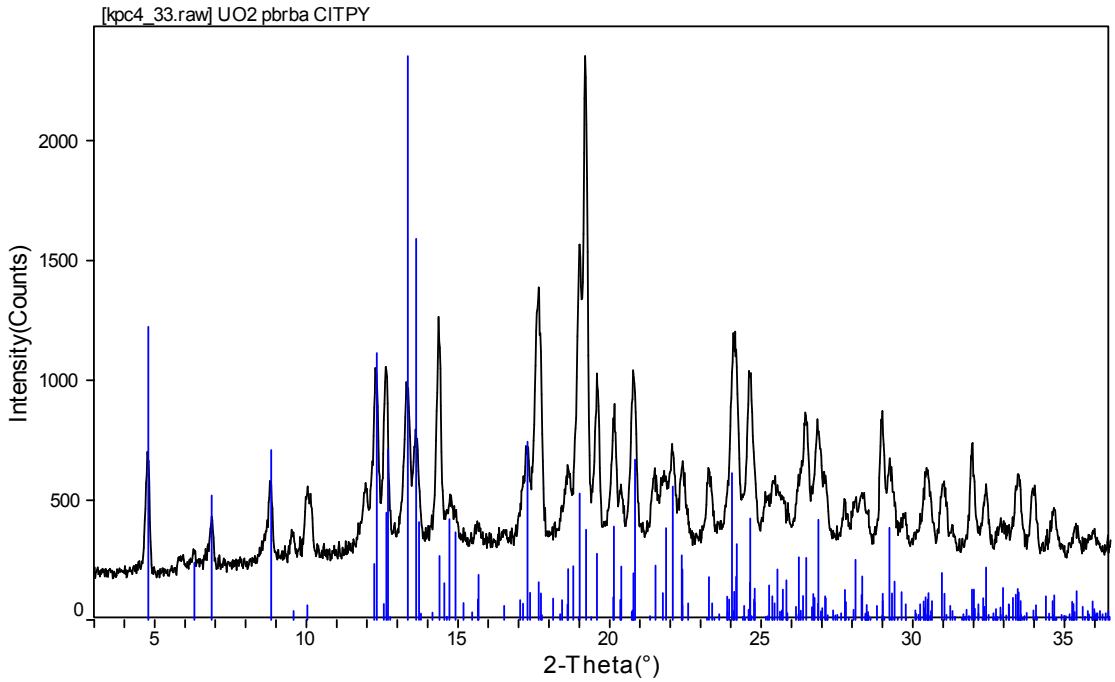

Figure S16: The observed PXRD pattern of structure **12** with calculated pattern overlaid in blue.

III. Thermal Ellipsoid Plots

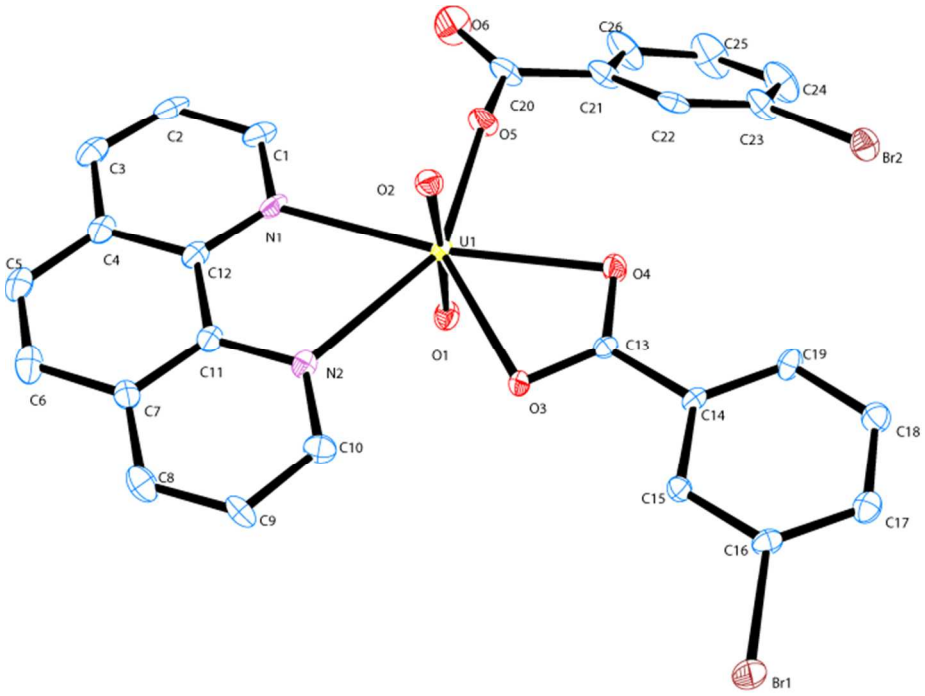

Figure S17: ORTEP illustration of complex **1**. Ellipsoids are shown at 50% probability level.

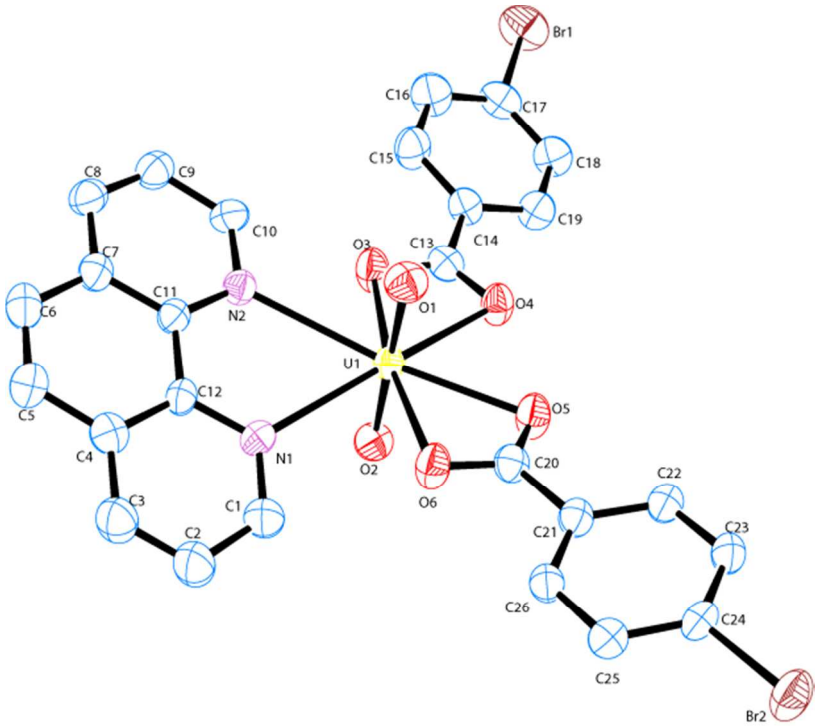

Figure S18: ORTEP illustration of structure **2**. Ellipsoids are shown at 50% probability level.

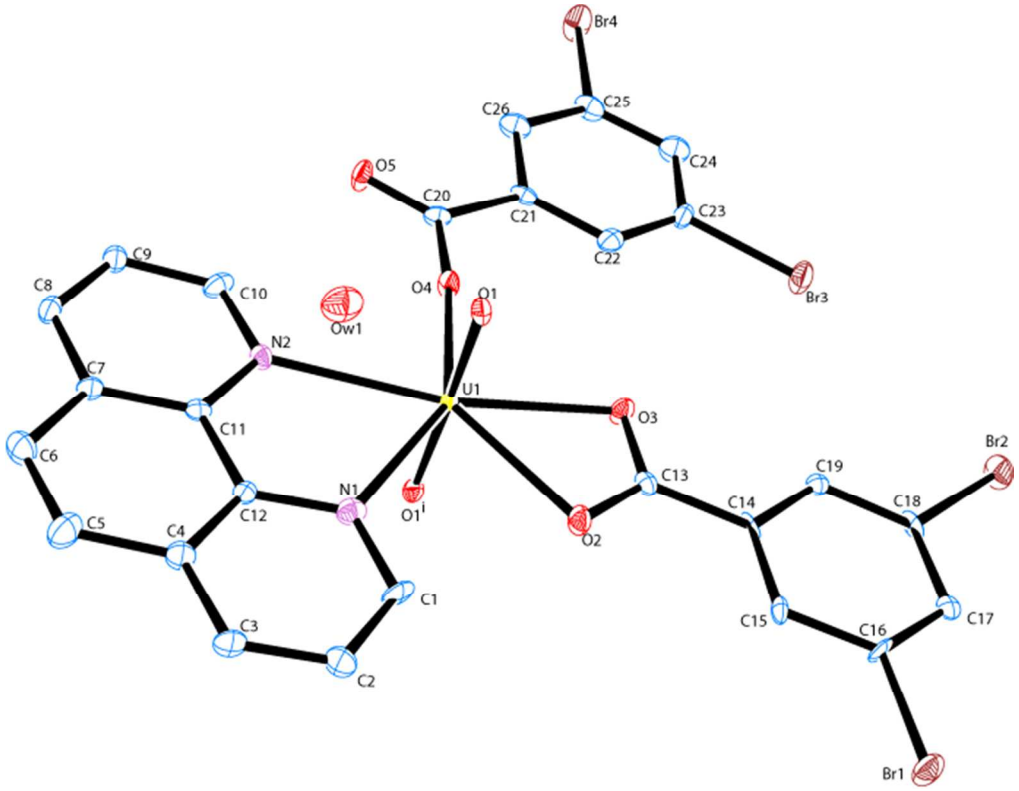

Figure S19: ORTEP illustration of structure **3**. Ellipsoids are shown at 50% probability level. Atoms labelled with an "^{i}" are reproduced through symmetry.

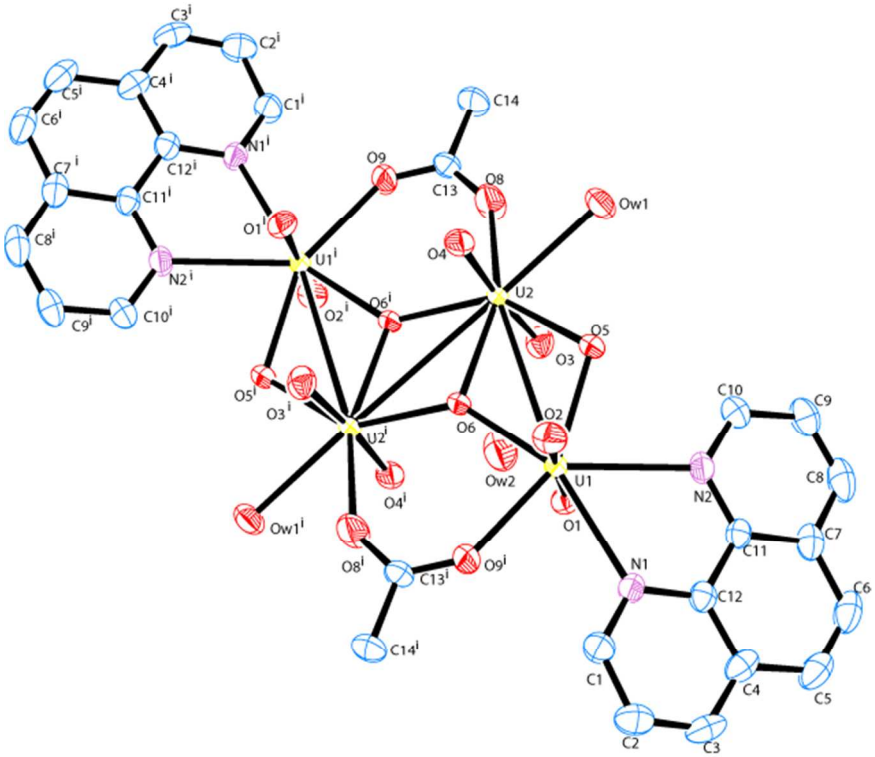

Figure S20: ORTEP illustration of structure **4**. Ellipsoids are shown at 50% probability level. Atoms labelled with an "^{i}" are reproduced through symmetry.

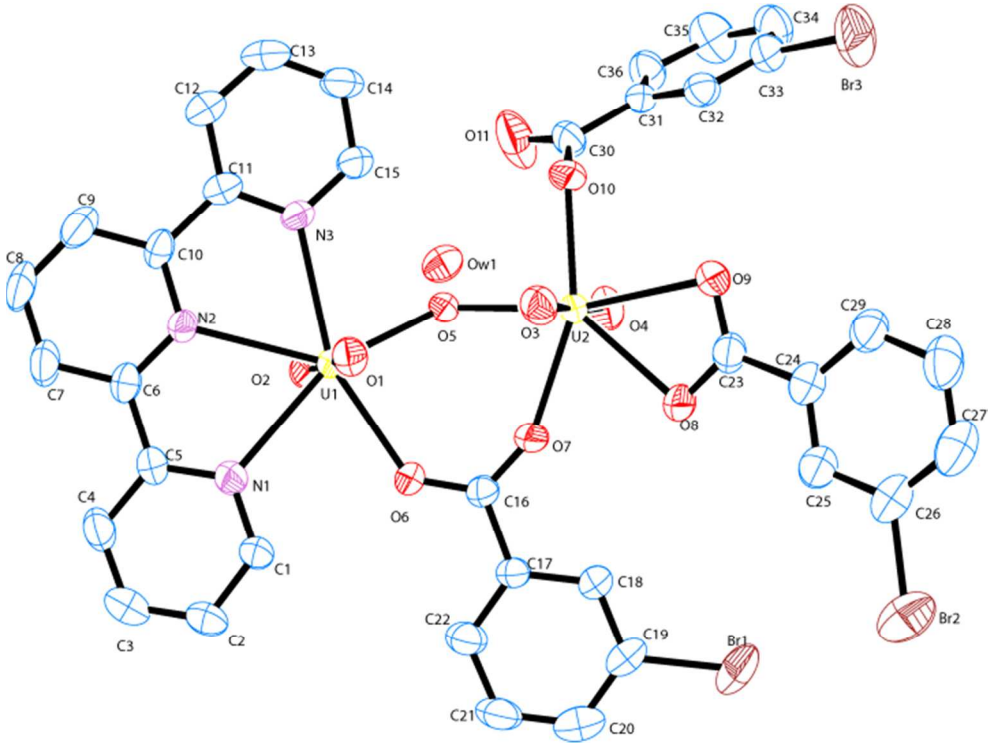

Figure S21: ORTEP illustration of complex **5**. Ellipsoids are shown at 50% probability level.

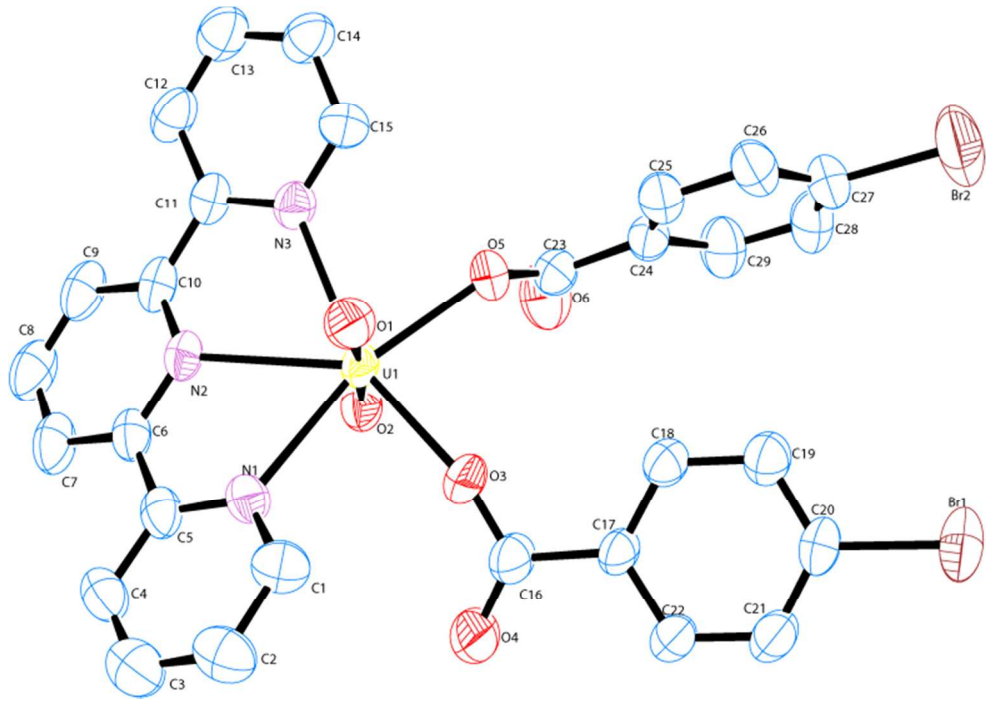

Figure S22: ORTEP illustration of structure **6**. Ellipsoids are shown at 50% probability level.

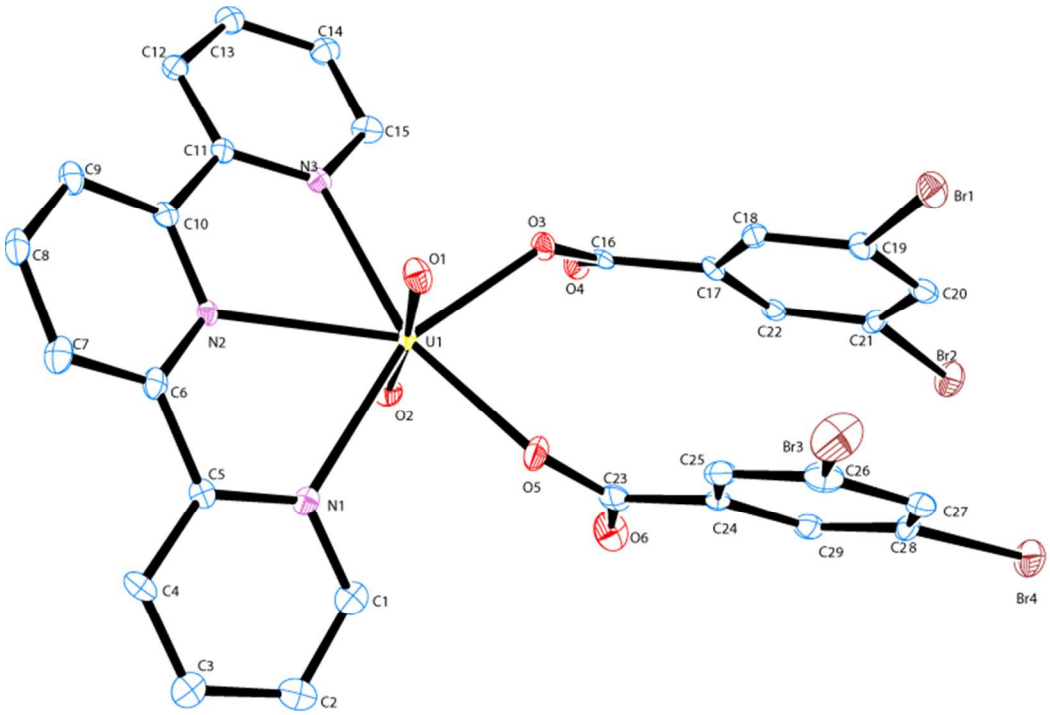

Figure S23: ORTEP illustration of structure **7**. Ellipsoids are shown at 50% probability level.

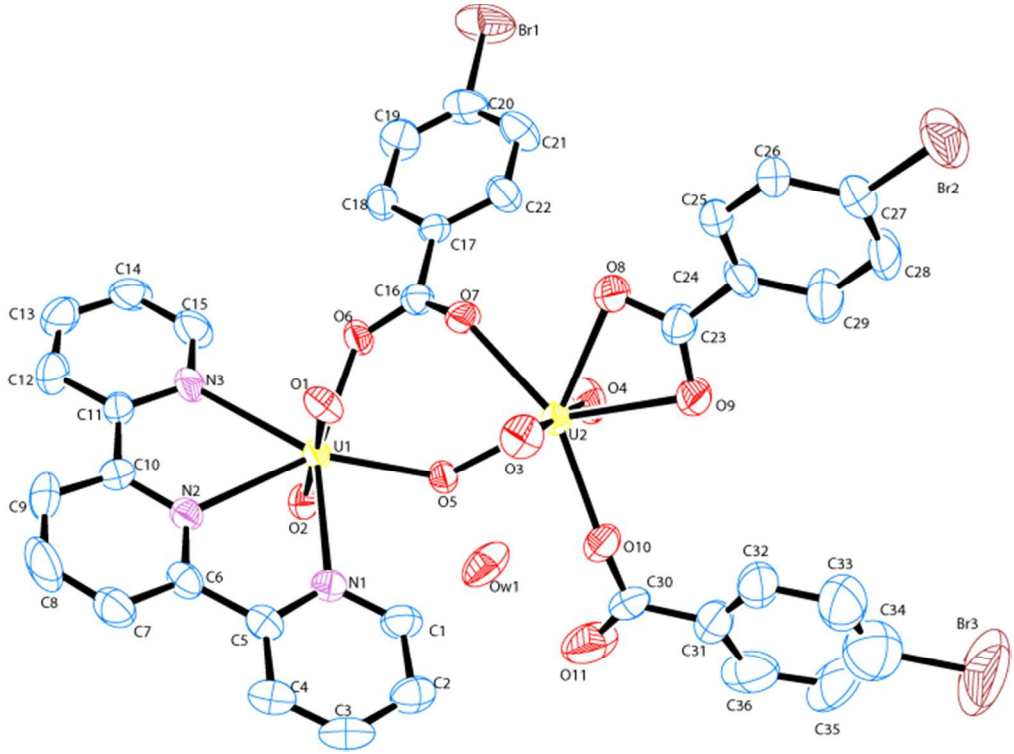

Figure S24: ORTEP illustration of structure **8**. Ellipsoids are shown at 50% probability level.

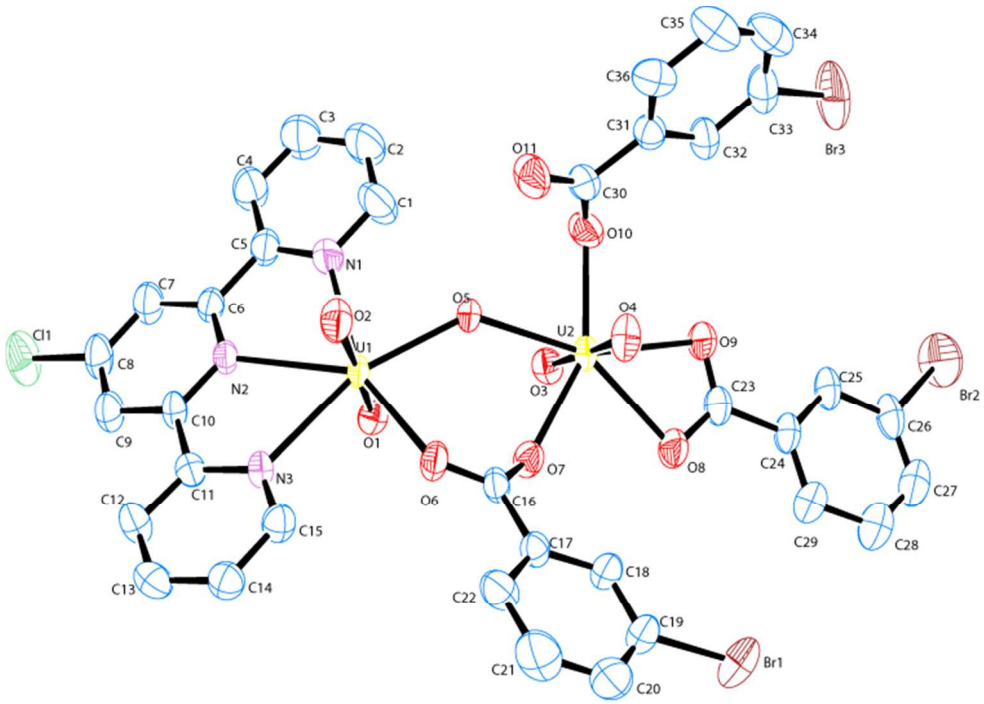

Figure S25: ORTEP illustration of structure **9**. Ellipsoids are shown at 50% probability level.

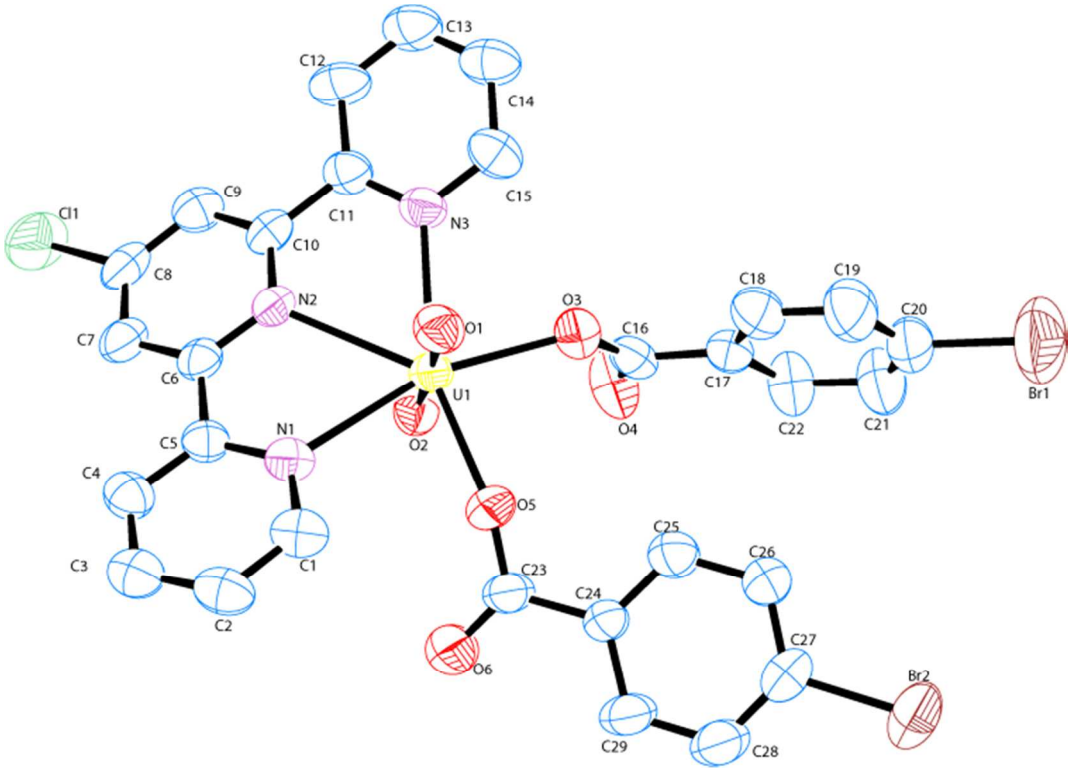

Figure S26: ORTEP illustration of structure **10**. Ellipsoids are shown at 50% probability level.

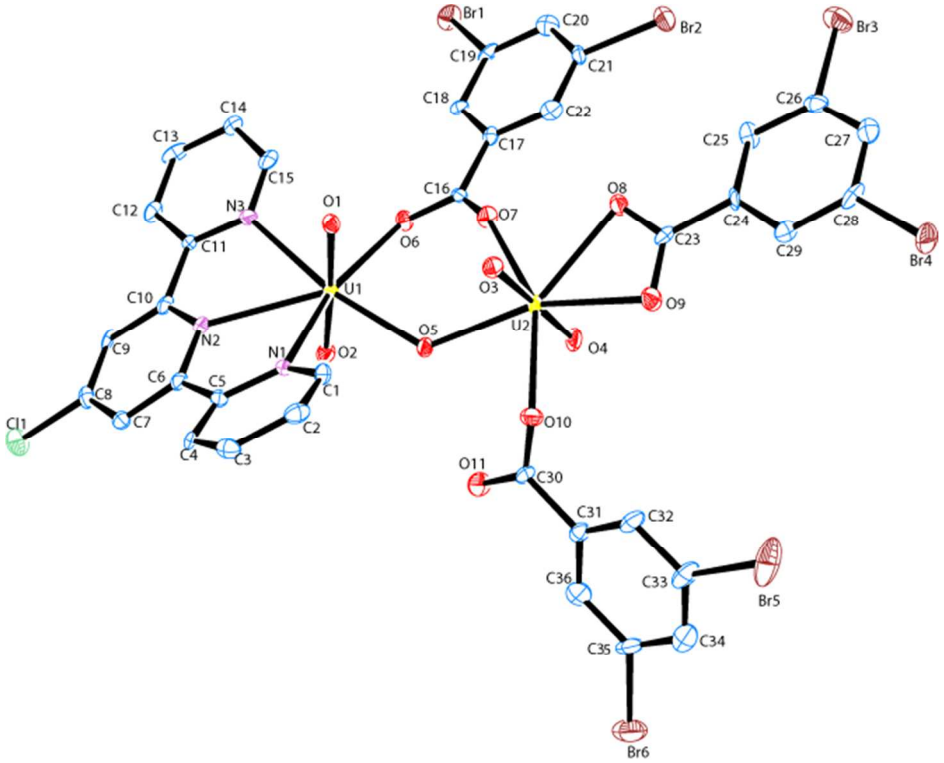

Figure S27: ORTEP illustration of structure **11**. Ellipsoids are shown at 50% probability level.

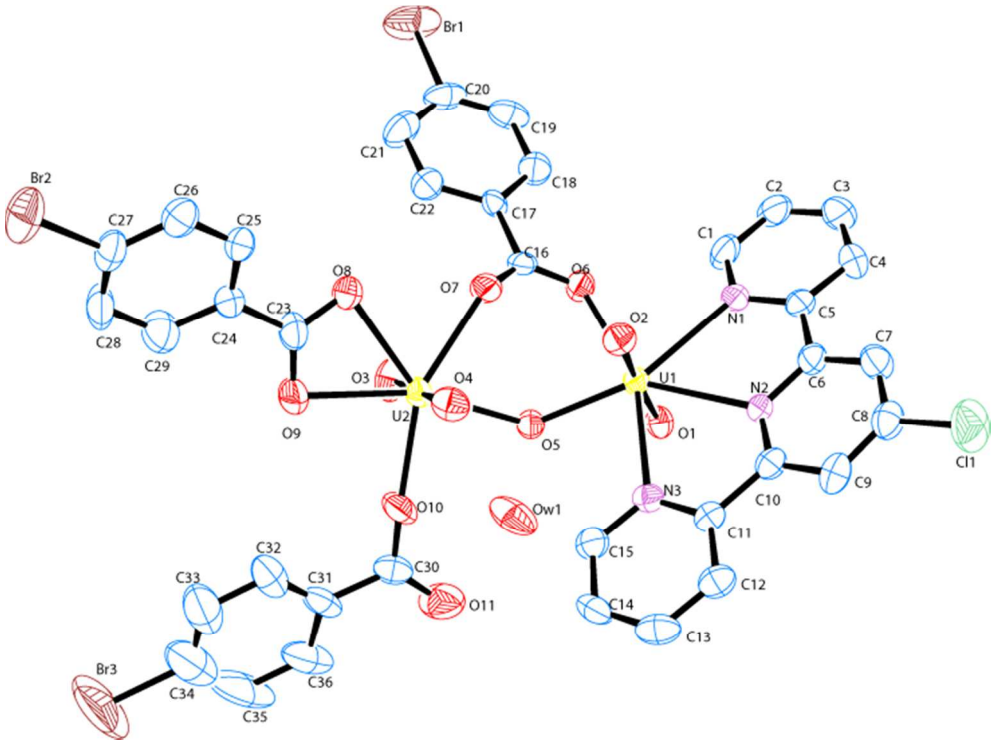

Figure S28: ORTEP illustration of structure **12**. Ellipsoids are shown at 50% probability level.

IV. Tables of Bond Distances

Table S1: U-O Axial Bond Lengths in UO_2^{2+} complexes (**1-12**).

Complex	d_{U1-O1} [Å]	d_{U1-O2} [Å]	d_{U2-O3} [Å]	d_{U2-O4} [Å]
1	1.780(3)	1.769(2)		
2	1.764(3)	1.755(3)		
3	1.773(3)			
4	1.776(3)	1.799(3)	1.794(3)	1.794(3)
5	1.765(3)	1.758(3)	1.760(4)	1.758(4)
6	1.760(3)	1.773(3)		
7	1.776(3)	1.772(3)		
8	1.774(7)	1.759(7)	1.749(7)	1.766(7)
9	1.763(3)	1.757(4)	1.764(4)	1.755(4)
10	1.755(4)	1.754(4)		
11	1.758(4)	1.760(4)	1.778(5)	1.769(5)
12	1.766(4)	1.756(4)	1.767(5)	1.765(4)

Table S2: U-O Equatorial Bond Lengths in UO_2^{2+} complexes (**1-12**).

Complex	d_{U1-O3} [Å]	d_{U1-O4} [Å]	d_{U1-O5} [Å]	d_{U1-O6} [Å]	d_{U2-O5} [Å]	d_{U2-O6} [Å]	d_{U2-O7} [Å]	d_{U2-O8} [Å]	d_{U2-O9} [Å]	d_{U2-O10} [Å]
1	2.405(2)	2.442(2)	2.225(3)							
2	2.404(3)	2.533(3)	2.488(3)	2.439(3)						
3	2.438(4)	2.438(4)	2.235(4)							
4			2.320(3)	2.233(3)	2.355(3)	2.322(3)		2.376(3)		
5			2.255(3)	2.398(3)	2.374(3)		2.314(4)	2.453(4)	2.548(3)	2.276(3)
6	2.230(3)		2.285(3)							
7	2.265(3)		2.268(3)							
8			2.241(6)	2.388(6)	2.361(6)		2.383(6)	2.435(7)	2.451(7)	2.263(7)
9			2.260(3)	2.409(3)	2.406(3)		2.346(3)	2.438(4)	2.436(3)	2.310(4)
10	2.290(4)		2.240(4)							
11			2.264(4)	2.402(5)	2.390(4)		2.336(4)	2.451(4)	2.428(4)	2.293(4)
12			2.226(4)	2.398(4)	2.390(4)		2.391(4)	2.440(4)	2.445(5)	2.244(5)

Table S3: U-N Bond Lengths in UO_2^{2+} complexes (**1-12**).

Complex	d_{U-N1} [Å]	d_{U-N2} [Å]	d_{U-N3} [Å]
1	2.552(3)	2.600(3)	
2	2.664(4)	2.705(4)	
3	2.561(5)	2.540(5)	

4	2.673(4)	2.663(4)	
5	2.592(4)	2.590(4)	2.580(4)
6	2.558(4)	2.600(3)	2.587(3)
7	2.576(3)	2.595(4)	2.560(3)
8	2.561(8)	2.583(8)	2.575(8)
9	2.581(5)	2.603(4)	2.574(4)
10	2.568(5)	2.604(4)	2.589(5)
11	2.568(6)	2.587(5)	2.560(5)
12	2.580(5)	2.585(5)	2.564(5)

V. Bond Valence Summations

Table S4: Bond Valence Summations for oxygen atoms in Compound **4**

O5	Distance (Å)	Bond Valence Sum	**O6**	Distance (Å)	Bond Valence Sum
Bound atoms			Bound atoms		
U1	2.320	0.5886	U1	2.233	0.6961
U2	2.355	0.5502	U2	2.322	0.5864
	Sum	1.138	U2’	2.236	0.6921
				Sum	1.974
OW1					
Bound atoms					
U2	2.595	0.3465			
	Sum	0.3465			

Bond valence summations for selected oxygen atoms in **4**. The values indicated that O5 is a hydroxyl group while O6 is an oxide group. [1, 2]

Table S5: Bond Valence Summations for hydroxide oxygen atom in Compound **5**

O5	Distance (Å)	Bond Valence Sum
Bound atoms		
U1	2.225	0.7069
U2	2.374	0.5305
	Sum	1.237

Table S6: Bond Valence Summations for hydroxide oxygen atom in Compound **8**

O5	Distance (Å)	Bond Valence Sum
Bound atoms		
U1	2.241	0.6854
U2	2.361	0.5439
	Sum	1.229

Table S7: Bond Valence Summations for hydroxide oxygen atom in Compound **9**

O5	Distance (Å)	Bond Valence Sum
Bound atoms		
U1	2.260	0.6608
U2	2.406	0.4987
	Sum	1.159

Table S8: Bond Valence Summations for oxygen atoms in Compound **11**

O5	Distance (Å)	Bond Valence Sum
Bound atoms		
U1	2.264	0.6557
U2	2.390	0.5144
	Sum	1.170

Table S9: Bond Valence Summations for oxygen atoms in Compound **12**

O5	Distance (Å)	Bond Valence Sum
Bound atoms		
U1	2.264	0.7055
U2	2.390	0.5144
	Sum	1.219

VI. References

1. N. E. Brese and M. O'Keeffe, *Acta Crystallographica Section B*, 1991, 47, 192-197.
2. P. C. Burns, R. C. Ewing and F. C. Hawthorne, *The Canadian Mineralogist*, 1997, 35, 1551-1570.

Combining coordination and supramolecular chemistry to explore uranyl assembly in the solid state

Korey P. Carter and Christopher L. Cahill*
Department of Chemistry, The George Washington University, 725 21st Street, NW, Washington, D.C. 20052, United States

Abstract

The syntheses and crystal structures of twelve new compounds containing the UO_2^{2+} cation, a bromo-substituted benzoic acid linker (*m*-bromo-, *p*-bromo, or 3,5-dibromobenzoic acid) and a chelating N-donor (1,10-phenanthroline, 2,2':6',2''-terpyridine, or 4'-chloro-2,2':6',2''-terpyridine) are reported. Single crystal X-ray diffraction analyses of these materials allowed for the exploration of the structural relationship between the benzoic acids and the chelating N-donor, as well as the influence of pH on uranyl speciation. At an unadjusted pH (~3) a mix of uranyl monomers and dimers are observed whereas at higher pH (5-6) uranyl dimers are usually produced with monomers and tetramers also observed. A systematic study of the supramolecular interactions present in these materials was executed by varying the bromine position on the benzoic acid groups along with substituents on the chelating N-donor. Assembly via halogen and hydrogen bonding interactions as well as π-π interactions, including four instances of uranyl oxo-functionalization via halogen bonding, was observed depending on the experimental conditions utilized.

Introduction

Hybrid materials incorporating hexavalent uranium are an area of continued interest due to their penchant for forming structurally diverse coordination polymers and molecular complexes, as well as their relevance to the nuclear fuel cycle.[1-9] Development of crystalline uranyl-organic hybrid materials is generally reliant on largely directional metal-ligand interactions to promote extended structures in 1-, 2- and 3-dimensions.[10] The resulting structural diversity of uranyl hybrid materials provides a platform for understanding the relationship between solution-phase $[UO_2]^{2+}$ speciation and solid-state manifestations thereof, as is relevant for the delineation of structure property relationships such as luminescence or actinide (An) transport in the environment. The unique chemistry of the linear triatomic $[UO_2]^{2+}$ cation, where bonding is generally constrained to the equatorial plane, results in three observed primary building units (square, pentagonal and hexagonal bipyramids) and additional hydrolysis of the U(VI) metal center results in an unpredictable range of secondary building units (dimers, trimers, tetramers, hexamers, sheets, chains, etc.).[11, 12]

Uranyl hydrolysis in aqueous solution proceeds via eq 1 and governs the formation of oligomeric/polymeric SBUs.

$$mUO_2^{2+} + nH_2O \leftrightarrows (UO_2)_m(OH)_n^{2m-n} + nH^+ \quad (1)$$

Metal cation hydrolysis can lead to oligomerization products through the creation of a point-shared hydroxyl group (olation) or thorough a two-step process that results in an oxo bridge (oxolation).[13, 14] Hydrolysis of the uranyl cation can be influenced by $[UO_2]^{2+}$ concentration and pH with oligomeric species more prevalent at pH values above 4.5.[15] Combined with a rich portfolio of ligands with a strong tendency to coordinate to the

uranyl cation (e.g. carboxylates and phosphonates) the literature is rich in both SBUs and extended assembly thereof.[5, 8, 16-19] Subsequently, the cumulative effects of both ligand contribution and metal-ion hydrolysis make the synthesis of materials with desired (or at least predictable) topologies rather challenging. While the rich diversity of uranyl materials have proven fruitful for structural characterization, the tuning of the electronic properties of the uranyl ion[6, 20, 21] remains challenging and thus an understanding of how to direct structure-property relationships in uranyl materials remains elusive.[4, 22, 23] As metal-ion hydrolysis prevents predictable construction of uranyl hybrid materials we turn to the molecular solid-state and supramolecular chemistry, as is the focus of this issue.

Supramolecular assembly of materials via attractive noncovalent interactions provides a platform to circumvent hydrolysis related synthetic challenges. A combination of chelating and linking ligands allows for the directed assembly of molecules into crystalline architectures.[24] Applications of supramolecular assembly in solid-state materials are broad and continue to expand, yet at present include drug design,[25, 26] catalysis,[27, 28] nanomaterials[29, 30] and organic materials design.[31, 32] Braga described crystal engineering as "making crystals by design,"[33] and by utilizing an understanding of intermolecular interactions in the context of crystal packing and metal-ligand coordination, one can address some of the challenges that stem from a diverse speciation profile. This is a concept that has been explored for transition metal chemistry[34] and that has more recently been extended to the actinide series, yet the area remains underexplored.[7, 35] To take a directed approach to assembly in a U(VI) system, one must find a way to restrict or "shut down" hydrolysis in order to end up with predictable molecular units (or tectons). Previous work in our group has demonstrated that synthesis

of $[UO_2]^{2+}$ materials in highly acidic and high halide media will limit uranyl hydrolysis to yield the $[UO_2X_4]^{2-}$ species (where X=Cl, Br)[36-38] or the analogous halide-nitrate ($[UO_2Cl_3NO_3]^{2-}$)[39] almost exclusively, which can then be assembled via the use of supramolecular (hydrogen- and halogen bonding) synthons. More recently, it has been shown that the use of acidic pseudo-halogens (SCN^-)[40, 41] is also quite effective in limiting uranyl speciation and producing anionic discrete building units that can be assembled via a diverse array of supramolecular interactions.

The formation of molecular $[UO_2]^{2+}$ materials does not exclusively require the use of harsh acidic conditions and indeed the literature is rich with a wide variety of uranyl molecular species.[16, 42-45] This has been highlighted by Forbes *et. al.* in the synthesis of uranyl hybrid materials containing carboxylates and amino acids that can be assembled via hydrogen bonding interactions.[46, 47] Previous work from our group has also shown that a combination of coordination chemistry principles with a series of halogen functionalized benzoic acids can yield discrete uranyl materials which utilize halogen-halogen interactions for assembly.[48] In that study, we relied on pH as a method for trying to control uranyl hydrolysis, which while effective, outcomes remain unpredictable. An approach to thwarting hydrolysis via coordination chemistry that does not require acidic media may be realized via the use of a chelating ligand to force *selection* of a single species with an inherent affinity for forming a specific coordination geometry about the $[UO_2]^{2+}$ cation. Due to their preorganization and relatively large binding affinities for f-element ions (specifically the $[UO_2]^{2+}$ cation),[49] chelating N-donors such as 1,10-phenanthroline (phen) and 2,2':6',2"-terpyridine (TPY) (and it's derivatives) have been explored as 'capping' ligands in the synthesis uranyl coordination polymers,[21, 50] uranyl

molecular materials[51] and the formation lanthanide molecular materials that also contain halogen functionalized benzoic acids.[52, 53]

Drawing inspiration from our previous work on uranyl coordination[21] and lanthanide supramolecular assembly,[52, 53] as well as the work of Loiseau and colleagues on uranyl molecular units with TPY,[54] we set out to explore a system that features both a halogen functionalized benzoic acid ligand and a chelating N-donor ligand (phen, TPY, Cl-TPY) used for the purpose of controlling hydrolysis and tailoring assembly of the uranyl tectons. Changes in ligand geometry and adjusting pH yield a rich array of molecular tectons containing a diverse array of supramolecular synthons sites (i.e. Br-O halogen bonds, Br-Br and Br-Cl halogen-halogen interactions, Br-π interactions, π-π interactions and hydrogen bonding interactions) that lie at the edge of the immediate coordination sphere. Herein we report the synthesis, crystal structures and modes of supramolecular assembly for a family of twelve new uranyl-bromo benzoic acid-N-donor materials. Additionally, the materials described herein have great potential for developing uranyl supramolecular assembly criteria based on the observed acceptor-donor pairings. As this is a *Frontiers* special issue we offer our first of many studies that will explore our motivation to establish a set of comprehensive criteria for supramolecular assembly of actinide species.

Experimental Section

Materials and Methods

Caution: Whereas the uranium oxyacetate dihydrate ($UO_2(CH_3COO)_2 \bullet 2H_2O$) used in this study consists of depleted U, standard precautions for handling radioactive and toxic substances should be followed.

All materials, including the various bromobenzoic acids (*m*-bromobenzoic acid, *p*-bromobenzoic acid and 3,5-dibromobenzoic acid) and chelating N-donors (1,10-phenanthroline, 2,2':6',2"-terpyridine and 4'-chloro-2,2':6',2"-terpyridine) were purchased and used without further purification.

Synthesis

All complexes discussed herein were synthesized via hydrothermal methods at autogeneous pressure in a 23 mL Teflon-lined Parr bomb at an oven temperature of 120 ˚C for 72 hours. A molar ratio of (1:2:2:667—UO_2^{2+}:benzoic acid:phen:water) was used for complexes **1-4**, while for complexes **5-12** a molar ratio of (1:2:1:667-- UO_2^{2+}:benzoic acid:terpy/Cl-terpy:water) was optimal for single crystal growth (Table 1). Complexes **4, 8** and **12** could only be produced after the synthesis pH was adjusted via the addition of 25 μL 5M NaOH. A comprehensive set of synthetic conditions for the UO_2^{2+}-bromo-benzoic acid-N-donor series are provided in Table 1.

Table 1: A summary of the conditions used to synthesize complexes **1-12**. Numbers in **bold** represent pH dependent syntheses.

	Unadjusted pH			**Adjusted pH**		
	m-bromo	*p*-bromo	3,5-dibromo	*m*-bromo	*p*-bromo	3,5-dibromo
phen	1 pH_f=2.5	**2** pH_f=3.0	3 pH_f=2.7	1 pH_f=5.2	**4** pH_f=5.8	3 pH_f=5.5
terpy	5 pH_f=2.9	**6** pH_f=2.8	7 pH_f=2.9	5 pH_f=5.2	**8** pH_f=5.8	7 pH_f=5.6
Cl-terpy	9 pH_f=2.6	**10** pH_f=2.8	11 pH_f=2.7	9 pH_f=5.4	**12** pH_f=5.5	11 pH_f=5.8

Characterization

X-Ray Structure Determination

Single crystals from each bulk sample were isolated and mounted on MiTeGen micromounts. Structure determination for each of the single crystals was achieved by collecting reflections using 0.5˚ ω scans on a Bruker SMART diffractometer furnished with an APEX II CCD detector using MoKα (λ=0.71073 Å) radiation at 100K (**1, 3, 7** and **11)** and (293 K) (**2, 4-6, 8-10** and **12)**. The data were integrated using the SAINT software package[55] contained within the APEX II software suite[56] and an absorption correction was performed using *SADABS*.[57] The crystal selected from the bulk product of complex **4** was a two component non-merohedral twin (77% of reflections in domain 1) that was accounted for using *TWINABS*.[58] Complexes **1, 2,** and **7-11** were solved via direct methods using SIR 92[59] and complexes **3-6** and **12** were solved via Direct Methods (SHELXS-2013).[60] All twelve complexes were refined using SHELXL-2013[60] contained within the WinGX[61] software suite. In each structure, all non-hydrogen atoms were located via difference Fourier maps and refined anisotropically. Aromatic hydrogen atoms were located via difference Fourier map, yet were placed at their idealized positions and allowed to ride on the coordinates of their parent carbon atom ((U_{iso}) fixed at 1.2U_{eq}). The hydrogen atoms on the bound water molecule in complex **4** were located via the difference Fourier map and refined isotropically. Structures **3-5, 8**, and **12** contain lattice water molecules and the hydrogen atoms on these molecules could not be located via difference Fourier maps and were not modeled. Hydrogen atoms on bridging hydroxide groups, identified via bond-valence summations (Tables S4-S9, Supporting Information), in **4-5, 8-9**, and **11-12** were not located via difference Fourier map and therefore could not be modeled via HFIX83 commands. Methyl hydrogen atoms on the bridging acetate group in **4** were placed in their idealized positions (HFIX137) and

allowed to ride on the coordinates of the parent atom ((U_{iso}) fixed at 1.5U_{eq}). Positional disorder in 3,5-dibromobenzoic acid ligands in complexes **3** (C14 and C18) and **11** (C1, C11 and C19) and in the *p*-bromobenzoic acid ligands in complex **8** (C11) was restrained via the ISOR command with uncertainty values ranging from 0.01 to 0.001 used depending on the extent of the disorder. All figures were prepared with CrystalMaker.[62] Data collection and refinement details for complexes **1-12** are included in Table 2.

Powder X-ray Diffraction

Powder X-ray diffraction (PXRD) data on the bulk reaction product of complexes **1-12** (Figures S5-S16, Supporting Information) were used to examine the bulk purity of each sample. All data were collected on a Rigaku Miniflex (Cu Kα, 2θ=3-60˚) and were analyzed using the JADE software program.[63] The bulk products of complexes **2-3, 6-7** and **9-11** contain multiple solid-state phases. Attempts were made to identify the impurities (SI) but the synthesis procedure described above was not optimized for phase purity and is thus a limitation of the presented study.

Table 2: Crystallographic Data for Compound **1-12**

	1	**2**	**3**	**4**
chem formula	$C_{26}H_{16}Br_2N_2O_6U$	$C_{26}H_{16}Br_2N_2O_6U$	$C_{26}H_{16}Br_4N_2O_7U$	$C_{28}H_{32}N_4O_{20}U_4$
formula weight	850.26	850.26	1026.08	1696.69
crystal system	triclinic	monoclinic	monoclinic	monoclinic
space group	P-1	$P2_1/c$	$P2_1/m$	$P2_1/n$
a (Å)	8.9104(8)	12.4466(8)	14.2282(8)	7.576(6)
b (Å)	12.1555(10)	21.6789(13)	6.5817(4)	15.177(6)

c (Å)	13.0201(11)	9.4110(6)	16.1780(9)	16.860(7)
α (deg)	63.614(4)	90	90	90
β (deg)	76.124(4)	95.249(4)	115.259(5)	102.094(6)
γ (deg)	84.538(3)	90	90	90
V (Å^3)	1226.32(19)	2528.7(3)	1370.15(15)	1895.6(19)
Z	2	4	2	2
T (K)	100	293	100	293
λ (Mo Kα)	0.71073	0.71073	0.71073	0.71073
D_{calc} (g cm^{-3})	2.303	2.233	2.487	2.941
μ (mm^{-1})	9.923	9.624	11.805	17.118
R_{int}	0.0375	0.0481	0.0622	0.0296
R1 [I>2σ(I)]	0.0255	0.0311	0.0279	0.0204
wR2 [I>2σ(I)]	0.0496	0.0623	0.0543	0.0453
	5	**6**	**7**	**8**
chem formula	$C_{36}H_{26}Br_3N_3O_{12}U_2$	$C_{26}H_{19}Br_2N_3O_6U$	$C_{29}H_{17}Br_4N_3O_6U$	$C_{36}H_{26}Br_3N_3O_{12}U_2$
formula weight	1408.39	903.32	1061.12	1408.39
crystal system	triclinic	triclinic	monoclinic	monoclinic
space group	P-1	P-1	$P2_1/c$	$P2_1/n$
a (Å)	8.1393(3)	8.7005(4)	13.8471(10)	20.6384(9)
b (Å)	14.2487(4)	10.3737(5)	17.0590(12)	7.4578(3)
c (Å)	17.1933(5)	16.6960(8)	14.0709(10)	26.5728(12)
α (deg)	91.870(3)	107.848(4)	90	90

β (deg)	97.985(2)	95.093(4)	115.488(1)	105.647(6)
γ (deg)	98.728(2)	95.359(3)	90	90
V (Å^3)	1948.84(11)	1417.13(12)	3000.3(4)	3938.4(3)
Z	2	2	4	4
T (K)	293	293	100	293
λ (Mo Kα)	0.71073	0.71073	0.71073	0.71073
D_{calc} (g cm^{-3})	2.400	2.117	2.349	2.375
μ (mm^{-1})	11.441	8.595	10.785	11.322
R_{int}	0.0389	0.0321	0.0600	0.0671
R1 [I>2σ(I)]	0.0322	0.0318	0.0273	0.0499
wR2 [I>2σ(I)]	0.0724	0.0695	0.0538	0.1350
	9	**10**	**11**	**12**
chem formula	$C_{36}H_{23}Br_3N_3ClO_{11}U_2$	$C_{29}H_{18}Br_2N_3ClO_6U$	$C_{36}H_{20}Br_6N_3ClO_{11}U_2$	$C_{36}H_{25}Br_3N_3ClO_{12}U_2$
formula weight	1424.81	937.76	1661.52	1442.83
crystal system	monoclinic	triclinic	monoclinic	monoclinic
space group	$P2_1/n$	P-1	$P2_1/c$	$P2_1/n$
a (Å)	20.7772(8)	8.9940(3)	18.8629(13)	20.7962(8)
b (Å)	7.9807(3)	10.4251(4)	8.6591(6)	7.5283(3)
c (Å)	25.7089(10)	16.3687(6)	26.9328(19)	26.7408(11)
α (deg)	90	104.094(1)	90	90
β (deg)	110.925(1)	94.879(1)	107.231(3)	106.168(5)
γ (deg)	90	96.417(2)	90	90

V (Å^3)	3981.8(3)	1469.19(9)	4201.6(5)	4021.0(3)
Z	4	2	4	4
T (K)	293	293	100	293
λ (Mo Kα)	0.71073	0.71073	0.71073	0.71073
D_{calc} (g cm^{-3})	2.377	2.120	2.627	2.383
μ (mm^{-1})	11.263	8.382	13.530	11.157
R_{int}	0.0438	0.0468	0.0790	0.0711
R1 [I>2σ(I)]	0.0300	0.0383	0.0374	0.0390
wR2 [I>2σ(I)]	0.0664	0.0859	0.0715	0.0769

Description of Structures

Single crystal X-ray crystallography analyses revealed three unique building units in this family of molecular complexes: monomers (one unique UO_2^{2+} cation) (**1**-**3, 6**-**7** and **10**), dimers (two unique UO_2^{2+} cations) (**5**, **8**-**9** and **11**-**12**) and a tetramer (two unique UO_2^{2+} cations) (**4**). Local structures are described in detail for complexes **1**-**6** only as they represent each of the unique observed coordination environments. Modes of supramolecular assembly are described for all complexes however as they are affected by systematic changes in the location of the bromine atoms on the benzoic acid groups and by the nature of the chelating N-donor ligands.

Complex **1**, $[UO_2(C_{12}H_8N_2)(C_7H_4BrO_2)_2]$, crystallizes in the space group P-1 and features an asymmetric unit that contains a uranyl monomer with pentagonal bipyramidal coordination geometry. The $[UO_2]^{2+}$ cation is chelated by a bidentate phen molecule and further coordinated to bidentate and monodentate *m*-bromobenzoic acid ligands (Figure

1). U1-O bond distances to the bidentate *m*-bromobenzoic acid (O3 and O4) are 2.405(2) Å and 2.442(2) Å respectively. The monodentate *m*-bromobenzoic acid is bound through O5 and is at a distance of 2.225(3) Å from the uranium center and the bromine atom (Br2) of this ligand facilitates intermolecular Br-O interactions that will be discussed in more detail in the following paragraph. Completing the equatorial coordination sphere of the uranyl ion is the bidentate phen molecule (N1 and N2) and the U1-N distances are 2.552(3) Å and 2.442(2) Å, respectively.

The uranyl monomers of **1** are assembled to form molecular dimers via halogen bonds between the axial uranyl oxygen atom (O2) on one unit and the bromine from an *m*-bromobenzoic acid ligand (Br2) of an adjacent monomer (Figure 1). The corresponding Br-O interaction distance and angle are 3.271(3) Å and ∠C-Br-O 162.82(14) º. Oxo-fuctionalization of the uranyl is known in some systems,[64-67] yet the uranyl oxygens are typically terminal in most hybrid materials (hence the bipyramidal building units). Some interactions involving the "yl" oxygen atoms are known (i.e cation-cation interactions (CCIs),[50, 68-73] yet these are observed much more frequently for the $[NpO_2]^+$ cation.[74] Efforts to 'activate' the "yl" oxygen atoms in molecular chemistry have primarily relied on the "yl" oxygen atoms ability to act as hydrogen bond acceptors.[75, 76] We have shown that the axial of the uranyl ion can act as a halogen bond acceptor with the $[UO_2(NCS)_4(H_2O)]^{2-}$ anion and the 4-chloropyridine cation[41] and in **1** we have the first of four examples where the "yl" oxygen atoms adopts the same function.

The dimers in **1** are assembled into an infinite 2D chain that propagates in the [100] direction via slightly offset π-π stacking interactions[77] between phenanthroline ligands on neighboring units. These non-covalent interactions are between the centroid (a

calculated centroid, Cg, corresponds to the center of the aromatic ring) of the phen moiety on one unit with the edge of the phen ring on the neighboring unit. Centroids were calculated in the center of the aromatic phen rings participating in these interactions in order to obtain the linear distance (Cg···Cg) between the centroids as well as displacement perpendicular to the plane of the phen rings for each of the unique π-stacks (Cg⊥···Cg⊥). Additionally, the angle (β) formed by the intersection of the line between centroids and the displacement perpendicular to the plane of the phen rings was determined. As such, the relevant distances and angles for these interactions are: Cg···Cg 3.803(2) Å; Cg⊥···Cg⊥ 3.3542(14) Å; β=27.81°.

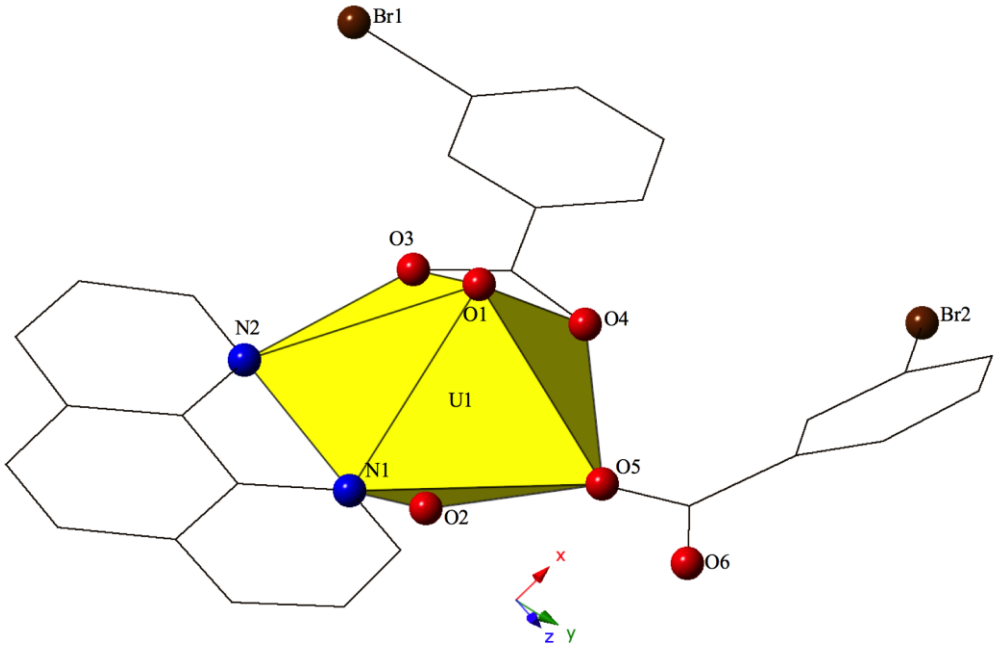

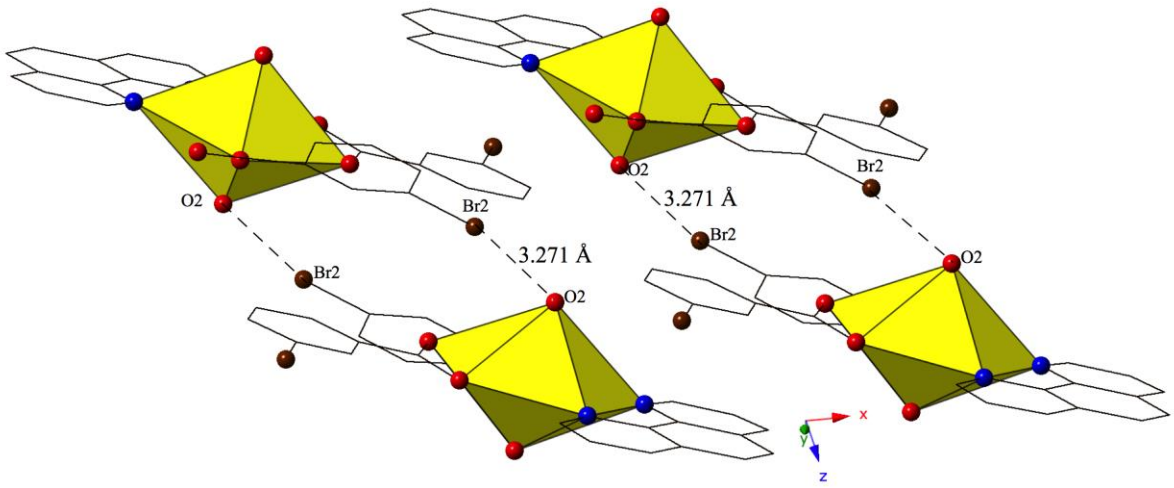

Figure 1 (Top) Polyhedral representation of asymmetric unit of **1**. Yellow polyhedra represent uranium metal centers, whereas spheres represent bromine (brown), nitrogen (blue) and oxygen (red). All H atoms have been omitted for clarity. **(Bottom)** Complex **1** viewed in the (101) plane highlighting the Br-O halogen bonding interactions between uranyl monomers.

Changing the position of the bromine from the *ortho*- to the *para*- position on the benzoic acid ligand yields complex **2**, $[UO_2(C_{12}H_8N_2)(C_7H_4BrO_2)_2]$, which crystallizes in the space group $P2_1/c$. The asymmetric unit of **2** contains a uranyl monomer with distorted hexagonal bipyramidal coordination geometry. The $[UO_2]^{2+}$ cation is chelated by a bidentate phen molecule along with two bidentate *p*-bromobenzoic acid ligands (Figure 2). U1-O bond distances to the two *p*-bromobenzoic acid ligands (O3, O4, O5 and O6) are at an average distance of 2.466 Å. U1-N distances to the bidentate phen molecule (N1 and N2) are 2.664(4) Å and 2.705 Å respectively and these values are consistent with expected distances for U-N bonds.[78, 79]

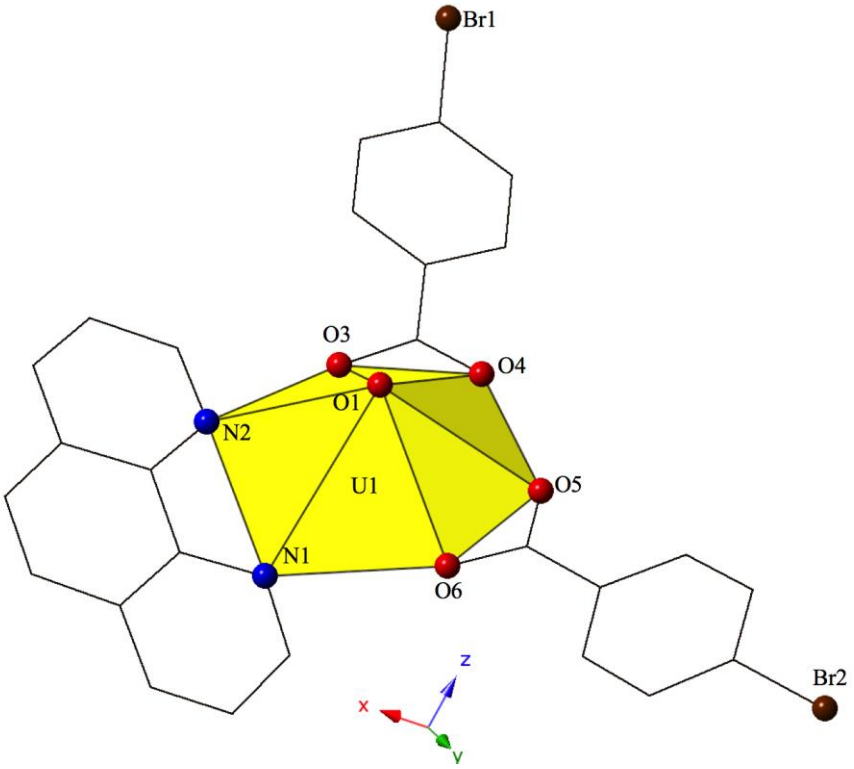

Figure 2 The local coordination geometry of **2** is shown. All H atoms have been omitted for clarity

Complex **3**, $[UO_2(C_{12}H_8N_2)(C_7H_3Br_2O_2)]\bullet H_2O$, crystallizes in the space group $P2_1/m$ and consists of uranyl monomers with a pentagonal bipyramidal coordination geometry. Each $[UO_2]^{2+}$ cation is chelated by a bidentate phen molecule and further coordinated to bidentate and monodentate 3,5-dibromobenzoic acid ligands (Figure 3). U1-O bond distances to the bidentate 3,5-dibromobenzoic acid (O2 and O3) are each 2.438(4) Å. The monodentate 3,5-dibromobenzoic acid is bound through O4 and is at a distance of 2.235(4) Å from the uranium center. U1-N distances to the bidentate phen molecule (N1 and N2) are 2.561(5) Å and 2.540(5) Å, respectively. The asymmetric unit further contains a lattice water molecule, OW1, which facilitates the supramolecular assembly of the uranyl monomers of **3** into infinite 1D chains.

Offset π-π stacking interactions between 3,5-dibromobenzoic acid ligands on adjacent units link monomers of **3** to form a 1D chain, which propagates infinitely in the [010] direction. The relevant distances and angles for these interactions are Cg···Cg 3.5832(14) Å; Cg⊥···Cg⊥ 3.2909(10) Å; β=23.30° (Figure 3). A bifurcated hydrogen bonding interaction from the lattice water, OW1, occurs with the uranyl axial oxygen atom (O1) and its symmetry equivalent (O1') and decorates the periphery of the chain (Figure S1, Supporting Information). Interaction distances from OW1 to O1 and O1' are equivalent at 3.234(5) Å.

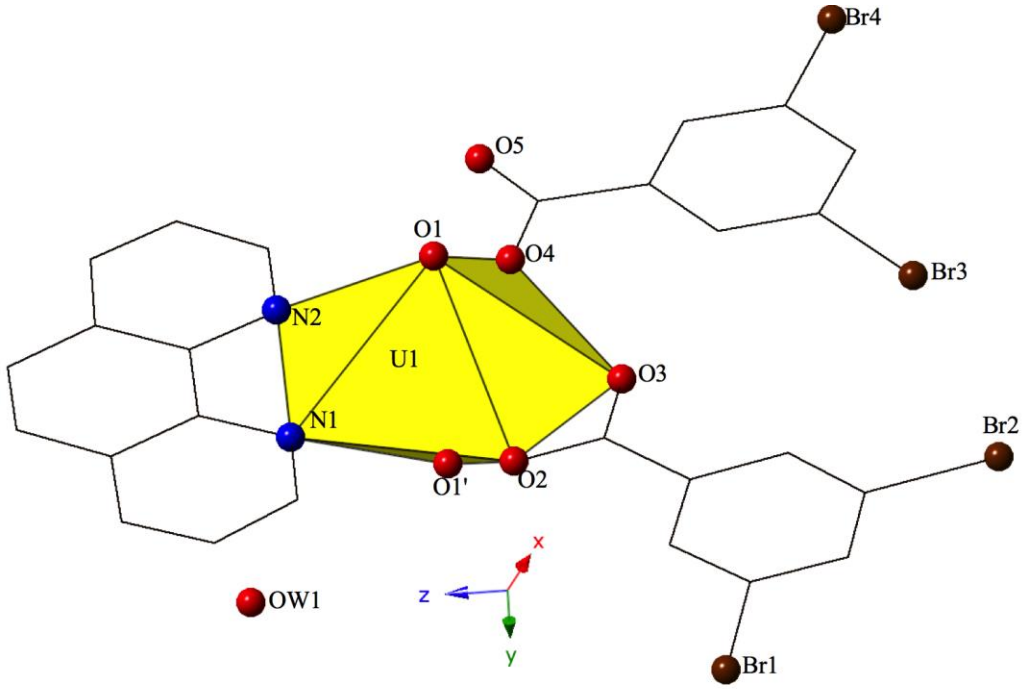

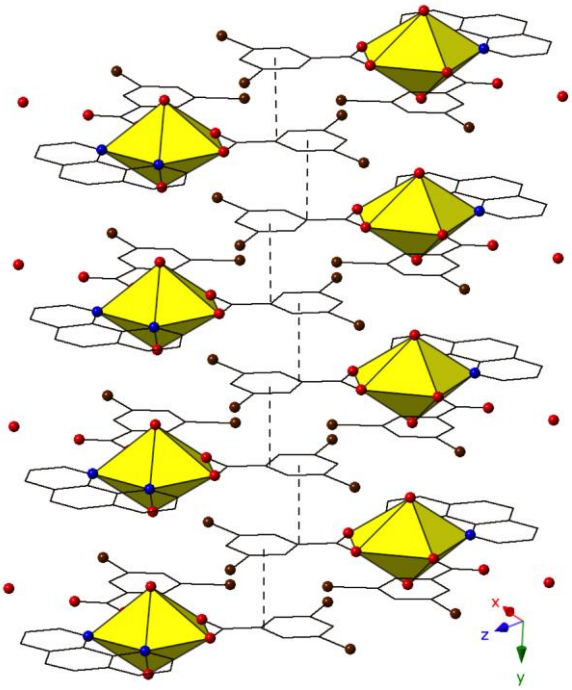

Figure 3 (Top) Polyhedral representation of local structure of **3**. All H atoms have been omitted for clarity. (**Bottom)** Complex **3** viewed down the [010] direction. π-π interactions between 3,5-dibromobenzoic acid ligands that assemble 1D chains of **3** are shown.

Complex **4,** $[(UO_2)_2(OH)(O)(C_{12}H_8N_2)(CH_3COO)(H_2O)]_2 \bullet 2H_2O$, is the first phase described herein to form exclusively at adjusted pH values (approximately 5-6) and crystallizes in the space group $P2_1/c$. The asymmetric unit of **4** consists of uranyl tetramer where two unique $[UO_2]^{2+}$ cations, and their symmetry equivalents, have adopted pentagonal bipyramidal coordination geometries (Figure 4). Both unique uranyl cations are bridged via a point-sharing μ_2-OH group (O5) with U-O bond distances of 2.320(3) Å (U1-O5) and 2.355(3) Å (U2-O5) (Confirmed via bond valence calculations, Table S4, Supporting Information). Oxolation yielded a μ_3-O bridge (O6) that connects U1, U2 and U2' with an average U-O bond distance of 2.264 Å. A third bridging interaction occurs through the coordinated acetate group (O8, O9) and this links U2 with

U1' to complete the tetramer. The corresponding U-O bond distances for the acetate group are 2.359(3) Å (U1'-O9) and 2.376(3) Å (U2-O8), respectively. Bidentate phen groups decorate the periphery of the uranyl tetramer in **4** and complete the equatorial coordination sphere of U1. U1-N distances are 2.673(4) Å (U1-N1) and 2.663(4) Å (U1-N2) which are consistent with the bond lengths observed in complexes **1-3.** A bound water molecule (OW1) lies at the apex of pentagonal bipyramid equatorial geometry of U2 at a distance 2.595(4) Å and the asymmetric unit of **4** further contains a lattice water molecule, OW2, which facilitates additional intermolecular interactions that will be discussed below. Despite its inclusion in the initial synthesis, the *p*-bromobenzoic acid ligand did not incorporate into the final structure of **4** nor was its presence as an impurity detected via PXRD. (Figure S8)

Looking at the global structure of **4**, the uranyl tetramers are assembled via offset π-π stacking interactions into a staggered 1D chain that propagates in approximately the [100] direction. (Figure 4). These non-covalent interactions are between the centroid of the phen moiety on one unit with the edge of the phen ring on the neighboring unit. The relevant distances and angles for these interactions are: Cg···Cg 3.667(4) Å; Cg⊥···Cg⊥ 3.4082(19) Å; β=21.67°. A bifurcated hydrogen bonding interaction from the lattice water, OW2, occurs with the axial uranyl oxygen atom (O3) of one tetramer and the bound water molecule (OW1) on the tetramer directly below. Interaction distances from OW2 are 2.817(5) Å to O3 and 2.798(6) Å to OW1 and the bifurcated interaction leads to the formation of a 2D sheet in approximately the (101) plane.

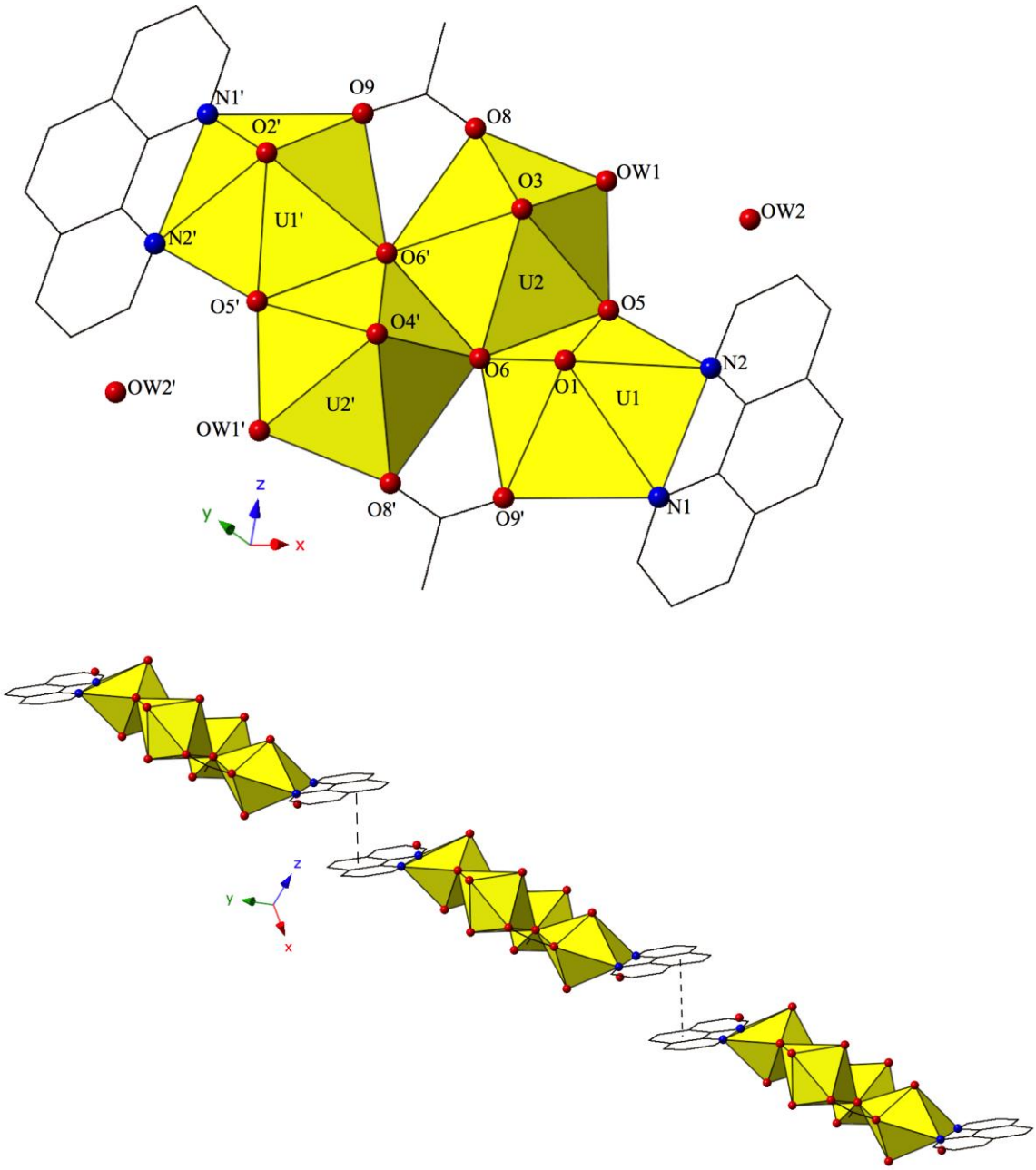

Figure 4 (Top) Polyhedral representation of local structure of **4**. All H atoms have been omitted for clarity. **(Bottom)** Complex **4** viewed down approximately the [101] direction. π-π interactions that stitch together the 1D chains of uranyl tetramers are highlighted.

The introduction of terpy as a chelating ligand yields complex **5**, $[(UO_2)_2(OH)(C_{15}H_{11}N_3)(C_7H_4BrO_2)_3]\bullet H_2O$, which crystallizes in the space group P-1. The asymmetric unit of **5** consists of a uranyl dimer where both $[UO_2]^{2+}$ cations display

pentagonal bipyramidal local coordination geometries (Figure 5). The two uranyl cations are linked via a bridging bidentate *m*-bromobenzoic acid ligand (O6 and O7) as well as a point-sharing μ_2-OH group (confirmed via bond valence calculations, Table S5, Supporting Information). Equatorial uranium-oxygen bond distances are 2.398(3) Å (U1-O6) and 2.341(4) Å (U2-O7) for the bridging *m*-bromobenzoic acid and 2.255(3) Å (U1-O5) and 2.374(3) Å (U2-O5) for the bridging hydroxide. The coordination sphere of U1 is completed by a tridentate terpy molecule bound through its three nitrogen atoms (N1, N2 and N3), with an average U1-N bond distance of 2.587 Å. Two additional *m*-bromobenzoic acid ligands decorate the U2 metal center and exhibit bidentate and monodentate coordination modes. U2-O bond distances to the bidentate *m*-bromobenzoic acid ligand (O8 and O9) are 2.453(4) Å and 2.548(3) respectively and the U2-O10 bond distance for the monodentate *m*-bromobenzoic acid is 2.276(3) Å. A lattice water molecule, OW1, which interacts with carboxylate oxygen (O11) via hydrogen bonding, completes the asymmetric unit.

Looking at the global structure of **5**, we see our first example of the halogen-halogen interaction as the uranyl dimers are linked via bromine atoms on adjacent units (Figure 5). Halogen-halogen interactions tend to adopt one of two geometries in order to minimize the overlap of regions of negative charge density.[80, 81] The interactions in complex **5** (Br3-Br3') meet the criteria described by Desiraju *et. al.*[82, 83] for a Type I halogen-halogen interaction with a distance of 3.4397(13) Å (93.0% vdW) and angles (θ_1,θ_2) equal to 139.00(19)º. The uranyl dimers of complex **5** propagate as infinite 1D chains via hydrogen bonds in approximately the [100] direction with the lattice water molecule, OW1, interacting with the point sharing hydroxide group, O5, of one dimer

directly above and the carboxylate oxygen, O9, of the dimer lying directly below at distances of 2.721(5) Å and 2.808(5) Å, respectively.

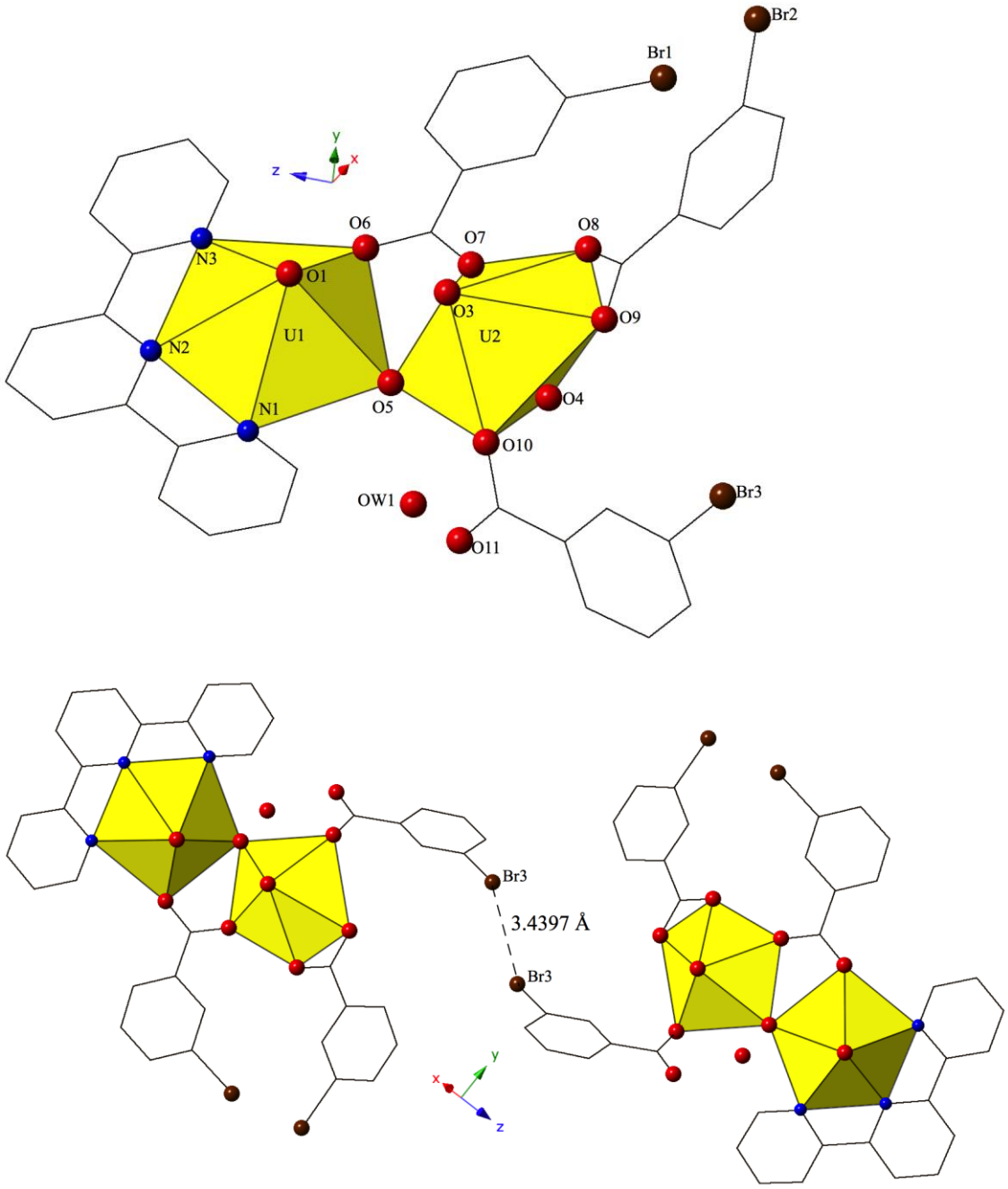

Figure 5 (Top) Polyhedral representation of asymmetric unit of **5**. All H atoms have been omitted for clarity. **(Bottom)** Complex **5** viewed down approximately the [011] direction featuring a Type I Br-Br interaction that links the adjacent uranyl dimers.

Complex **6**, $[UO_2(C_{15}H_{11}N_3)(C_7H_4BrO_2)_2]$, crystallizes in the space group P-1 and features an asymmetric unit that contains one pentagonal bipyramidal uranyl PBU. Each $[UO_2]^{2+}$ cation is chelated by a tridentate terpy molecule and coordinated by two monodentate *p*-bromobenzoic acid ligands (Figure 6). U1-O bond distances to the monodentate *p*-bromobenzoic acid ligands (O3 and O5) are 2.230(3) Å and 2.285(3) Å, respectively. The tridentate terpy molecule (N1, N2 and N3) caps the uranyl coordination sphere and the average U1-N distance is 2.582 Å.

The uranyl monomers of **6** form molecular dimers via halogen bonding interactions between the axial uranyl oxygen atom (O1) on one unit and the bromine from a *p*-bromobenzoic acid ligand (Br1) on the neighboring monomer (Figure 6). The corresponding Br-O interaction distance and angle are 3.320(3) Å and ∠C-Br-O 144.52(17) º. Additional supramolecular connectivity in **6** is achieved through a series a series of weak hydrogen bonding interactions.

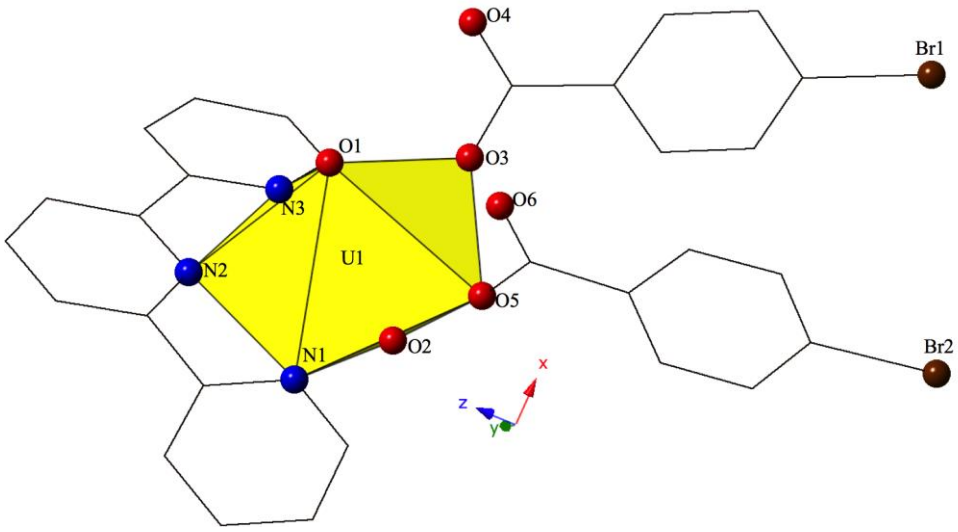

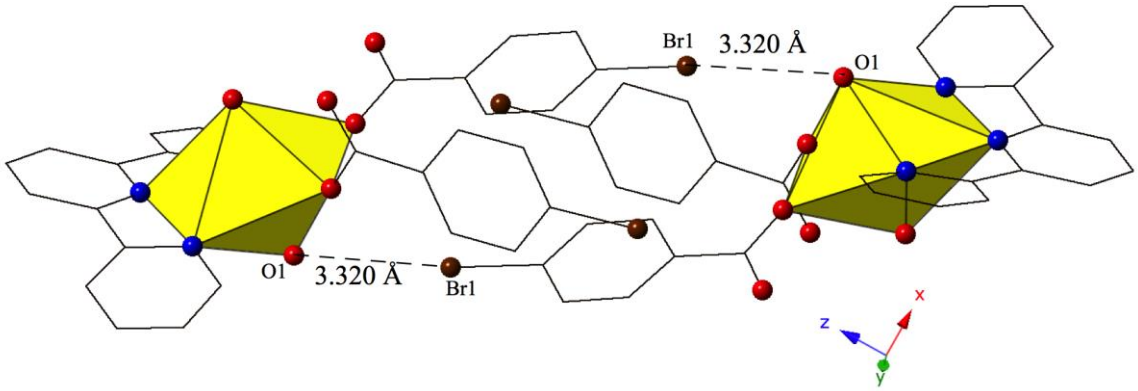

Figure 6 (Top) Polyhedral representation of asymmetric unit of **6**. All H atoms have been omitted for clarity. **(Bottom)** Complex **6** viewed down approximately the [001] direction highlighting Br-O halogen bonding interactions that assemble uranyl monomers into molecular dimers.

The combination of terpy and the 3,5-dibromobenzoic acid ligand yields complex **7**, $[UO_2(C_{15}H_{11}N_3)(C_7H_3Br_2O_2)]$, which crystallizes in the space group $P2_1/c$. Complex **7** features nearly identical uranyl coordination geometry to **6**, and thus will not be described in detail. The modes of supramolecular assembly appear to be similar when comparing **6** and **7**, yet a detailed look reveals significant differences. Similar to **6**, uranyl monomers of **7** are tethered to form molecular dimers via halogen bonding interactions between the axial uranyl oxygen atom (O1) on one unit and the bromine from a 3,5-dibromobenzoic acid ligand (Br1) on the neighboring monomer (Figure 7). The corresponding Br-O interaction distance and angle are 3.246(3) Å and ∠C-Br-O 152.80(13)º. Whereas additional dimensionality in **6** was achieved via weak hydrogen bonding interactions, the supramolecular dimers of **7** are assembled into a zigzag 1D chain via a pair of moderately strong[84] localized Br-π (Br2-C7) and (Br4-C3) interactions[85] between two 3,5-dibromobenzoic acid ligands on the same uranyl unit with the periphery of the terpyridine moiety on a neighboring unit (Figure S2, Supporting Information). Halogen-π interactions are defined as either moderate or strong lone pair-π interactions by Reedijk

and colleagues[84] based on whether the interaction distance is less than equal to the corresponding sum of the van der Waals radii (3.550 Å for bromine and carbon). The halogen-π interactions of **7** are at distances of 3.441(4) Å (Br2-C7) and 3.315(4) Å (Br4-C3) respectively and as both of these interactions are well within the sum of the corresponding vdW radii of bromine and carbon this is suggestive that the vdW overlap of the bromine atoms (Br2 and Br4) of the 3,5-dibromobenzoic acid ligands and the aromatic rings of the terpyridine molecules in **7** are significant.

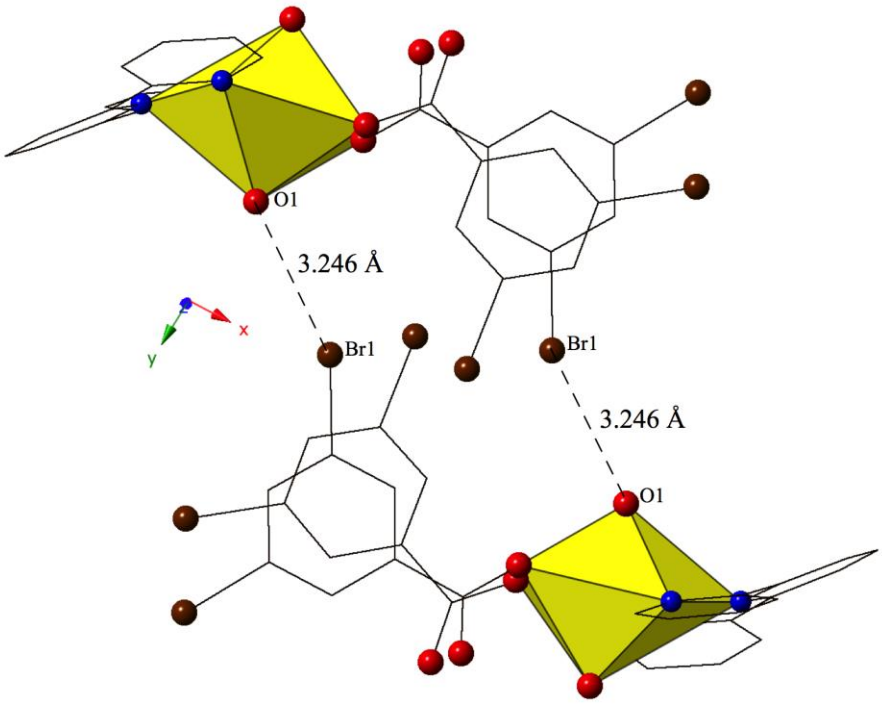

Figure 7 Complex **7** viewed down approximately the [010] direction showing the Br-O halogen bonding interactions that stitch together neighboring uranyl monomers.

Complex **8**, $[(UO_2)_2(OH)(C_{15}H_{11}N_3)(C_7H_4BrO_2)_3]$, forms at adjusted pH values (5-6) and crystallizes in the space group $P2_1/n$. Although the *p*-bromobenzoic acid is used in the synthesis of **8**, the local coordination geometry is similar to **5** and will not be described in detail. The structure of **8** contains uranyl dimers that are linked via localized

Br-π interactions, stemming from the bromine of a *p*-bromobenzoic acid ligand on one unit (Br1) and the periphery of a benzoic acid ring on the neighboring uranyl unit (C31) (Figure 8). The chains formed from these Br-π interactions propagate in approximately the [101] direction with Br1-C31 interaction distances of 3.315(12) Å. Additionally, a lattice water molecule is absent in **8**, which represents a slight variation from the asymmetric unit of **5**.

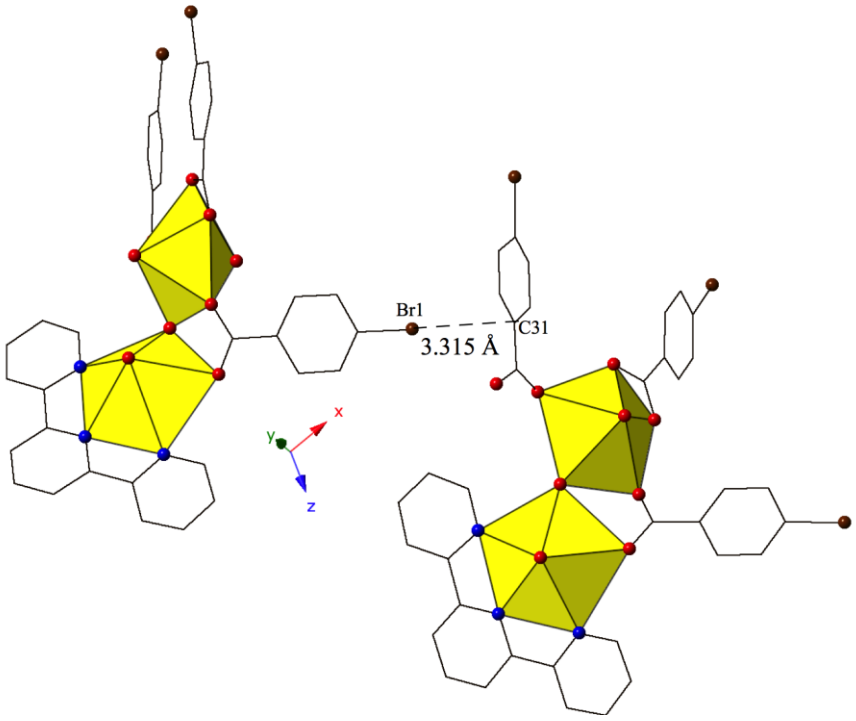

Figure 8 Complex **8** viewed down approximately the [101] direction highlighting the localized Br-π interaction that ties together neighboring uranyl dimers.

Complex **9**, $[(UO_2)_2(OH)(C_{15}H_{10}ClN_3)(C_7H_4BrO_2)_3]$, crystallizes in the space group $P2_1/n$. Beyond the introduction of Cl-terpy as a capping ligand, **9** features a nearly identical local coordination geometry to **5** so it will not be described in detail. The only changes from **5** to **9** are the absence of a crystallized lattice water molecule and the addition of a chlorine atom at the 4'-position of the terpy molecule in **9**. Whereas these

changes may seem insignificant, the resulting supramolecular interactions in **9** have changed dramatically. A bifurcated halogen-halogen interaction (Br3-Cl1 and Br3-Br1) where the bromine atom of one *m*-bromobenzoic acid ligand (Br3) acts as a halogen bond donor links together the uranyl dimers of **9** into a 1D chain that propagates in the [100] direction (Figure 9). The bifurcated interaction is made up of a type II[83] interaction between the halogen bond donor Br3 and a chlorine (Cl1) at the 4'-position of the terpyridine moiety on an adjacent uranyl unit. The Br3-Cl1 distance is 3.550(2) Å, which is 98.6% of the sum of the van der Waals radii, and the θ_1 and θ_2 angles are very near type II geometry (θ_1=180 º, θ_2=90 º) at 174.5(2) ºand 83.4(2) ºrespectively. Completing the bifurcated halogen-halogen interaction is a quasi-type I interaction[83] between the halogen bond donor Br3 and a bromine (Br1) from an *m*-bromobenzoic acid ligand on a different neighboring unit. The Br1-Br3 distance is 3.4661(14) Å (93.7% of the sum of the vdW radii) and the θ_1 (C19-Br1-Br3) and θ_2 (C33-Br3-Br1) values are 163.6(3) ºand 148.2(2) º, respectively.

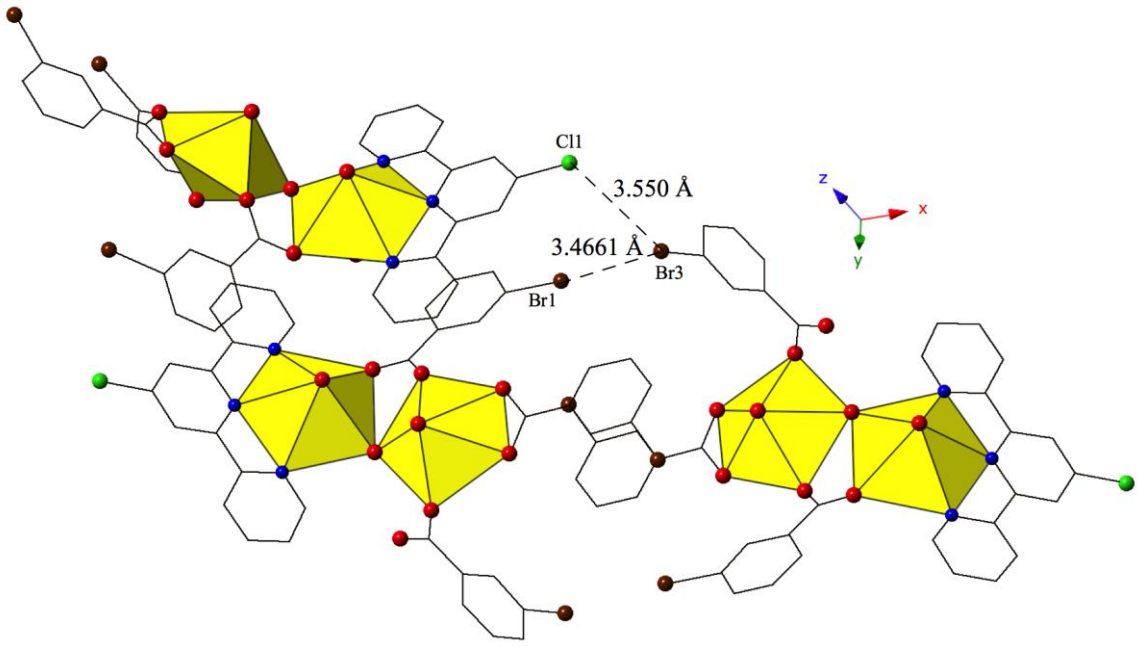

Figure 9 Polyhedral representation of complex **9** viewed down the [100] direction. Green spheres represent chlorine. The bifurcated halogen bonding interaction that connects three neighboring uranyl dimers is highlighted.

Complex **10**, $[UO_2(C_{15}H_{10}ClN_3)(C_7H_4BrO_2)_2]$, crystallizes in the space group P-1 and features nearly identical local coordination geometry to **6** so it will not be described here in detail. The only change from **6** to **10** is the addition of a chlorine atom at the 4' position of the terpy molecule in **10**, which once again results in significant changes in the modes of supramolecular assembly. The uranyl monomers of **10** are assembled into an infinite 1D chain extending approximately along the [011] direction via cooperative Br-O halogen bonding and Br-Cl halogen-halogen interactions (Figure 10, Figure S3, Supporting Information). Halogen bonding interactions between the axial uranyl oxygen of one uranyl monomer (O1) and the bromine of a *p*-bromobenzoic acid ligand (Br2) on the neighboring unit are similar to those observed in **6** with corresponding interaction distances and angles of 3.319(3) Å and 148.9(2) º, respectively (Figure 10). In addition, **10** features a type I halogen-halogen interaction[83] between the bromine of the *p*-bromobenzoic acid ligand (Br1) of the uranyl monomer and the chlorine at the 4'-position of the terpy on an adjacent unit. The Br1-Cl1 interaction distance is 3.588(2) Å (99.6% vdW) with a θ_1 value of 120.7(2) º and a θ_2 value of 118.4(2). (Figure S3, Supporting Information)

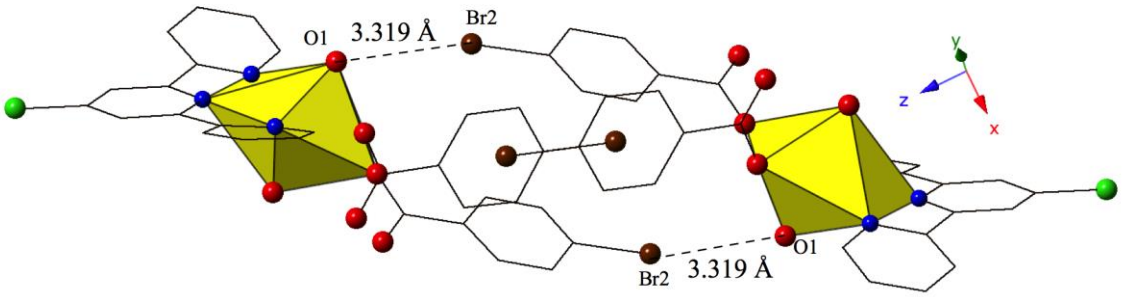

Figure 10 Complex **10** viewed down approximately the [001] direction showing the Br-O halogen bonding interactions that in concert with Br-Cl interactions link neighboring uranyl monomers.

Complex **11**, $[(UO_2)_2(OH)(C_{15}H_{10}ClN_3)(C_7H_3Br_2O_2)_3]$, crystallizes in the space group $P2_1/c$ and has nearly identical local coordination geometry to **5,** so it will not be described here in detail. Similar to **9**, **11** lacks a lattice water molecule and features the addition of a chlorine atom at the 4'-position of the terpy molecule as well as the use of 3,5-dibromobenzoic acid ligand in place of the *m*-bromobenzoic acid ligand used in **5**. These changes in ligand geometry yield a global structure that is unlike those observed for complexes **1**-**10.** The major mode of supramolecular assembly is a trifurcated halogen-halogen interaction originating from the chlorine atom at the 4'-position of the TPY molecule, which is acting as both a halogen bond acceptor and donor in **11** (Figure 11). Generally it is the heavier, more polarizable halogens that behave as halogen bond donors (i.e iodine)[86] but here we observe both a bromine (Br5) and a chlorine (Cl1) atom adopting the role. All three halogen-halogen interactions involving Cl1 (Cl1-Br4, Cl1-Br5 and Cl1-Br6) meet the criteria for type II halogen-halogen interactions ($|\theta_1-\theta_2| > 30°$) described by Desiraju *et. al*.[83] and feature interaction distances of 3.347(2) Å (Cl1-Br4, 93.0% vdW), 3.415(2) Å (Cl1-Br5, 94.9% vdW) and 3.512(2) Å (Cl1-Br6, 97.6 % vdW), respectively. Increased connectivity in the structure of **11** is achieved via further supramolecular interactions in the form of a fourth halogen-halogen interaction and a localized Cl-π interaction between Cl1 and the periphery of a 3,5-dibromobenzoic acid ligand on a fourth neighboring unit. The additional halogen-halogen interaction (Br3-Br5) also adopts a type II orientation with an interaction distance of 3.6893(13) Å (99.7 vdW) and θ_1 and θ_2 values of 150.7(2)° and 68.03(2)°, respectively. The moderate,[84] localized Cl-π interaction (Cl1-C20) is at an interaction distance 3.423(7) Å (99.2% of

the sum of the vdW radii of chlorine and carbon) and is suggestive of some vdW overlap between the chlorine atom and the benzoic acid ring of the 3,5-dibromobenzoic acid ligand.

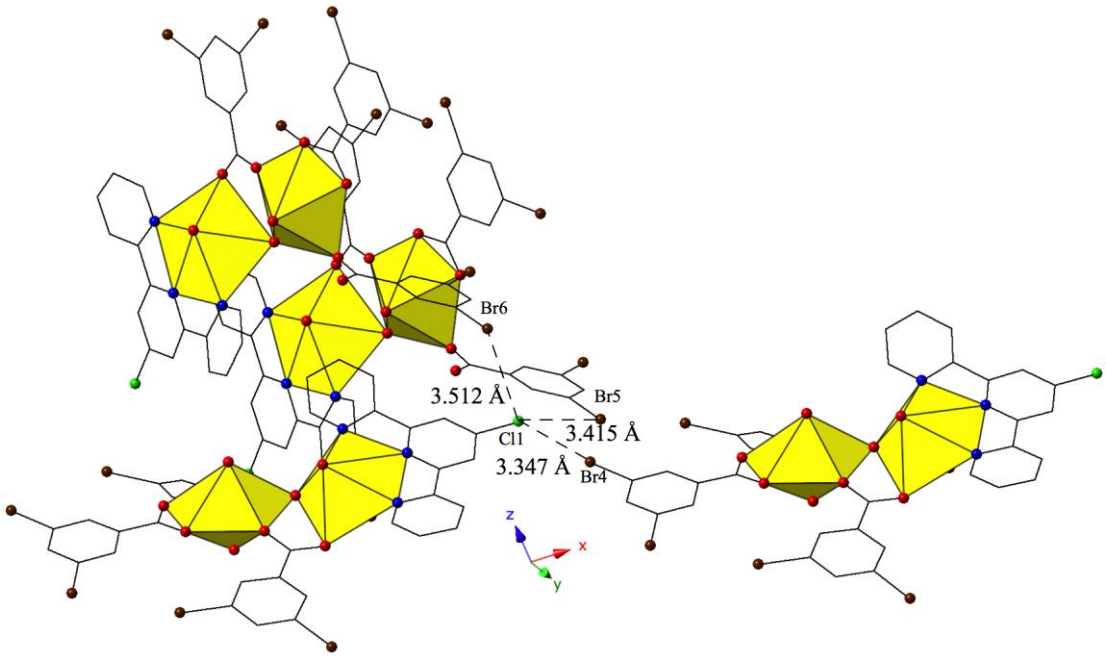

Figure 11 Complex **11** viewed in the (110) plane illustrating the trifurcated halogen-halogen interaction that links together four neighboring uranyl dimers.

Complex **12**, $[(UO_2)_2(OH)(C_{15}H_{10}ClN_3)(C_7H_4BrO_2)_3]$, is the third phase (along with **4** and **8**) that forms only at adjusted pH values (5-6) and crystallizes in the space group $P2_1/n$. **12** features nearly identical local coordination geometry to **5** and is isostructural with complex **9**, and thus will not be described in detail. Whereas at unadjusted pH with the *p*-bromobenzoic acid and Cl-TPY ligands we observed a uranyl monomer (**10**), **12** is a uranyl dimer where the two unique $[UO_2]^{2+}$ cations are bridged by a *p*-bromobenzoic acid ligand and a point sharing hydroxyl group that is a result of olation.

Similar to **9, 12** features halogen-halogen interactions that assemble the uranyl dimers in approximately the [101] direction (Figure 12). The interactions between the chlorine at the 4'-position of the TPY molecule (Cl1) and the bromine from the monodentate *p*-bromobenzoic acid ligand on the neighboring dimer (Br3) can be classified as a type II interaction[83] and feature a Cl1-Br3 interaction distance of 3.485(3) Å (96.8% of the sum of the vdW radii) and θ_1 and θ_2 values of 155.4(5) ° and 108.6(3) °, respectively. Further assembly is the result of localized Cl-π interactions between the chlorine at the 4'-position of the TPY molecule and the periphery of an adjacent *p*-bromobenzoic ligand (C32) (Figure S4, Supporting Information). These strong[84] Cl-π interactions are at distance of 3.296(9) Å (95.5% vdW) and originate from the same chlorine atoms that are also participating in halogen-halogen interactions described above.

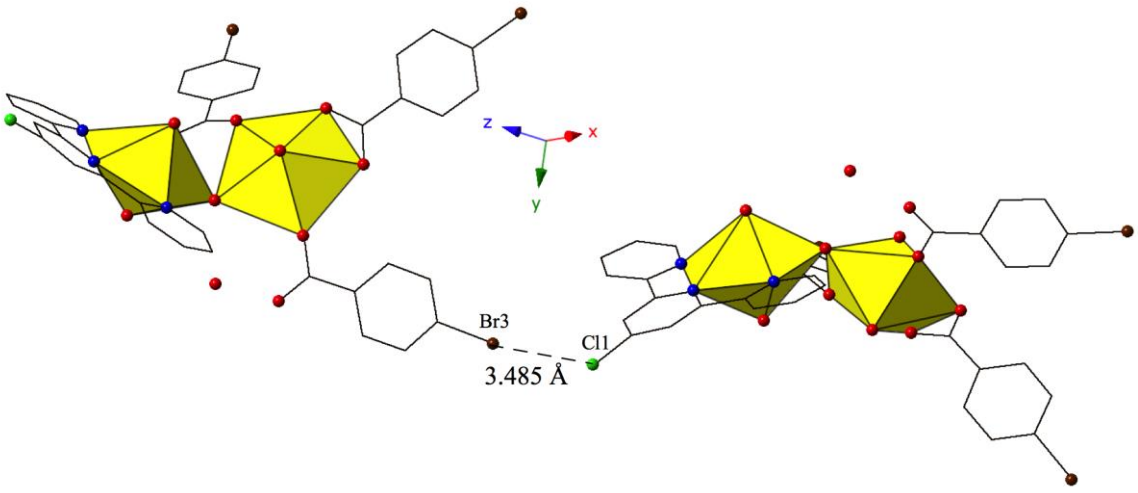

Figure 12 Complex **12** shown in approximately the [101] direction highlighting the Type II Br-Cl interaction that assembles neighboring uranyl dimers.

Structural Discussion

As structures **1-12** were synthesized from similar reaction conditions, the resulting structure types and supramolecular synthons provide an opportunity to assess

the influence of ligand sterics, the selected chelating N-donor and to a lesser extent hydrolysis on supramolecular assembly. (Table 3)

Table 3: A Summary of the Observed Supramolecular Synthons in Complex **1-12**

Complex	**Observed Synthons**	**Benzoic Acid Ligand**	**Chelating Ligand**
1	Br-O	*m*-BrBA	Phen
2	N/A	*p*-BrBA	Phen
3	H-Bonding, π-π	3,5-diBrBA	Phen
4	H-Bonding, π-π	*p*-BrBA* (did not incorporate into final structure)	Phen
5	Br-Br	*m*-BrBA	Terpy
6	Br-O	*p*-BrBA	Terpy
7	Br-O, Br-π	3,5-diBrBA	Terpy
8	Br-π	*p*-BrBA	Terpy
9	Br-Br, Br-Cl	*m*-BrBA	Cl-terpy
10	Br-Cl, Br-O	*p*-BrBA	Cl-terpy
11	Br-Cl (x3), Br-Br, Cl-π	3,5-diBrBA	Cl-terpy
12	Br-Cl, Cl-π	*p*-BrBA	Cl-terpy

m-BrBA=*m*-bromobenzoic acid, *p*-BrBA=*p*-bromobenzoic acid, 3,5-diBrBA=3,5-dibromobenzoic acid

Family 1: Complexes with Phen (1-4)

Compounds **1-4** feature a uranyl cation capped by the chelating N-donor phen and further coordinated by bromo-fuctionalized benzoic acid ligands, except in the case of **4** where the *p*-bromobenzoic acid ligand did not incorporate into the final structure. In **1** and **3** we observe uranyl monomers that adopt pentagonal bipyramidal coordination

geometry whereas in the case of **2,** we have our only example of a hexagonal bipyramidal coordination geometry**.** The two unique uranyl cations in the tetramer of **4** also adopt the pentagonal bipyramidal geometries seen in **1** and **3.** In this family of phen complexes, supramolecular interactions are observed for complexes **1**, **3** and **4**, but not complex **2** as hexagonal bipyramidal uranyl geometry does not facilitate additional assembly. These results suggest that uranyl coordination geometry may play some role in supramolecular assembly, yet this was not explored systematically. Complex **1** features uranyl monomers assembled into molecular dimers via halogen bonding interactions between *m*-bromobenzoic acid ligands and uranyl axial oxygen atoms. In complex **3**, where the larger 3,5-dibromobenzoic acid ligand is incorporated, halogens are not involved in supramolecular assembly and the monomers are assembled into 1D chains via bifurcated hydrogen bonding interactions. Finally, in complex **4** where the *p*-bromobenzoic acid ligand did not incorporate we observe assembly of the uranyl tetramers into a 2D sheet via a combination of π-π stacking interactions between phen ligands and bifurcated hydrogen bonding interactions similar to those observed in complex **7.**

Family 2: Complexes with TPY (5-8)

In compounds **5-8**, the unique uranyl cations are chelated by the tridentate N-donor terpy and then feature additional coordination to bromo-fuctionalized benzoic acid ligands. Complex **5** is a uranyl dimer that features the *m*-bromobenzoic acid ligand and is made at both unadjusted (2.5-3) and adjusted pH (5-6). Complexes **6** and **7** both contain uranyl monomers that incorporate the *p*-bromobenzoic acid and 3,5-dibromobenzoic acid ligands respectively. The former species forms only at unadjusted pH whereas the latter can be made under a range of synthetic conditions. When the pH of the synthesis of **6** is

raised to approximately neutral (pH 5-6) the result is complex **8**, which is a uranyl dimer that also features the *p*-bromobenzoic acid ligand. Looking at the modes of assembly of the molecular species in family 2, we see that the dimers of complex **5** are tethered via symmetrical Type I halogen-halogen interactions, the monomers of complexes **6** and **7** utilize halogen bonding interactions to assemble into dimers and 1D chains respectively and the dimers of complex **8** are also stitched into 1D chains via localized Br-π interactions. Br-π interactions, made possible by the additional bromine atoms on the 3,5-dibromobenzoic acid ligands, are also observed in complex **7** and are utilized to achieve additional supramolecular dimensionality.

Family 3: Complexes with Cl-TPY (9-12)

Compounds **9-12** all feature the chelating Cl-terpy ligand and a bromo-fuctionalized benzoic acid ligand. Complex **10**, with the *p*-bromobenzoic acid ligand, is a monomer made at low (~3) pH while all other members of this family are uranyl dimers. **9** and **11** are produced at both unadjusted (2.5-3) and adjusted (5-6) pH while **12** is only produced when utilizing the latter conditions. Whereas in families 1 and 2 we observed some variation in the modes of supramolecular assembly, the addition of the chlorine atom at the 4'-position of the terpy molecule in the complexes of family 3 provided the necessary conditions for halogen-halogen interactions to be the dominant mode of assembly. In all four complexes (**9-12**) we observe at least one unsymmetrical[87] ($X_1 \neq X_2$) Cl-Br interaction between molecular units and in complexes **9** and **11** we observe two and three respectively. These interactions, except in complex **10**, all adopt type II halogen-halogen geometries,[83] which arise from electrophile-nucleophile pairings, and the electrostatic nature of these interactions allows them to be viable at interaction distances

near the sum of the vdW radii. In complex **10**, the Br-Cl interactions adopt the quasi-type I orientation,[83] which is most commonly observed for Cl-Cl contacts,[87] yet is not unknown for unsymmetrical Br-Cl interactions.

From the results in structural families 1-3 we have noted that the use of the *m*-bromobenzoic ligand yields assembly via halogen bonding interactions, either halogen-halogen or halogen-heteroatom, independent of the N-donor. Despite its similarities, the *p*-bromobenzoic acid ligand yields very different results with modes of assembly varying with both the accompanying N-donor and the reaction pH. The sterically larger 3,5-dibromobenzoic acid ligand uses halogen bonding as means of assembly when the N-donor is also of sufficient size (terpy or Cl-terpy). With regards to the chelating N-donors used herein, the bidentate phen was not very useful as crystal engineering tool as it yielded a variety of local coordination modes, yet did not offer much control over the modes of supramolecular assembly. The terpy molecule, however, was able to selectively utilize halogen bonding as means of assembly in all members of family 2, yet there was still some variance in these interactions, whether they were between two halogens, a halogen and a heteroatom or a halogen and a π-system. The Cl-terpy was found to be best tool for crystal engineering the uranyl molecular complexes described herein as all that incorporated the Cl-terpy as a capping ligand were then assembled via unsymmetrical halogen-halogen interactions into extended solid-state structures of varying dimensionalities.

Returning to the participation of the axial uranyl oxygen atoms, the non-covalent coordination observed in **1**, **6**, **7** and **10** are likely not a consequence not be a function of "activation" that has been described previously where careful choice of equatorial ligands

affect Lewis basicity.[64-67] Instead our results suggest that the participation of the weakly Lewis basic uranyl oxo ligands in non-covalent interactions is possibly a function of having an agreeable donor with which to pair—in this case a polarizable bromine atom.

Conclusions

The synthesis and crystal structures of twelve uranyl complexes containing bromine functionalized benzoic acids, *m*-bromobenzoic acid, *p*-bromobenzoic acid and 3,5-dibromobenzoic acid, and the chelating N-donors phen, terpy and Cl-terpy obtained using hydrothermal reaction conditions have been reported, and their resulting means of supramolecular assembly have been investigated. Throughout the series of structurally diverse materials that were characterized herein, we observe that subtle changes in ligand geometry often lead to significant changes in the interactions utilized for supramolecular assembly. In the materials containing the chelating N-donor Cl-terpy, halogen-halogen interactions were always observed as the functionalization of the back-end of the terpy moiety proved to be a consistent method for the generation of halogen-halogen interactions. In four materials we observed oxo-functionalization of the uranyl via halogen bonding interactions and the 'activation' of the uranyl via non-covalent methods is a topic we are continuing to explore. A correlation between the SBU and pH was observed for the materials containing the *p*-bromobenzoic acid ligand, but not for the *m*-bromobenzoic acid or 3,5-dibromobenzoic acid ligands. The mechanism for these seemingly divergent results is under investigation. Follow up studies to investigate changing the character of halogens (more electron withdrawing or more electron donating) on the benzoic acid group can effect the resulting local structures and the corresponding modes for supramolecular assembly. Design of mixed-synthon systems

(Br and NO_2) and modeling efforts to better understand the role of partial charge in supramolecular interaction strength are also ongoing.

Supporting Information Available

X-ray crystallographic files in CIF format, ORTEP figures of all compounds, PXRD spectra of all compounds, tables of selected supramolecular interaction distances and bond lengths, additional figures for complexes **3**, **7**, **10** and **12** and bond valence calculations are all available. CIFs have also been deposited at the Cambridge Crystallographic Database Centre and may be obtained from http://www.ccdc.cam.ac.uk by citing reference numbers 1025739-1025750 for compounds **1-12**, respectively.

Author Information

Corresponding Author

*E-mail: cahill@gwu.edu Phone: (202) 994-6959

Notes

The authors declare no competing financial interest.

Acknowledgement

This material was supported by the U. S. Department of Energy—Chemical Sciences, Geosciences and Biosciences Division, Office of Basic Sciences, Office of Science, Heavy Elements Program, under grant number DE-FG02-05ER15736.

References

1. M. Ephritikhine, *Dalton Transactions*, 2006, 2501-2516.
2. C. L. Cahill and L. A. Borkowski, in *Structural Chemistry of Inorganic Actinide Compounds*, eds. S. V. Krivovichev, P. C. Burns and I. G. Tananaev, Elsevier, Amsterdam, 2007.
3. C. L. Cahill, D. T. de Lill and M. Frisch, *CrystEngComm*, 2007, 9, 15-26.
4. K.-X. Wang and J.-S. Chen, *Accounts of Chemical Research*, 2011, 44, 531-540.
5. K. E. Knope and C. L. Cahill, in *Metal Phosphonate Chemistry: From Synthesis to Applications*, eds. A. Clearfield and K. Demadis, Royal Society of Chemistry, London, UK, 2012.
6. L. S. Natrajan, *Coordination Chemistry Reviews*, 2012, 256, 1583-1603.
7. M. B. Andrews and C. L. Cahill, *Chemical Reviews*, 2013, 113, 1121-1136.
8. T. Loiseau, I. Mihalcea, N. Henry and C. Volkringer, *Coordination Chemistry Reviews*, 2014, 266–267, 69-109.
9. P. Thuéry and J. Harrowfield, *Crystal Growth & Design*, 2014, 14, 1314-1323.
10. C. Janiak, *Dalton Transactions*, 2003, 2781-2804.
11. C. E. Rowland and C. L. Cahill, *Inorganic Chemistry*, 2010, 49, 6716-6724.
12. M. B. Andrews and C. L. Cahill, *Angewandte Chemie International Edition*, 2012, 51, 6631-6634.
13. C. F. Baes and R. E. Mesmer, *The Hydrolysis of Cations*, John Wiley and Sons, New York, NY, 1976.
14. K. E. Knope and L. Soderholm, *Chemical Reviews*, 2013, 113, 944-994.
15. I. Grenthe, J. Fuger, R. J. M. Konings, R. J. Lemire, C. Nguyen-Trun and H. Wanner, *Chemical Thermodynamics of Uranium*, Organization for Econmoic Cooperation and Development, Issy-les-Moulineaux, France, 2004.
16. J. Leciejewicz, N. Alcock and T. Kemp, in *Coordination Chemistry*, Springer Berlin Heidelberg, 1995, vol. 82, ch. 2, pp. 43-84.
17. K. E. Knope and C. L. Cahill, *European Journal of Inorganic Chemistry*, 2010, 2010, 1177-1185.
18. W. Yang, T. Tian, H.-Y. Wu, Q.-J. Pan, S. Dang and Z.-M. Sun, *Inorganic Chemistry*, 2013, 52, 2736-2743.
19. B. Monteiro, J. A. Fernandes, C. C. L. Pereira, S. M. F. Vilela, J. P. C. Tome, J. Marcalo and F. A. Almeida Paz, *Acta Crystallographica Section B*, 2014, 70, 28-36.
20. R. G. Denning, *The Journal of Physical Chemistry A*, 2007, 111, 4125-4143.
21. S. G. Thangavelu, M. B. Andrews, S. J. A. Pope and C. L. Cahill, *Inorganic Chemistry*, 2013, 52, 2060-2069.
22. G. Liu, N. P. Deifel, C. L. Cahill, V. V. Zhurov and A. A. Pinkerton, *The Journal of Physical Chemistry A*, 2012, 116, 855-864.
23. G. Liu, L. Rao and G. Tian, *Physical Chemistry Chemical Physics*, 2013, 15, 17487-17495.
24. C. B. Aakeroy, P. D. Chopade, C. Ganser and J. Desper, *Chemical Communications*, 2011, 47, 4688-4690.
25. Y. Lu, T. Shi, Y. Wang, H. Yang, X. Yan, X. Luo, H. Jiang and W. Zhu, *Journal of Medicinal Chemistry*, 2009, 52, 2854-2862.

26. R. Wilcken, M. O. Zimmermann, A. Lange, A. C. Joerger and F. M. Boeckler, *Journal of Medicinal Chemistry*, 2012, 56, 1363-1388.
27. R. R. Knowles and E. N. Jacobsen, *Proceedings of the National Academy of Sciences*, 2010, 107, 20678-20685.
28. W. Tang, S. Johnston, J. A. Iggo, N. G. Berry, M. Phelan, L. Lian, J. Bacsa and J. Xiao, *Angewandte Chemie International Edition*, 2013, 52, 1668-1672.
29. P. H. Dinolfo and J. T. Hupp, *Chemistry of Materials*, 2001, 13, 3113-3125.
30. T. Kudernac, S. Lei, J. A. A. W. Elemans and S. De Feyter, *Chemical Society Reviews*, 2009, 38, 402-421.
31. S. I. Stupp and L. C. Palmer, *Chemistry of Materials*, 2014, 26, 507-518.
32. D. Wang, G. Tong, R. Dong, Y. Zhou, J. Shen and X. Zhu, *Chemical Communications*, 2014, 50, 11994-12017.
33. D. Braga, *Chemical Communications*, 2003, 2751-2754.
34. Y. E. Alexeev, B. I. Kharisov, T. C. H. Garcá and A. D. Garnovskii, *Coordination Chemistry Reviews*, 2010, 254, 794-831.
35. R. J. Baker, *Chemistry – A European Journal*, 2012, 18, 16258-16271.
36. N. P. Deifel and C. L. Cahill, *CrystEngComm*, 2009, 11, 2739-2744.
37. N. P. Deifel and C. L. Cahill, *Comptes Rendus Chimie*, 2010, 13, 747-754.
38. M. B. Andrews and C. L. Cahill, *Dalton Transactions*, 2012, 41, 3911-3914.
39. M. B. Andrews and C. L. Cahill, *CrystEngComm*, 2013, 15, 3082-3086.
40. C. E. Rowland, M. G. Kanatzidis and L. Soderholm, *Inorganic Chemistry*, 2012, 51, 11798-11804.
41. R. G. Surbella III and C. L. Cahill, *CrystEngComm*, 2014, 16, 2352-2364.
42. N. W. Alcock, D. J. Flanders and D. Brown, *Journal of the Chemical Society, Dalton Transactions*, 1985, 1001-1007.
43. J.-C. Berthet, M. Nierlich and M. Ephritikhine, *Dalton Transactions*, 2004, 2814-2821.
44. P. Thuéry, *Inorganic Chemistry*, 2012, 52, 435-447.
45. X.-S. Zhai, Y.-Q. Zheng, J.-L. Lin and W. Xu, *Inorganica Chimica Acta*, 2014, 423, Part A, 1-10.
46. D. K. Unruh, K. Gojdas, E. Flores, A. Libo and T. Z. Forbes, *Inorganic Chemistry*, 2013, 52, 10191-10198.
47. J. de Groot, K. Gojdas, D. K. Unruh and T. Z. Forbes, *Crystal Growth & Design*, 2014, 14, 1357-1365.
48. N. P. Deifel and C. L. Cahill, *Chemical Communications*, 2011, 47, 6114-6116.
49. R. D. Hancock, *Chemical Society Reviews*, 2013, 42, 1500-1524.
50. P. O. Adelani and P. C. Burns, *Inorganic Chemistry*, 2012, 51, 11177-11183.
51. P. Thuéry, *European Journal of Inorganic Chemistry*, 2013, 2013, 4563-4573.
52. K. P. Carter, S. J. A. Pope and C. L. Cahill, *CrystEngComm*, 2014, 16, 1873-1884.
53. K. P. Carter, C. H. F. Zulato and C. L. Cahill, *CrystEngComm*, 2014, 16, 10189-10202.
54. J. Lhoste, N. Henry, T. Loiseau, Y. Guyot and F. Abraham, *Polyhedron*, 2013, 50, 321-327.
55. *SAINT*, Bruker AXS Inc., Madison, Wisconsin, USA, 2007.
56. *APEX2*, Bruker AXS Inc. , Madison, Wisconsin, USA, 2008.
57. *SADABS*, Bruker AXS, Madison, Wisconsin, USA, 2008.

58. *TWINABS*, Bruker AXS, Madison, Wisconsin, USA, 2008.
59. A. Altomare, G. Cascarano, C. Giacovazzo, A. Guagliardi, M. C. Burla, G. Polidori and M. Camalli, *Journal of Applied Crystallography*, 1994, 27, 435-435.
60. G. Sheldrick, *Acta Crystallographica Section A*, 2008, 64, 112-122.
61. L. Farrugia, *Journal of Applied Crystallography*, 2012, 45, 849-854.
62. *Crystal Maker*, Crystal Maker Software Limited, Bicester, England, 2009.
63. *JADE*, Materials Data Inc., Livermore, California, USA, 2003.
64. M. J. Sarsfield and M. Helliwell, *Journal of the American Chemical Society*, 2004, 126, 1036-1037.
65. S. Fortier and T. W. Hayton, *Coordination Chemistry Reviews*, 2010, 254, 197-214.
66. P. L. Arnold, A.-F. Pécharman, E. Hollis, A. Yahia, L. Maron, S. Parsons and J. B. Love, *Nat Chem*, 2010, 2, 1056-1061.
67. A. J. Lewis, H. Yin, P. J. Carroll and E. J. Schelter, *Dalton Transactions*, 2014, 43, 10844-10851.
68. P. Thuéry, M. Nierlich, B. Souley, Z. Asfari and J. Vicens, *Journal of the Chemical Society, Dalton Transactions*, 1999, 2589-2594.
69. Y. Li, C. L. Cahill and P. C. Burns, *Chemistry of Materials*, 2001, 13, 4026-4031.
70. K.-A. Kubatko and P. C. Burns, *Inorganic Chemistry*, 2006, 45, 10277-10281.
71. J. Lhoste, N. Henry, P. Roussel, T. Loiseau and F. Abraham, *Dalton Transactions*, 2011, 40, 2422-2424.
72. R. C. Severance, M. D. Smith and H.-C. zur Loye, *Inorganic Chemistry*, 2011, 50, 7931-7933.
73. V. N. Serezhkin, G. V. Sidorenko, D. V. Pushkin and L. B. Serezhkina, *Radiochemistry*, 2014, 56, 115-133.
74. N. N. Krot and M. S. Grigoriev, *Russian Chemical Reviews*, 2004, 73, 89-100.
75. D. L. Clark, S. D. Conradson, R. J. Donohoe, D. W. Keogh, D. E. Morris, P. D. Palmer, R. D. Rogers and C. D. Tait, *Inorganic Chemistry*, 1999, 38, 1456-1466.
76. L. A. Watson and B. P. Hay, *Inorganic Chemistry*, 2011, 50, 2599-2605.
77. C. Janiak, *Journal of the Chemical Society, Dalton Transactions*, 2000, 3885-3896.
78. N. W. Alcock, D. J. Flanders, M. Pennington and D. Brown, *Acta Crystallographica Section C*, 1988, 44, 247-250.
79. J.-C. Berthet, M. Nierlich and M. Ephritikhine, *Chemical Communications*, 2003, 1660-1661.
80. F. F. Awwadi, R. D. Willett, K. A. Peterson and B. Twamley, *Chemistry – A European Journal*, 2006, 12, 8952-8960.
81. L. Brammer, G. Minguez Espallargas and S. Libri, *CrystEngComm*, 2008, 10, 1712-1727.
82. G. R. Desiraju and R. Parthasarathy, *Journal of the American Chemical Society*, 1989, 111, 8725-8726.
83. A. Mukherjee, S. Tothadi and G. R. Desiraju, *Accounts of Chemical Research*, 2014, 47, 2514-2524.
84. T. J. Mooibroek, P. Gamez and J. Reedijk, *CrystEngComm*, 2008, 10, 1501-1515.
85. D. Schollmeyer, O. V. Shishkin, T. Ruhl and M. O. Vysotsky, *CrystEngComm*, 2008, 10, 715-723.

86. P. Metrangolo, F. Meyer, T. Pilati, G. Resnati and G. Terraneo, *Chemical Communications*, 2008, 1635-1637.
87. S. Tothadi, S. Joseph and G. R. Desiraju, *Crystal Growth & Design*, 2013, 13, 3242-3254.